Synthesis and Characterisation of Monodisperse Sub-10 nm Alkali Metal Rare Earth Fluoride Nanocrystals

Doctoral Thesis

to obtain the Degree of Doctorate in Natural Sciences
(Dr. rer. nat.)
in the Department of Biology/Chemistry
University of Osnabrueck

Submitted by

Athira Naduviledathu Raj

Osnabrueck, Germany

December 2016

The work presented in this thesis was carried out under the guidance of Prof. Dr. Markus Haase in Inorganic Chemistry I- Functional Nanomaterials department at the Institute of Chemistry of new Materials, University of Osnabrueck, Germany during the period from April 2011 to December 2016.

Parts of the results of this work have already been published in the following articles.

A. Naduviledathu Raj, T. Rinkel and M. Haase, Ostwald ripening, particle size focusing, and decomposition of sub-10 nm $NaREF_4$ (RE = La, Ce, Pr, Nd) nanocrystals, *Chem. Mater.*, **2014**, 26, 5689.

C. Drees, **A. Naduviledathu Raj**, R. Kurre, K. B. Busch, M. Haase and J. Piehler, Engineered upconversion nanoparticles for resolving protein interactions inside living cells, *Angew. Chem. Int. Ed.*, **2016**, 55, 11668.

T. Rinkel, **A. Naduviledathu Raj**, S. Dühnen and M. Haase, Synthesis of 10 nm β-$NaYF_4$: Yb,Er/$NaYF_4$ core/shell upconversion nanocrystals with 5 nm particle cores, *Angew. Chem. Int. Ed.*, **2016**, 55, 1164.

T. Rinkel, J. Nordmann, **A. Naduviledathu Raj** and M. Haase, Ostwald-ripening and particle size focussing of sub-10 nm $NaYF_4$ upconversion nanocrystals, *Nanoscale*, **2014**, 6, 14523.

J. Nordmann, B. Voß, R. Komban, K. Kömpe, **A. Naduviledathu Raj**, T. Rinkel, S. Dühnen and M. Haase, Synthesis of β-phase $NaYF_4$:Yb,Er upconversion nanocrystals and nanorods by hot-injection of small particles of the α-phase, *Z. Phys. Chem.* **2015**, 229, 247.

Expert Committee

1. **Prof. Dr. Markus Haase**

   Anorganische Chemie I - Funktionale Nanomaterialien

2. **Prof. Dr. Lorenz Walder**

   Organische Chemie II - Molekulare Elektrochemie

Universität Osnabrück

Fachbereich Biologie/Chemie

Institut für Chemie neuer Materialien

Table of Contents

List of Abbreviations

Abbreviation	Expansion
Z	Atomic number
e. g.	For example
IUPAC	International Union of Pure and Applied Chemistry
Xe	Xenon
Ar	Argon
NCs	Nanocrystals
NP	Nanoparticles
UCNP	Upconversion nanoparticles
Kr	Krypton
Ln	Lanthanide elements
RE	Rare earths
REE	Rare earths elements
LREE	Light rare earth elements
HREE	Heavy rare earth elements
MREE	Middle rare earth elements
MRI	Magnetic resonance imaging
OA /H-OA	Oleic acid
OM	Oleylamine
TOPO	Trioctylphosphine oxide
ODE	1-Octadecne
eq.	Equation
i.e.	That is
RE-oleate	Rare earth element oleate
Li-oleate	Lithium oleate
Na-oleate	Sodium oleate
nm	Nanometer (10^{-9} meter)
mmol	Milli mole (10^{-3} mol)
min	Minute
s	Second
h	Hour
A°	Angstrom (10^{-10} meter)
kW	Kilo-watt (10^{3} watt)
mA	Mill ampere (10^{-3} ampere)
λ	Wavelength
W/cm^2	Watt per square centimetre
mL	Milliliter (10^{-3} litre)
XRD	X-ray diffractogram
XRF	X-ray fluorescence spectroscopy
TEM	Transmission electron microscopy
NIR	Near infra red
UV-Vis	Ultra violet- visible

Abstract

During the past decade, lanthanide doped alkali metal rare earth fluorides have been intensively studied due to their unique properties. Also, nanoparticles of these materials have gained much importance because $NaYF_4$, $NaGdF_4$, $NaLuF_4$ and $LiYF_4$ nanocrystals doped with Yb/Er or Yb/Tm display efficient upconversion emission. The synthesis of $NaREF_4$ nanocrystals (RE = rare earths) has therefore attracted many researchers worldwide. While a large number of procedures is already available for the synthesis of $NaREF_4$ particles of the heavier rare earth ions and for $NaYF_4$, only a very limited number of methods exists for nanocrystals of the lighter rare earth ions, RE = La, Ce, Pr and Nd. In this work, a synthesis method was therefore developed to produce monodisperse sub-10 nm sodium rare earth fluoride nanocrystals of the lighter rare earths, $NaREF_4$ (RE = La, Ce, Pr and Nd) from single-source precursors. Based on this method, the Ostwald ripening, the size focusing and the stability of these nanocrystals were studied; also, the versatility of the method was demonstrated by developing doped nanocrystals of these particles. The procedures developed in this thesis not only allow to prepare the hexagonal β-phase of these materials but also the meta-stable cubic α-phase. The latter is found to be very sensitive to decomposition. This decomposition affects also the synthesis of $NaREF_4$ particles of the hexagonal β-phase where particles of the cubic α-phase form an intermediate product. This thesis also shows that highly sodium deficient α-$NaYF_4$ nanocrystals with a size of less than 10 nm can be prepared which contain much less sodium than the bulk material. These nanocrystals were used as precursor to produce monodisperse sub-10 nm lithium rare earth fluoride ($LiREF_4$, RE = Y, Gd, Lu) nanocrystals. Using this new approach also $LiYF_4$:Yb,Er/$LiYF_4$ core/shell upconversion nanocrystals were prepared, displaying a 35 times enhancement in luminescence intensity compared to the corresponding core particles. Further, this approach provided new insights on intermediate phases formed during the synthesis. Our studies confirmed, for instance, that $LiREF_4$ nanocrystals were formed through an 'available intermediate phase', that is, a phase having a composition which is determined by the available cations in the reaction mixture.

Chapter 1

Introduction on Nanomaterials, Rare Earth Elements and Alkali Metal Rare Earth Fluorides

1.1. Nanomaterials

Scientific Committee on Consumer Products (SCCP) and British Standards Institution (BSI) defined nanomaterial as material for which at least one side or internal structure is in the nanoscale, and that according to the Federal Institute for Occupational Safety and Health (BAuA - Germany), it is a material consisting of nanostructure or nano-substance. So in general, if nanomaterials are composed of particles, with a size in the nanometer (nm) range, typically within 1 to 100 nm, these particles are called nanoparticles (NPs). In fact, the range is somewhat arbitrary and is not defined in a uniform manner. Sometimes particles with a diameter in the range between 1 and 1000 nm are also considered as nanomaterials. A nanometer is one billionth of a meter (1 nm=10^{-9} m), this is approximately 100,000 times smaller than the diameter of a human hair. The prefix ‘‘nano” is derived from the Greek word “nanos”, which means “dwarf”. In the literature the term nanocrystals (NCs) or nanocrystalline is used to emphasize the crystalline character of the nanoparticles. Even though depending on the shape and morphology of nanomaterials are categorized as several types, especially as nanoparticles, nanorods, nanotubes and nanowires, the term NPs is often used to represent them generally. Though there is no true hard definition for these nanostructures, a summarized description is provided in Table 1.1. NPs are fundamental building units of nanostructures, which are also an integral part of nature, present in the environment and living organisms where they play important roles in many chemical and biological processes [1, 2].

Historical background in connection with NPs shows that suspensions containing gold particles were known even in 1200-1300 BC. Until the Middle Ages, silver and gold colloids were used for health treatment (antibacterial, venereal diseases, dysentery, epilepsy and syphilis) [3]. The first book on colloidal gold was published by Francisci Antonii, a philosopher and medical doctor, in 1618. The colloidal suspensions were also used for colouration of ceramics and clothes [4]. A famous antiquity in this regard is the Lycurgus cup, a Roman goblet from the 4th century A.D., whose coloration is green or red when observed in reflection or transmission respectively, due to light scattering induced

by metallic NPs dispersed in the glassy matrix [5, 6]. A well-known application of early nanotechnology is the ruby red colour of finely dispersed gold that was used for stained glass windows during the Middle Ages, which are found in glass windows of many Gothic European cathedrals, like the stained glass in the Cathédrale Notre-Dame de Chartres (France), León Cathedral (Spain), Santiago de Compostela (Spain) etc.

Table 1.1: Definition of nanoparticles, nanorods, nanotubes and nanowires:

Structures	**Definition***
Nanoparticles	Nanostructure with all dimensions in the nanometer range and are part of the zero-dimensional nanostructures.
Nanorods	One-dimensional nanostructures where the standard aspect ratio (length to width) is larger than one but less than 10.
Nanowires	One-dimensional nanostructures with the diameter of the order of a nanometer which generally have aspect ratio exceeding 10 or the length at least approach the micron scale.
Nanotubes	One-dimensional structures like nanowires, in terms of aspect ratio; but unlike wires, tubes are hollow

* *There is no true hard definition*

The modern perspective on nanotechnology was perhaps first envisioned and articulated by the American theoretical physicist Richard Phillips Feynman in his famous speech on top-down nanotechnology called "*There's plenty of room at the bottom*" at an American Physical Society meeting at Caltech on December 29, 1959 [7, 8] 8]. In his speech he mentioned that ''at the atomic level, we have new kinds of forces and new kinds of possibilities, new kinds of effects''. His vision has opened new opportunities in science and technology. In the mid-1980s, Marquardt and co-workers pioneered the systematic investigation of nanostructured materials and they coined the terms "nanocrystalline" and "nanocrystal" for crystalline NPs [9, 10].

As they are effectively a bridge between bulk materials and atomic or molecular structures, NPs are of high scientific interest. Bulk materials should have constant physical properties regardless of their size, but at the nano-scale this is often not the case. The properties of materials change as their size approaches to nanoscale as the percentage of atoms at the surface of a material becomes significant due to high surface to volume ratio. However, the interesting and sometimes unusual properties of

nanoparticles are not fully due to the aspects of the surface atoms. This is known as quantum confinement effects, another primary factor that causes nanomaterials to behave significantly differently than bulk materials [11]. Both these effects influence the chemical reactivity as well as their mechanical, optical, catalytic, electric and magnetic behaviour. Size- dependent properties are observed particularly in semiconductors and metals(gold, silver) [12, 13, 14] as well as catalytic properties in some other metal (platinum, nickel, copper) NPs [15], quantum confinement in semiconductor NPs or quantum dots (cadmium selenide, cadmium sulphide, cadmium telluride, lead sulphide, indium phosphide, indium arsenide, zinc sulphide) [16, 17, 18, 19, 20] and superparamagnetism in magnetic NPs (iron oxide) [21]. Apart from the inorganic nanomaterials given by these examples, nanoparticles of organic and biomolecules are also known [22].

Due to the amazing properties of NPs, nanoscience emerged as a unique discipline of research with applications in different fields, such as life science-medicine, energy, catalyst, opto-electronics, displays, cosmetics, sensors, tribology etc. The art and science of manipulating matter at the nanoscale to create new and unique materials, technologies, devices and products now comes under the term nanotechnology. Among the inorganic nanoparticles, the semiconductor quantum dots such as CdSe, CdS, ZnS, InAs, InP, CdTe etc., having a size of less than 10 nm, are widely used in biolabeling and displays and, in the future probably also LEDs, solid state lighting and photovoltaics [23, 24, 25]. Nanoparticles of TiO_2 [26], SiO_2 [27] and ZnO [28] and metallic nanoparticles such as Ag, Au, Pt [29, 30, 31] are also extensively used in the field of solar cells, catalysis, coatings, ceramics, cosmetics and life science.

Since many inorganic NPs show size-dependent properties, high quality particles with narrow particle size distribution, well-defined structure and shape are of high interest. General strategies for the synthesis of NPs are the bottom-up and the top-down approaches [32]. In the top down approach NPs are synthesized by breaking down respective bulk materials gradually into smaller sizes by physical or chemical methods. However, in the bottom up approach NPs are built up atom by atom or molecule by molecule to form final NPs, which also can be done by different physical and chemical routes.

A detailed description of each nanomaterial, its properties and applications as well as different synthesis methods is out of scope of this thesis. In my own work, I have focused

on rare earths containing inorganic, particularly fluoride based NPs, forming a unique class of materials for versatile applications. Before discussing such nanomaterials, a description of rare earth elements and their properties is given in the following section of the thesis.

1.2. Rare Earth Elements (REE)

As stated by the International Union of Pure and Applied Chemistry (IUPAC), REE comprise fifteen lanthanides (Ln) metal elements in the f-block, lanthanum to lutetium (Z = 57 to 71), along with scandium (Z = 21) and yttrium (Z = 39), since they exhibit similar chemical behaviors and have an almost similar valence electronic configuration [Ar]$3d^1 4s^2$ (Sc), [Kr]$4d^1 5s^2$ (Y) and [Xe]$5d^1 6s^2$ (La). Also, scandium and yttrium generally occur with the Lanthanides in the same ore deposits. The word lanthanide comes from the Greek "lanthaneien" and means "to lie hidden". The REE occur in nature, although promethium, the rarest, only occurs in trace quantities in natural materials as it has no stable or long lived isotopes. Regardless of the name “rare earth”, most of the REE are much more abundant than some other elements. For example, cerium is the most abundant rare earth element and is more common than lead or copper in the earth’s crust [33]. Also, all of the REE, except promethium, are more abundant on average than gold, platinum or silver. However, most REE are not concentrated enough to make them easily exploitable economically [34].

On the basis of their atomic weight, REE are divided into two groups as light rare earth elements (LREE; lanthanum to europium or gadolinium) and heavy rare earth elements (HREE; gadolinium or terbium to lutetium). In fact, the division is somewhat arbitrary and the term middle rare earth elements (MREE) is sometimes used to refer to those elements between europium and dysprosium. Scandium and yttrium are, although light, usually grouped with the HREE group because of their similar physical and chemical properties [35].

The lanthanide elements have the general electronic configuration [Xe] $4f^{0\text{-}14}5d^1 6s^2$. The 4f level is consecutively filled from left to right in the series, that is, from cerium ([Xe]$4f^1 5d^1 6s^2$) to lutetium ([Xe]$4f^{14}5d^1 6s^2$). Lanthanum has no $4f$ electron ([Xe]$4f^0 5d^1 6s^2$). Since the inner $4f$ electrons of trivalent lanthanide ions (Ln^{3+}) are effectively shielded by outer 5d and 6s orbitals, the electrons are less affected by the chemical environment of the ions. So the $4f$ electrons are closer to the nucleus and are removed or ionized in rare cases, and have less participation in chemical bond

synergism. The electrons of the outer shells, 5*d* and 6*s*, have less ionisation energy and are easily removed or ionized to give the REE the most predominant oxidation state +3, one reason behind the similar chemical properties throughout the series. Some of the lanthanides show +2 and +4 oxidation state e.g. Ce^{4+}, Eu^{2+} and Yb^{2+}.

Though the trivalent lanthanide ions (Ln^{3+}) have almost similar chemical properties, their optical properties are interestingly distinct. Since, as mentioned above, the inner 4*f* are less affected by the chemical environment of the ions, the luminescent Ln^{3+} ions show a characteristic sharp emission line that occurs anywhere from UV to IR region, depending on their electronic states and transition probabilities. These emission lines correspond to f-f transitions of the 4f electrons which are Laporte forbidden and exhibit a low extinction coefficient. On the other hand they show long lifetimes of their excited states which is associated with the low transition probabilities of forbidden transition. Some of the most widely used ions for luminescence in the visible region are $Eu^{3+}$and Tb^{+3}. In contrast, Y^{3+}, Sc^{3+}, La^{+3} and Lu^{+3} do not show any luminescence in the visible region due to their empty or completely filled *f*-orbitals. The excellent optical properties of lanthanides enable their use individually or in combination as phosphors for many types of flat panel displays and x-ray tubes widely. Plasma displays were developed with the aid of new europium based blue phosphor which retains brightness ten times longer than previous blue phosphor [36]. Some lanthanides, chiefly europium and terbium, are used as phosphor compounds in fluorescent lamps and LEDs, and are therefore basis of energy efficient lighting [37, 38].

Another end user of REE is the glass industry where REE are used in glass polishing materials and as additives that provide colour and special optical properties [39, 40]. Rare earth based glass is used in 50% of digital and cell phone camera lenses [41]. The catalytic property of REE is well known and REE based materials are widely used in automotive catalytic converters [42]. For example, cerium oxide is part of the catalyst substrate and used as component of the converter's oxidising catalyst system [43, 44]. In the petroleum industry, REE based materials are being used in fluid cracking catalysts in the process of refining crude oil [45, 46]. Also the REE can be used as heterogeneous catalyst in chemical reactions and it is also possible to use it at high temperatures [47, 48].

The highest value commercial application of REE is their use in strong permanent magnets. The strongest permanent magnets are based on Nd-Fe-B and Co-Sm, and are

very useful when weight and space are limiting factors [49]. It leads to the production of small, light-weight and high performance electric motors which are used in different carbon reducing technologies such as in hybrid engines and wind turbines. The strength of the magnets used in the engines is one of the factors which determine the amount of electricity generated. REE magnets are commonly used in automotive power steering, electric windows, power seats, DVD and CD ROM disk drives and in computer hard disks. Terbium and dysprosium are also used in magnets and show magnetic property even at high temperatures. Another example is gadolinium, known for its strong paramagnetism [50].

REE can be used for numerous other applications and also in many new technologies. As anode materials consist of mixed REE alloy (mostly lanthanum) in the Nickel-metal hydride (NiMH) rechargeable batteries, it can be used in hybrid cars and countless other electronic products [66]. Cerium, lanthanum, neodymium and praseodymium, commonly in the form of a mixed oxide known as mischmetal, are used in steel making to remove impurities and in the production of special alloys. It has been found that gadolinium based special magnetic materials can be used in magnetic refrigeration [51] [67]. REE are essential in solid oxide fuel cells, and it has been shown that electrolytes made up of industrial grade lanthanum, cerium and praseodymium mixed carbonate are able to achieve excellent fuel cell performance at low temperatures [52].

As advances are made in materials science there are a number of REE containing materials are developed. Among them there are several nanoparticles consisting of REE that have been synthesized and are being used for various applications. Rare earth doped or undoped nanoparticles such as oxides [53], phosphates [54, 55, 56], sulphates [57, 58, 59], sulfides [60], vanadates [61, 62] etc found to be interesting from the past decades because of their excellent optical, magnetic and electrical properties arising from the f-f transitions of the 4f electrons. Since the thesis focuses on synthesis and characterization of rare earth fluoride nanoparticles, the following section is dedicated to providing a brief overview about these nanoparticles, their application and general synthesis strategies.

1.3. Rare Earth Fluoride Nanoparticles

It has been considered that rare earth fluorides are very appropriate host materials for optically active lanthanide ions (Ln^{3+}). These fluoride materials own properties such as excellent thermal and chemical stability along with conventional oxide and phosphate

host materials. Apart from that, fluoride based host materials have low phonon frequencies, one of the important factors that affect the luminescence efficiency of Ln^{3+} where non-radiative relaxation occurs due to multi-phonon relaxation. So by choosing an appropriate host material with low phonon frequency it is possible to improve the luminescence efficiency. Based on this it has been found that the rare earth fluorides including trifluorides (REF_3) and alkali rare earth fluorides ($AREF_4$, RE = rare earth, A = alkali metal) are excellent host materials with low phonon frequencies (ca. $350cm^{-1}$) [85] compared to other host materials such as oxides and phosphates (>500-1000 cm^{-1}) [86, 87]. Hence the rare earth fluoride materials have been extensively used as an ideal host for luminescent ions showing upconversion [63, 64, 65, 66, 67], downshifting [68, 69] and down conversion or quantum cutting [70, 71, 72]. These materials can be used for different applications, mainly in life science [73, 74], for lasers [75, 76, 77], solar cells [78, 79, 80, 81] or as sensor for detecting heavy and toxic ions [82, 83] as well as gas [84, 85] and biological molecules [86, 87].

Among them, nanosized $NaYF_4$ or $NaGdF_4$ or $LiYF_4$ doped with Yb/Er or Yb/Tm or Yb/Ho ions is most widely studied as upconversion materials. Upconversion process is the generation of high energy photons (particularly in the visible region) by the sequential absorption of two or more photons in the lower energy region (for example, near infra red, NIR). Upconversion nanoparticles (UCNPs) are promising fluorophores for biological assays and medical imaging since the conventional organic fluorophores are limited due to photobleaching. Moreover, organic fluorophores are excited generally with UV or visible radiations, which often cause autofluorescence by the biological samples that may interfere with the fluorescent emission signals of the fluorophore. In addition, prolonged UV radiation may cause photobleaching, photodamage or even mutation in the biological samples. However, inorganic UCNPs have shown high chemical stability, long luminescence lifetime, tunable emission wavelength and low toxicity. Also, the particles are excited by NIR radiation, which shows high penetration depth in the biological tissue is less harmful due to its low photon energy. The absence of autofluorescence and blinking leads to high signal to noise ratio [88, 89, 90] and enable them tremendously exploitable in biolabeling [91], bioimaging [92, 93], biodetection [94, 95, 96], FERT-based sensor [97] and drug delivery [98, 99, 100] applications. Most importantly, the upconversion (UC) emission can be induced by low power continuous wave laser excitation (1-10^3 W/cm^2) as opposed to the costly high-

intensity pulse laser sources (10^6-10^9 W/cm^2) required for the generation of simultaneous two-photon processes. UC ions doped $NaGdF_4$ host materials show not only UC emission, but also paramagnetic properties due to the presence of Gd^{3+} ions and these NPs can be used as contrast agent in magnetic resonance imaging (MRI) [101, 102, 103, 104]. Such NPs are known as multimodal imaging probes that work for both optical imaging and MRI. $AREF_4$ UCNPs have also been used in in-vivo studies for plant cell imaging [105] and uptake of nanoparticles [106].

1.4. Synthesis of Alkali Metal Rare Earth Fluoride ($AREF_4$) Nanoparticles

Owing to their interesting properties, methods for synthesizing NPs of $AREF_4$ materials with well-defined crystal phase, high crystallinity and narrow particle size distribution have gained much attention in recent years. In particular, the optical properties of $AREF_4$ nanocrystals (NCs) have been extensively investigated with respect to its crystal phases and particle size distribution [107]. The molecular scale building of NCs via solution phase synthesis methods result in very high composition homogeneity and morphology which often lack in case of solid state synthesis methods [108]. Also, these methods allow to control the size, morphology and crystal structure by varying the synthesis temperature, solvent, reaction time, concentration and precursor materials. The chemical methods adopted for the synthesis of $AREF_4$ NCs are synthesis in high-boiling organic solvents, hydro thermal/solvo thermal growth, co-precipitation, sol-gel processes, combustion and microwave techniques. In the following section some of these synthesis methods are briefly discussed.

1.4.1. Synthesis in High-boiling Organic Solvents

High quality nanocrystals of $AREF_4$ can be produced with control over the size and shape of the particles using this method. It mainly involves decomposition of organic precursors of REE at an elevated temperature in high boiling organic solvents with surfactants to stabilize the nanocrystals. The commonly used precursors for the thermal decomposition are fluoroorganic acid salts of REE, e.g. trifluoroacetate. Oleic acid (OA), oleylamine (OM), trioctylphosphine oxide (TOPO) etc. can act as both solvents and surfactants along with 1-octadecene (ODE), squalene or paraffin oil as co-solvents. The rapid decomposition of precursor particles at high temperature leads to a burst of nucleation, which is the key to achieve monodisperse particles. The concentration of precursors, choice of solvents, reaction temperature and time are also critical factors

that affect the final size, morphology, crystal phase, luminescence efficiency and homogeneity of the nanocrystals.

By using this method, Yan and co-workers prepared LaF_3 from trifluoroacetate of lanthanum ($La(CF_3COO)_3$) for the first time [109]. Monodisperse rare earth trifluorides, REF_3 were also successfully prepared using rare earth trifluoroacetate ($RE(CF_3COO)_3$) as single source precursor [110] in OA/OM/ODE solvent mixture. As an extension to this procedure Capobianco and co-workers successfully employed a similar method for the synthesis of alkali metal rare earth fluoride ($AREF_4$). In this case, a co-thermolysis of $RE(CF_3COO)_3$ and $ACOOCF_3$ (A = Li, Na) in organic solvents resulted in the formation of $AREF_4$ [111, 112]. Before this, in a detailed study, Mai and co-workers extensively examined the formation temperature, size and crystal structure of hexagonal and cubic phased $AREF_4$ for the entire series of rare earth elements by using different solvent ratios (OA/OM/ODE), reaction times and temperatures [107]. In addition, Shan and co-workers [113, 114, 115, 116] reported that trioctylphosphine (TOP) and ODE with OA are effective co-solvents in the co-thermolysis method. Many research groups working in the area developed modified thermal decomposition methods to tune the emission colour, morphology and size of the particles. As a result, protocols for the synthesis of monodisperse and uniform UCNPs based on different hosts such as $NaYF_4$ [117], $NaGdF_4$ [118, 119], $NaYbF_4$ [120, 121], $LiYF_4$ [122, 123], and KY_3F_{10} [124] are now available.

One advantage of the use of trifluoroacetates is the rapid formation of reactive fluoride compounds at elevated temperatures. However, the main drawbacks of the thermal decomposition of trifluoroacetate are small yields and exhale of highly toxic oxyfluorinated carbon species as by-product during decomposition. In addition, since the solvents using this method are purely organic, the particles obtained are hydrophobic in nature and need surface modification to enable them to be used for further applications, especially water solubility for life science applications.

As an alternative to trifluoroacetate, respective rare earth oleates can be used as precursor material along with NaF or NH_4F as fluoride source to achieve $AREF_4$ or REF_3 nanocrystals with the desired size and properties. The molecules used as surfactants (OA, OM or TOPO) also play an important role on the manoeuvring of narrow particle size distribution, morphology and crystal phase transition of $AREF_4$ nanocrystals [125, 126, 127, 128]. In such a case, the reaction is free of toxic by-products and also provides the possibility to scale up the product in grams. Of course, surface modifications of the

hydrophobic nanocrystals are required to transfer them into hydrophilic solvents. Chen and co-workers prepared doped $NaYF_4$ and $NaGdF_4$ nanocrystals using RE-oleate and NaF in OA/ODE as solvents [129, 130]. Li and Zhang demonstrated the use of other precursors, such as rare earth chlorides instead of oleates, but the chlorides subsequently converted to oleates due to the presence of oleic acid [131]. Thus, rare earth oleates are widely used as precursors to produce different kinds of $AREF_4$ or REF_3 NCs with various sizes, shapes and crystal structures.

1.4.2. Hydrothermal and Solvothermal Methods

Hydrothermal and solvothermal synthesis techniques are important wet-chemical methods, where the reactions take place in water (hydrothermal) or other solvents (solvothermal) at pressures above 1 bar. The high pressure increases the boiling point of the solvent and therefore allows to conduct the synthesis at high temperatures. It helps to increase the solubility and reactivity of the reactants and supports crystallization of the products [132, 133, 134, 135]. The reactions are conducted in a sealed vessel called autoclave. Since this method is usually based on water or nontoxic solvents, it is considered to be more environment- friendly. It has been shown that the shape and size of particles can be controlled through appropriate addition of organic additives which act as complex agents or structure directing agents [136, 137]. The commonly used organic additives for the fabrication of $AREF_4$ nanoparticles are oleic acid, as polyvinylpyrrolidone (PVP) and polyethylenimine (PEI) [138], ethylenediamine tetraacetic acid (EDTA) [139, 140], cetyltrimethylammonium bromide (CTAB) [141] and tri-sodium citrate (TSC) [142, 143].

Usually, rare-earth chlorides, nitrates, or oxides are chosen as the rare earth ion precursors and these are combined with HF or NH_4F for synthesizing rare earth trifluoride nanoparticles (REF_3), while either NaF or LiF is used for rare earth-alkali metal rare earth fluoride ($AREF_4$). Li and co-workers synthesised highly uniform rare earth fluoride nanocrystals by using a special hydrothermal method called liquid-solid-solution (LSS) strategy [138]. By adapting this technique, rare earth fluoride such as YF_3 [144, 145], LaF_3 [146, 147, 148], GdF_3 [149]as well as alkali metal fluorides like $NaYF_4$ [150, 151], $NaLaF_4$ [152], $NaLuF_4$ [153, 154], were successfully synthesised. Zhao and co-workers prepared uniform $NaYF_4$ nanorods, nanotubes and nanodisks using another hydrothermal method called OA mediated process [155]. Liu and co-workers developed a novel Gd^{3+}-doping approach to give simultaneous control over the crystal phase, size,

and optical properties of the resulting $NaYF_4$ UCNPs during the hydro (solvo) thermal synthesis [156]. It has been found that the morphology of these nanocrystals is affected by the experimental parameters such as temperature, reaction time, pH, concentration, solvents and doping concentration.

1.4.3. Other Synthesis Methods

Methods involving as co-precipitation, sol-gel techniques, microwave heating and solvents like polyols and ionic liquids have also been used for producing different rare earth fluorides. Among them, co-precipitation is considered as one of the simplest methods due to simple steps to follow and low cost of reaction equipment. However, in most of the cases post-treatment like annealing of as prepared co-precipitated particles is needed to gain better physical and chemical properties. Veggel and co-workers synthesised NCs of LaF_3:Ln^{3+} (Ln=Eu, Er, Nd and Ho) using the co-precipitation method [157]. Commercially available ligands such as polyvinylpyrrolidone (PVP) and polyethylenimine (PEI) are also widely used to control particle growth and endow solubility as well as surface functionality [158, 159].

The sol-gel process is a typical wet-chemical process involving mainly two steps, hydrolysis and condensation. The process has been widely used for developing glass materials and thin film coating formulations containing nanomaterials. Again, a post heat treatment or calcinations at high temperature is usually required for instance, to improve the luminescence efficiency of the deposited materials. Different groups have synthesised various rare earth fluorides NPs via this method [160, 161, 162]. The sol-gel-derived NPs are supposedly not particularly suitable as luminescent probes for biological assays due to lack of size control as well as aggregation of the particles happens to occur.

Apart from the synthetic strategies mentioned above, there are other known processes like solid state reaction, synthesis in ionic liquid as well as polyol [163]] and the microwave assisted method [164] have been adopted for the preparation of rare earth fluoride particles. In the work presented here the nanocrystals were synthesised in the high-boiling coordinating solvent oleic acid because the method yields NPs with narrow size distribution, high luminescence efficiency and particle size tunability.

1.5. Motivation of the Thesis

Luminescent nanoparticles are particularly useful for biologically and other applications, if their

- Mean size is below 10 nm
- Size distribution is narrow

Since $NaLaF_4$, $LiYF_4$, $LiGdF_4$ and $LiLuF_4$ are suitable host lattices for doping with luminescent lanthanide ions, the synthesis of monodisperse nanocrystals of these materials with a size below 10 nm was studied.

1.6. Aims of the Thesis

The aims of the work presented here are as follows;

1. Developing a new synthesis procedure for monodisperse β-$NaREF_4$ (RE = La, Ce, Pr, Nd) nanocrystals with sizes below 10 nm.
2. Investigating the growth mechanism of these (1) particles with special emphasis on the formation of transient of sodium deficient particles of cubic α-$NaREF_4$.
3. Development of a new synthesis procedure for monodisperse $LiREF_4$ (RE = Y, Gd, Lu) nanocrystals.

1.7. Outline of Chapters 3 - 5

In accord with the aims of this thesis given above (1.6), the main results are structured as follows.

In **Chapter 3** the synthesis of sub-10 nm $NaREF_4$ NCs of the LREE (RE = La, Ce, Pr, Nd) is described. We observed that NCs of some of these materials behave thermodynamically different from corresponding bulk particles. We successfully established a synthesis procedure for such NCs with sizes less than 10 nm and a narrow size distribution using single-source precursors. A detailed study on Ostwald ripening, size focusing and decomposition effects of these NCs was also performed and the results are presented in this chapter. Further, successful doping of $NaLaF_4$ and $NaCeF_4$ with different luminescent lanthanides ions, especially Ce, Tb and Pr, were demonstrated and their optical properties were studied.

The studies presented in chapter 3 indicated that highly sodium deficient $NaREF_4$ particles of the cubic α-phase are formed as intermediate products before $NaREF_4$ particles of hexagonal β-phase are obtained as final products. This motivated us to examine the existence as well as the stability of highly sodium deficient cubic α-phase $NaYF_4$ NCs. So **Chapter 4** provides a detailed description for the synthesis of highly sodium deficient cubic α-phase $NaYF_4$ NCs with sub-10 nm size. In addition, Ostwald ripening and size focusing of these particles were investigated in detail.

Chapter 5 discusses the synthesis and the characterisation of monodisperse sub-10 nm lithium rare earth fluoride ($LiREF_4$, RE = Y, Gd, Lu) NCs, another unique class of rare earth fluoride materials. We have successfully developed a new approach to prepare monodisperse sub-10 nm sized $LiREF_4$ NCs using highly sodium deficient rare earth fluoride NCs. Also, this approach was used to check the intermediate phase formation during the synthesis of $LiYF_4$ NCs, since this was not clear from previous studies. Our studies confirm that $LiYF_4$ NCs are formed through an 'available intermediate phase' and formation of the available intermediate phase was determined by the available cations in the reaction mixture. In addition, we found that the approach is readily $LiLuF_4$. The new approach was finally used to grow a shell of $LiYF_4$ on the core particle of $LiYF_4$:Yb,Er demonstrating the feasibility of the method to prepare the core/shell particles.

Chapter 2

Theory for the Formation of Monodisperse Nanocrystals and Characterisation Techniques

2.1. Formation of Monodispersed Nanocrystals in Solution

Generally, the formation of NCs can be divided into three stages as nucleation, growth and ripening, and the following section may give a brief overview on these stages.

2.1.1. Nucleation, Growth and Ripening

In the classical model of crystal or solid growth in solution, growth is explained based on dissolved 'monomers', the term used to refer to ions, atoms or molecules present in the reaction medium. Nuclei are formed from these monomers and follow different growth regimes to form crystals or solids. Nucleation is the process whereby a new phase is generated in the form of 'nuclei or seeds'. Generally, there are three kinds of nucleation processes. If nuclei are formed from a homogeneous supersaturated bulk solution or parent phase, this process is referred to as 'primary nucleation', whereas if nuclei are generated in a supersaturated bulk solution in the presence of other particles or materials with the same, this is called 'secondary nucleation'. On the other hand, the 'heterogeneous nucleation' process occurs due to structural inhomogeneities, that is the presence of foreign interfaces, like impurities, grain boundaries, dislocations and container surfaces. For the rest of the discussion in this section I will focus on homogeneous primary nucleation, which is the one to take place most likely in the synthesis procedure adopted for developing NCs mentioned in the thesis.

The growth mechanism of highly uniform or monodisperse NCs or colloids from a homogeneous supersaturated monomer reaction medium was first studied by LaMer and Dinegar [165]. They pioneered the concept of 'burst nucleation', in which many nuclei are generated at the same time when the concentration of the monomers increases rapidly, rising above the saturation concentration for a concise period. A short period of time during which nucleation occurs is, in fact, very important to obtain narrow particle size distribution. Otherwise, if the nuclei formation occurs throughout the synthesis, the growth histories of particles would differ largely from one another, and would result in polydisperse particles. The LaMer plot, shown in **Figure 2.1**, is very

useful for understanding how burst nucleation and the subsequent growth of the seeds occur by consuming the monomers in the supersaturated solution with time.

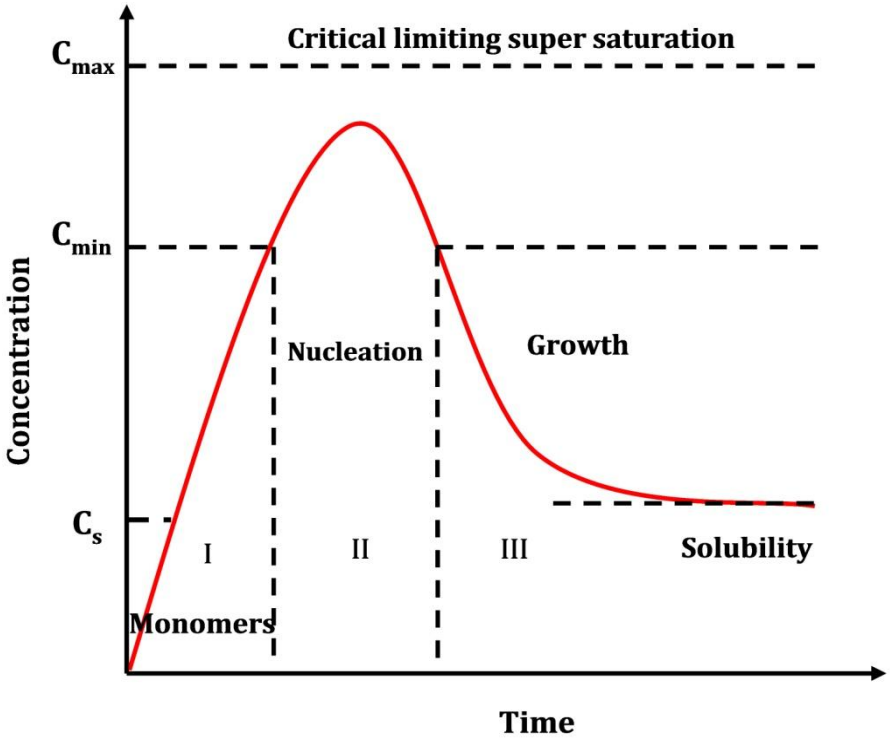

Figure 2.1: LaMer plot: Concentration of monomers as function of time [165].

As is depicted, the mechanism mainly proceeds through three different stages. In stage I, the concentration of monomers constantly increases with time as thermal decomposition of precursors occurs. However, precipitation does not happen below the critical supersaturation concentration (C_{min}) because the energy barrier for spontaneous homogeneous nucleation is high. In stage II, the formation of stable nuclei occurs because C_{min} is high enough to overcome the energy barrier for nucleation. Since the rate of monomer consumption resulting from nucleation and fast growth of the nuclei exceeds the rate of monomer supply, the monomer concentration (C_{mono}) decreases until it reaches the level at which the nucleation rate (the number of nuclei formed per unit time) is zero. This leads the system to the next growth stage (stage III), in which nucleation has effectively stopped and the solution now consists of the crystal nuclei, free monomers and any remaining precursor, which may release monomers further. At this stage, the existing nuclei will grow to nanocrystals with increasingly larger size until an equilibrium state is reached between the monomers on the surface of the nanocrystals and the monomers in the solution. The resulting monomer concentration in solution is called equilibrium concentration, C_{∞}^{eq}. In general, the ratio

between the concentration of monomers, C_{mono} and the equilibrium concentration, C_{∞}^{eq} is called supersaturation, S (eq. 2.1).

$$S = \frac{C_{mono}}{C_{\infty}^{eq}} \qquad (2.1)$$

The widely accepted and simplest theory that describes the nucleation process is the classical nucleation theory, which was originally derived for describing the condensation of a vapor into a liquid. Later on, it has also been employed by analogy to explain the formation of crystals from supersaturated solution and melts. At the end of the 19th century, Gibbs developed the thermodynamic description of this process. According to this theory, the total free energy change required for the crystal formation (ΔG) is given by the sum of the free energy change required for the phase transformation to a unit volume of the crystal (ΔG_v) and the free energy change required for the formation of the surface of the crystal (ΔG_s). For a spherical particle with radius, r and surface energy, γ the total free energy is given by eq. 2.2. The resulting free energy diagram for nucleation is shown in **Figure 2.2**. In a saturated solution with increasing radius of the crystal, ΔG_v becomes more negative due to the high thermodynamic stability of a solid state material. On the other hand, the formation of the solid/liquid interface increases the free energy by an amount proportional to the surface of the crystal. Since the positive surface free energy ΔG_s dominates at small radii, the total free energy change ΔG increases initially.

However, as the crystal size increases, the total energy goes through a maximum at a critical size (r_{cr}) above which the total free energy decreases continuously and growth of the nucleus becomes energetically favorable.

$$\Delta G = 4\pi r^2 \gamma + \frac{4}{3}\pi r^3 \Delta G_v \qquad (2.2)$$

The crystal free energy ΔG_V depends on the temperature T, the surface energy γ, the molar volume of solid material V_m and the supersaturation of the solution S.

$$\Delta G_V = -\frac{RT \ln S}{V_m} \qquad (2.3)$$

Eq 2.3 shows that the volume term favors the formation of crystals as long as $S > 1$, that is, ΔG_V is negative as long as the solution is supersaturated

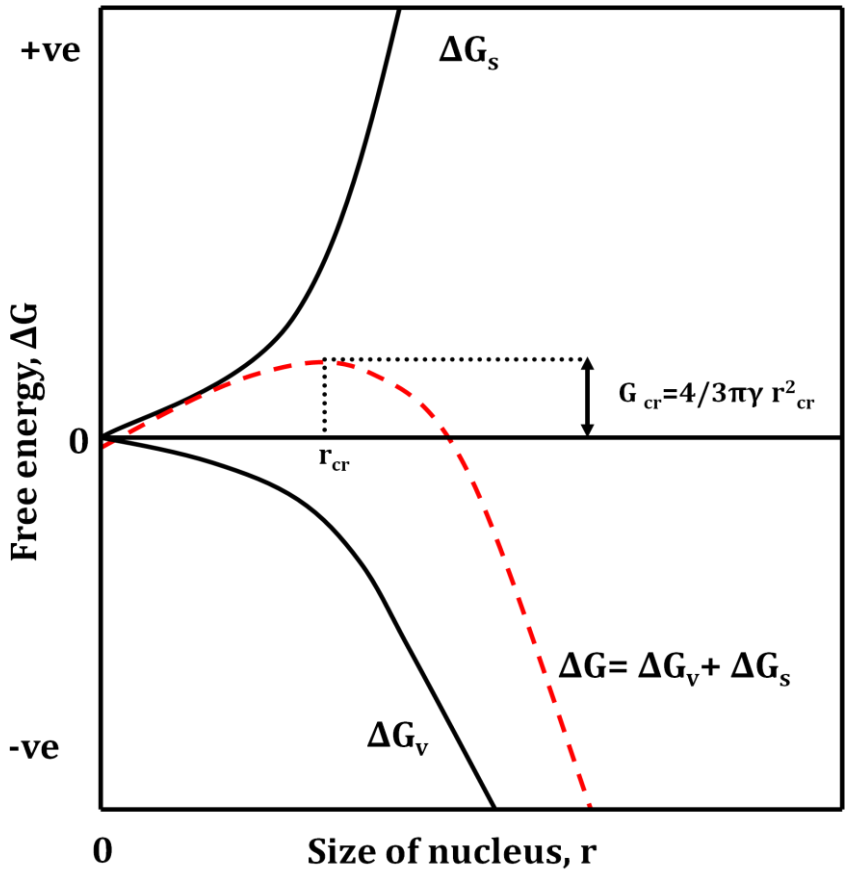

Figure 2.2: Free energy diagram for nucleation explaining the existence of 'a critical nucleus' [166].

However, the surface term ΔG_s imposes an extra free energy requirement for the formation of nuclei. Due to the contribution of ΔG_s, nuclei smaller than the critical radius (r_{cr}) dissolve again because this decreases their total free energy ΔG. So the critical radius r_{cr} is the minimum size of a nucleus that can resist dissolution and grow further. By differentiating ΔG with respect to r and setting the derivatives equal to zero, it is possible to calculate the maximum free energy (ΔG_{cr}) (eq. 2.4) which a nucleus will pass through to form a stable nucleus as well as the corresponding critical radius (eq. 2.5).

$$\Delta G_{cr} = \frac{4}{3}\pi\gamma r_{cr}^2 \qquad (2.4)$$

$$r_{cr} = \frac{2\gamma V_m}{RT\ ln\ S} \qquad (2.5)$$

The growth process involves deposition of monomers from the solution on to the surface of the NCs. According to the classical growth theory, the growth rate of a particle is determined by the number of monomers reacting at the particle surface per unit time by diffusion and the rate of their reaction with the particle surface. If the diffusion of monomers on the particle surface limits the growth rate of the particle, the reaction is called diffusion controlled. If the reaction of the monomers with the particle is slower than their transport to the surface via diffusion, the reaction is called kinetically controlled, reaction controlled or surface controlled.

The growth rate of a seed or particle depends on three factors; particle size r, supersaturation S and the constant K, which indicates, whether the growth reaction is more diffusion or reaction controlled. It is determined by the quotient of the diffusion coefficient D of the monomers in solution and the rate constant k_∞ of the reaction between the monomer and the particle surface. In 1961 Wagner has published the following equation for the growth rate of a particle (eq. 2.6) [167].

$$\frac{dr}{dt} = \frac{2\gamma\, C_\infty^{eq} V_m^2}{RT}\, \frac{k_\infty D}{k_\infty r + D} \left(\frac{1}{r_{cr}} - \frac{1}{r}\right) \qquad (2.6)$$

In eq. 2.6 R is the ideal gas constant, T is the absolute temperature, γ is the surface energy, V_m is the molar volume, D is the diffusion coefficient and r_{cr} is the critical radius.

For the limiting cases of a purely diffusion controlled and purely kinetic controlled reactions, eq. 2.6 simplifies to equation 2.7 and eq. 2.8 respectively. For a diffusion controlled reaction $D \ll r.k_\infty$ and hence

$$\frac{dr}{dt} = \frac{K_D}{r}\left(\frac{1}{r_{cr}} - \frac{1}{r}\right) \qquad (2.7)$$

Where

$$K_D = \frac{2\gamma\, C_\infty^{eq} V_m^2 D}{RT}$$

Correspondingly, the reaction controlled growth, where $D \gg r.k_\infty$ is explained by the equation (eq. 2.8),

$$\frac{dr}{dt} = K_R\left(\frac{1}{r_{cr}} - \frac{1}{r}\right) \qquad (2.8)$$

Where

$$K_R = \frac{2\gamma C_\infty^{eq} V_m^2 k_\infty}{RT}$$

These two equations (also derived by Wagner) were used in 1987 by Sugimoto who realized that eq. 2.7 leads to focussing of the particles size distribution [168].

Several months before Wagner, Lifshitz and Slyozov published a very similar work and the theory is now known as LSW theory [167, 169, 170]. However, the expression for the growth law given above is only valid for larger particles, since LSW theory just considers the linear term of the Taylor expansion of the Gibbs-Thomson equation (refer eq. 2.11). Wagner explained that this approximation fails only for very small particles, for which $2\gamma v/rRT \geq 0.3$, i. e., that particles whose radius is of the order of 3 x 10^{-7} cm or less [167]. Crystals of this size were considered at that time as insignificant.

By using the Gibbs-Thompson equation without this approximation and by obeying the dependence of the rate constant k_∞ on particle size, Talapin and co-workers obtained the following modified expression for the growth rate [171].

$$\frac{dr}{dt} = V_m D C_\infty^{eq} \left\{ \frac{\frac{C}{C_\infty^{eq}} - exp\left[\frac{2\gamma V_m}{rRT}\right]}{r + \frac{D}{k_\infty} exp\left[\propto \frac{2\gamma V_m}{rRT}\right]} \right\} \qquad (2.9)$$

Further, based on the modified growth law they described the temporal evolution of the particle size distribution of NCs by numerical simulation. Also in the modified growth law a NC having a radius smaller than some critical radius r_{cr} dissolves and shows a negative growth rate. The value of this critical radius corresponding to a growth rate equal to zero can be easily evaluated by setting equation 2.9 (or eq. 2.6) equal to zero. For equation 2.9 this yields

$$r_{cr} = \frac{2\gamma V_m}{RT lnS} \qquad (2.10)$$

Consequently, particles with a radius $r < r_{cr}$, have a negative growth rate, consequently dissolve and thus release monomers in to the solution. Particles with a radius $r > r_{cr}$ have a positive growth rate and as a result, they consume monomers from the solution and grow. Eq.2.10 shows that a high supersaturation S results in a very small critical

radius r_{cr}. If r_{cr} is smaller than the smallest particles of the size distribution, all particles have a positive growth rate and increase in size. The dependence of growth rate on size of the NCs is schematically represented in **Figure 2.3** for the diffusion controlled case. The left hand side of the curve shows that very small crystals are unstable owing to their large fraction of active surface atoms, as indicated by the negative growth rate. Larger crystals with smaller surface to bulk ratio are stable and grow further, as illustrated by the positive growth rates in the right hand side of the curve. The NCs neither grow nor shrink at the zero-crossing point which indicates the critical size of the particles.

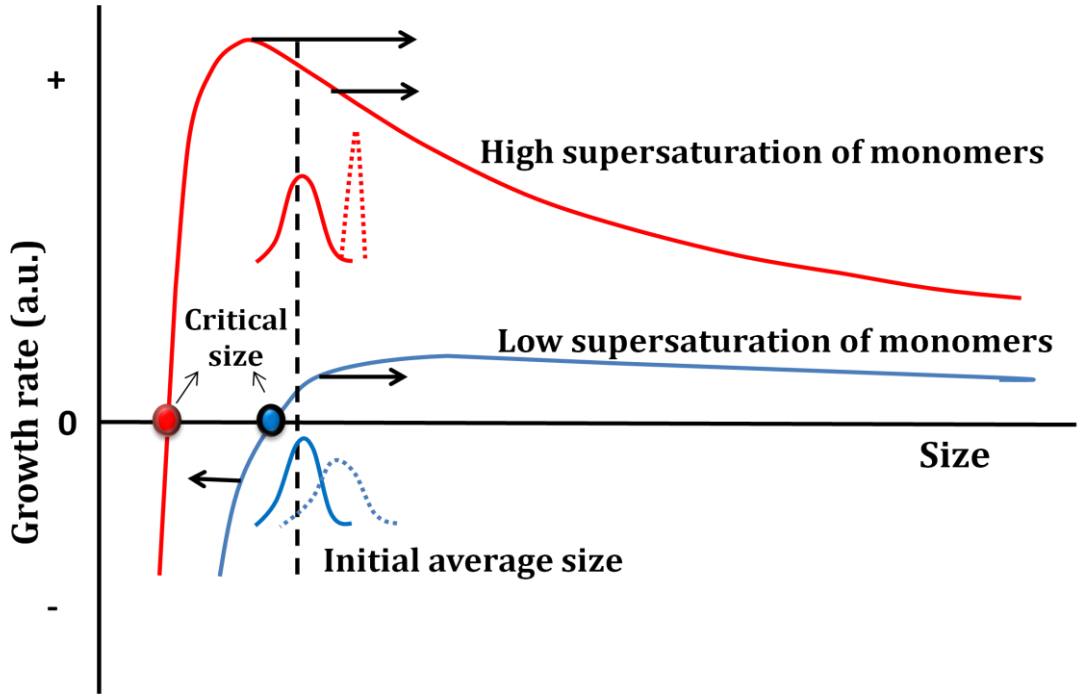

Figure 2.3: The dependence of the growth rate of a spherical nanocrystal on its particle radius focusing for the case of high and low supersaturation. The temporal evolution of a particle size distribution is also sketched [172].

If the monomer supersaturation S is sufficiently high, all particles of the size distribution grow because their size is larger than the critical radius. Their growth, however, consumes monomers and therefore decreases S and increases the critical radius. It can be shown mathematically that the mean radius of the particle ensemble increases slower than the critical radius. Therefore, after some time of the growth, the value of the critical radius moves into the size range covered by the particle ensemble. The fraction of particles with sizes smaller than the critical size now decreases in size because their growth rates are negative. Conversely, all particles with a size larger than the critical

radius still grow in size. This leads to an increase of the mean particle size of the ensemble, but its size distribution broadens with time. This process is called Ostwald ripening and was first proposed by Ostwald in 1900 [173]. Since the monomers released by the dissolution of the smaller particles are consumed by the larger particles, "the larger particles grow on the expense of the smaller particles".

The process of Ostwald ripening is described by the LSW model which is based on the Gibbs-Thompson equation.

$$C_r^{eq} = C_\infty^{eq}\, exp\left(\frac{2\gamma V_m}{RTr}\right) \cong C_\infty^{eq}\left(1 + \frac{2\gamma V_m}{RTr}\right) \qquad (2.11)$$

According to the Gibbs-Thompson equation, the solubility of a small particle C_{mono}^{eq} increases with decrease in size. The solubility of a "bulk" precipitate of the solid is given by C_∞^{eq}. The solubility C_r^{eq} corresponds to the monomer concentration in solution which is in equilibrium with a particle of size r .

It is possible to recover monodisperse particles from Ostwald ripened sample or particles with broad sized distribution by separating out fractions of particles with a narrow distribution using the size selective precipitation approach [174, 175]. However, the concept of 'size-distribution focusing' (Figure 2.3) is considered a more robust approach to obtaining NCs with narrow size distributions. In fact, figure 2.3 shows that the small NCs will grow more rapidly than larger ones if monomer concentrations are sufficiently high. This was first predicted by Reiss and co-workers [176], several years before Sugimoto. As a result, the size distribution can be focused down to one that is nearly monodisperse, provided that supersaturation can be kept sufficiently high to prevent the critical radius to enter the size range of the particle ensemble [172]. So monodisperse NCs can be achieved by stopping the reaction, while it is still in the focusing regime and it is a key step in kinetic control over the NCs synthesis. Another way is providing monomer by secondary hot injection or fast dropping during slow growth conditions. The distribution of nanocrystal sizes present does not change immediately after injection, however, the critical size, which depends on monomer concentration, shifts to a smaller value. If the shift is large enough, the distribution will spontaneously narrow or focus. The concept of size distribution focusing has now been experimentally demonstrated [177].

2.2. Characterisation Techniques

2.2.1. X-ray Powder Diffractometer (XRD): is one of the most powerful, non-destructive analytical tools to identify the crystal structural of a material. When a monochromatic X-ray beam with a certain wavelength strikes onto a crystalline material at angle theta, diffraction at the lattice plane of the crystal occurs and the constructive interference of the diffracted x-rays, which take places only when the conditions satisfy Bragg's Law, $(n\lambda = 2d\,sin\theta)$, is monitored by the diffractometer. All possible diffractions from the crystal lattices will be captured by scanning through preferable 2θ angles. Different forms of samples can be used for analysis such as powder, films, discs and semi-solid etc. For analyzing the samples presented in the thesis, only powder XRD was performed by plating the sample on the sample holder. The XRD patterns were recorded by an X'Pert Pro Diffractometer (Pananlytical) with Bragg-Brentano geometry using Cu Kα radiation (1.5406 Å), a voltage of 40 kV, a current of 40 mA and a step size of 0.033423°. The crystal structure of samples was deduced by comparing the position and intensity of the reflections of the measured diffractograms with those of a database (the powder diffraction files, PDF).

2.2.2. X-ray Fluorescence (XRF) Spectrometry: is a quantitative non-destructive elemental analysis technique suitable for analysing solids, liquids and powder samples. X-ray fluorescence is the emission of characteristic X-rays from a material that has been excited with X-ray with sufficient photon energy. X-ray fluorescence is observed when the atoms in the sample absorb enough X-ray energy ejecting electrons from the lower (usually K and L) energy levels and creating vacancies. The vacancies can be replaced by electrons from an outer orbital, higher energy orbital. Inner electrons have higher binding energies than outer electrons. So an electron loses some energy when it drops from a higher electron shell to an electron shell that is closer to the nucleus. The energy released or lost due to the decreased binding energy is equivalent to the difference in energy between the two electron shells. Since these energy differences are unique with each element, elemental analysis is easily possible through XRF. The detection limit depends on the element and the sample matrix. In general heavier elements have lower detection limits to the ppm level. The elemental composition of the samples presented in this thesis was determined with a 1 kW AXIO^{SmAX} X-ray fluorescence spectrometer (PANalytical).

2.2.3. Transmission Electron Microscopy (TEM): is used to image nanometer ranged particles. Owing to the small wavelength of the electrons, a much higher resolution is achieved compared to optical microscopy. With an additional EDAX unit, elemental analysis can be performed by detecting characteristic X-rays formed due to the interaction between the electrons and the sample. The maximum resolution of TEM is determined by the acceleration voltage quality of the electronic lenses. For the work presented here, a TEM (JEOL 2010) with an accelerating voltage of 200 kV and a resolution limit of 2 Å was used to image the synthesized samples. The TEM samples were prepared by placing 10 µL of a dilute colloidal solution in hexane on a carbon film coated copper grid (200 mesh) and evaporating the solvent. Size histograms of the samples were derived from TEM images using the software Image-J. The TEM images used for this purpose are shown in appendix A2.

2.2.4. Luminescence Spectroscopy: Lanthanides are well known for their distinct luminescence properties. Therefore, the emission and excitation spectra of all lanthanide doped samples were recorded at room temperature with a Fluorolog 3 spectrometer (Jobin Yvon, Horiba). A 450 W xenon lamp was used as excitation source and the emission light was measured at the right angle to the excitation light. Powder samples were filled in 1 mm quartz cuvette and mounted at a 45 angle using a solid sample holder (model 1933, Horiba). Usually, the wavelength of maximum absorption was chosen as excitation wavelength, which is mentioned in the respective part of the thesis. For the measurement of emission spectra, a step size of 0.5 nm and a slit width of 1 nm were used for the emission monochromator and of 3 nm for excitation monochromator. In order to eliminate higher order spectra, respective filters were used. Upconversion luminescence spectra of the synthesized samples were recorded at room temperature with the same spectrophotometer by replacing the 450 W xenon lamp against 980 nm CW- laser diode. The samples were measured as powders filled in 1 mm quartz cuvettes.

2.3. Synthesis and Chemicals

Since several rare earth fluorides were prepared in this thesis, it is difficult to generalize the synthesis procedure, and therefore each synthesis method is presented in the respective chapter. The details of the chemicals and amount used in each reaction presented in this thesis are given in appendix A3.

Table 2.2 gives the details, including purity and manufacturer, of the chemicals used for the synthesis.

Table 2.2: Details of chemicals used for the synthesis

Chemicals	**Manufacturer**	**Purity, %**
Rare earth chloride hydrated $YCl_3.6H_2O$;$LaCl_3.7H_2O$;$CeCl_3.7H_2O$; $PrCl_3.6H_2O$;$NdCl_3.6H_2O$;$GdCl_3.6H_2O$; $YbCl_3.6H_2O$; $ErCl_3.6H_2O$; $LuCl_3.6H_2O$	Treibacher Industries AG	99.9
Lithium hydroxide monohydrate ($LiOH.H_2O$)	Sigma-Aldrich	98
Ammonium fluoride (NH_4F)	Sigma-Aldrich	98
Sodium fluoride	Sigma-Aldrich	99
Tetramethylammonium fluoride (TMAF) tetrahydrate	Alfa Aesar	98
Sodiumoleate	Sigma-Aldrich	82
Silver nitrate ($AgNO_3$)	Merck	99.5
Oleic acid	Alfa Aesar	90
Octadecene	Alfa Aesar	90
n-Hexane	Sigma-Aldrich	99.9
Ethanol	AHK Alkoholhandel GmbH & Co KG	99.9

Chapter 3

Synthesis and Characterisation of Monodisperse Sub-10 nm Sodium Rare Earth Fluoride of Lighter Lanthanides ($NaREF_4$, RE = La, Ce, Pr, Nd) Nanocrystals

3.1. Introduction

In recent years, as previously mentioned in the sections 1.3 and 1.4, nearly monodisperse nanocrystals of sodium rare earth fluorides ($NaREF_4$) have been intensively investigated. The majority of papers deal with $NaREF_4$ nanocrystals containing heavy or middle rare earth elements (HREE or MREE). It has been found that the crystal phase, size distribution, morphology and doping concentration are important parameters which determine the physical, chemical, and especially the optical properties of the particles. Generally $NaREF_4$ particles can crystallise in two different crystallographic phases, the cubic α-phase (metastable at room temperature) and the hexagonal β-phase (thermodynamically stable). Each phase can be produced, depending on the synthesis conditions. In the structure of α-$NaREF_4$, Na^+ and RE^{3+} cations are randomly distributed in the cationic sub-lattice; while in the β-$NaREF_4$, there are three cation sites: one site only occupied by RE^{3+}, a second site occupied randomly by ½ Na^+ and ½ RE^{3+}, and a third site occupied randomly by ½ Na^+ and ½ vacancies [178]. Yb,Er doped $NaYF_4$ in the hexagonal β-phase displays stronger upconversion emission than in the cubic α-phase.

$NaREF_4$ NCs of the lighter rare earth elements (LREE, RE = La, Ce, Pr, Nd), are significantly more difficult to prepare than those of the HREE and MREE since these materials are more sensitive to decomposition [179]. Mai and co-workers tried to synthesise the whole series of $NaREF_4$ (RE = Y, Pr-Lu) by an oleic acid based synthesis method [107]. By tuning the ratio of Na/RE, the solvent compositions (oleic acid/octadecene/oleylamine), the reaction temperature and the reaction time, they succeeded to manipulate the crystal phase (cubic or hexagonal), shape, and size of the $NaREF_4$ nanocrystals. Moreover, they suggested that the cubic (α) to hexagonal (β) -phase transition occurs during the decomposition of metal trifluoroacetate and that the phase transition plays an important role in determining the particle size distribution and shape of the final particles. Even though they successfully synthesised β-$NaPrF_4$ and

β-$NaNdF_4$, there was no description for the synthesis of β-$NaLaF_4$ and β-$NaCeF_4$, and no mention about its possibility of existence. Though high quality β-$NaLaF_4$ was synthesized by Chow and co-workers, they adopted drastic reaction conditions, i.e., the decomposition of excess metal trifluoroacetate in oleylamine at a very high temperature of 345 °C [180]. Li and co-workers investigated a solvothermal synthesis of β-$NaCeF_4$ in oleic acid/ethanol mixtures and reported the formation of rather large nanorods with a length of approximately 200 nm [181]. In another work, Wu and co-workers synthesised small β-$NaCeF_4$ particles by using diethylene glycol as solvent and poly(acrylic acid) (PAA) as stabilizer, but obtained comparatively broad size distributions [182]. Yang and co-workers prepared spherical and rod shaped nano as well as micrometer sized crystals of $NaREF_4$ (RE = Pr-Yb, Y) using water-ethanol as solvent, oleic acid as stabilising agent and prolonged heating, 12 - 24 h. They found that the F/RE ratio plays an important role to determine the shape of the particles [183]. However, as we mentioned in the previous chapter, the large particle size, the polydispersity and the drastic synthesis conditions may restrict use of these materials.

So through this chapter we discuss our efforts to identify the reason for the difficulty in the formation of these $NaREF_4$ nanomaterials (RE = La, Ce, Pr, Nd), further their Ostwald ripening, size focusing and decomposition behaviour. As in a previous work reported from our group on $NaSmF_4$, $NaEuF_4$, $NaGdF_4$ and $NaTbF_4$ nanocrystals, we prepared first sub-10 nm particles of these materials, purified them and use these particles then as single-source precursor for the synthesis of larger β-phase particles of the same material [184]. The final particles are thereby formed solely by Ostwald ripening and in the absence of any molecular precursors apart from the "monomers" exchanged among the particles during Ostwald ripening. This "clean" reaction allows us to identify the problems as well as the conditions to obtain nearly monodisperse β-$NaREF_4$ particles of the lighter lanthanides i.e., La, Ce, Pr, Nd. Using our new approach, we have developed procedures to prepare not only monodisperse particles but also sub-10 nm sized particles of both crystal phases (β-$NaLaF_4$, β- $NaCeF_4$, β-$NaPrF_4$ and β-$NaNdF_4$, as well as of α-$NaCeF_4$, α-$NaPrF_4$ and α-$NaNdF_4$) which may facilitate the use of these particles in different applications.

3.2. Experimental Section

Synthesis of sodium fluoride: Sodium fluoride was freshly prepared by slowly adding a solution (0.05 mol/L) of NaOH in methanol to a suspension (0.05 mol/L) of NH_4F in methanol and stirring the mixture for 30 min at room temperature. The precipitate of NaF was isolated by centrifugation, washed two times with methanol, and dried at room temperature.

Synthesis of rare earth oleates: The rare earth oleates were prepared by reacting solutions of the corresponding rare earth chlorides with sodium oleate, as given in the literature [185]. In a typical preparation of neodymium oleate, 60 mmol of neodymium chloride ($NdCl_3 \cdot 6H_2O$, 21.52 g) and 180 mmol of sodium oleate (54.8 g) were dispersed in 120 mL of ethanol, 90 mL of water, and 210 mL of hexane, and the resulting turbid mixture was heated under reflux (at about 60 °C). After 14 h of heating, the transparent pale purple coloured organic phase containing the neodymium oleate was separated. The neodymium oleate was isolated as a waxy solid by removing the hexane with a rotavap. Praseodymium oleate (green), cerium oleate (pale brown) and lanthanum oleate (pale yellow) were prepared analogously.

Synthesis of small cubic phase nanocrystals: Sub-10 nm particles of α-$NaREF_4$ (RE = Ce, Pr, and Nd) were prepared by combining a 1:6 mixture (RE:Na) of rare earth oleates and freshly prepared sodium fluoride with oleic acid, oleylamine and octadecene (2.5 mL of oleic acid, 2.5 mL of oleylamine, and 5 mL of octadecene per 1 mmol of rare earth oleate), and degassing the mixture on a vacuum Schlenk line (1 mbar) for 1 h at 100 °C under vigorous stirring. The reaction mixture was heated at 200 °C for 60 min under nitrogen flow and strong stirring. A turbid solution was obtained due to the excess of sparingly soluble sodium fluoride, which was removed by centrifugation after cooling to room temperature. The clear supernatant was merged with an equal volume of ethanol, leading to precipitation of the small particles, which were separated by centrifugation. The particles were purified by redispersing the precipitate in hexane (3 mL of hexane per 1 mmol of rare earth oleates), followed by precipitation with ethanol and separation by centrifugation.

Synthesis of small hexagonal phase nanocrystals: Sub-10 nm particles of β-$NaREF_4$ (RE = La, Ce, Pr, Nd) were prepared by using rare earth oleate and sodium oleate in a molar ratio of 1:2.5. The combined oleates were dissolved in a mixture of oleic acid,

oleylamine, and octadecene (2.5 mL of oleic acid, 2.5 mL of oleylamine, and 5 mL of octadecene per 1 mmol of rare earth oleate), and the solution was degassed on a vacuum Schlenk line (1 mbar) for 1 h at 100 °C under vigorous stirring. Subsequently, 4 mmol of ammonium fluoride per 1 mmol of rare earth oleate was added under nitrogen flow. The setup was cycled three times between a nitrogen atmosphere and vacuum (vacuum was applied for only 5 s in each cycle) before the reaction mixture was heated at 290 °C for 60 min under nitrogen flow and vigorous stirring. After cooling to room temperature, the nanocrystals were precipitated by adding an equal volume of ethanol and separated by centrifugation. Purification was performed as given above for particles of the cubic phase.

The hexagonal NCs of 15% Tb^{3+} doped $NaCeF_4$, 5% Ce^{3+} doped $NaLaF_4$ and 5% Pr^{3+} doped $NaLaF_4$ were also synthesised by the same procedure.

Synthesis of large hexagonal phase nanocrystals: Larger particles of β-$NaREF_4$ (RE = Ce, Pr, Nd) were prepared by Ostwald ripening of smaller $NaREF_4$ particles in oleic acid/octadecene, as follows. The reaction was performed in a 25 mL three-neck flask with an attached thermo sensor and reflux condenser. After filling 5 mL of oleic acid and 5 mL of octadecene into the flask, 2.5 mmol of small particles of the α-phase or the β-phase was added and the setup was connected to a Schlenk line. The particles were redispersed in the solvent by heating the mixture at 100 °C for 60 min under vacuum. Thereafter, the solution was heated to 320 °C for 60 min under nitrogen flow and vigorous stirring. After the desired reaction time, the solution was rapidly cooled to room temperature. A 1:2 mixture of hexane and ethanol was added, and the nanocrystals were separated by centrifugation. The precipitate was purified as given above for the small particles. For TEM investigations, the nanocrystals were redispersed in hexane using ultrasonication.

3.3. Results and Discussion

Small $NaREF_4$ particles of the cubic α-phase or the hexagonal β-phase were used as single source precursors in all of our synthesis procedures. A Considerably large amount, in gram level, of nearly monodispersed sub-10 nm $NaREF_4$ particles (RE = La, Ce, Pr and Nd) of the β-phase were prepared by the reaction of ammonium fluoride with sodium oleate and rare earth oleate dissolved in a solvent mixture of oleic acid, oleylamine and octadecene. TEM images of the particles are shown in **Figure 3.1**. It was

found to be crucial that oleylamine is part of the solvent mixture to obtain particles of the β-phase. In the case of cerium and praseodymium, CeF_3 and PrF_3 particles are formed instead, if oleylamine was omitted. Size histograms generated from corresponding TEM images in figure 3.1 are given in **Figure 3.2**. The histograms show that the mean particle sizes ⟨d⟩ are in the range of 5–7 nm and that narrow size distributions with standard deviations of σ/⟨d⟩ = 5–10 % are obtained in all cases. For all materials, the XRD reflections are well in accord with the hexagonal β-phase of $NaREF_4$ (**Figure 3.3**).

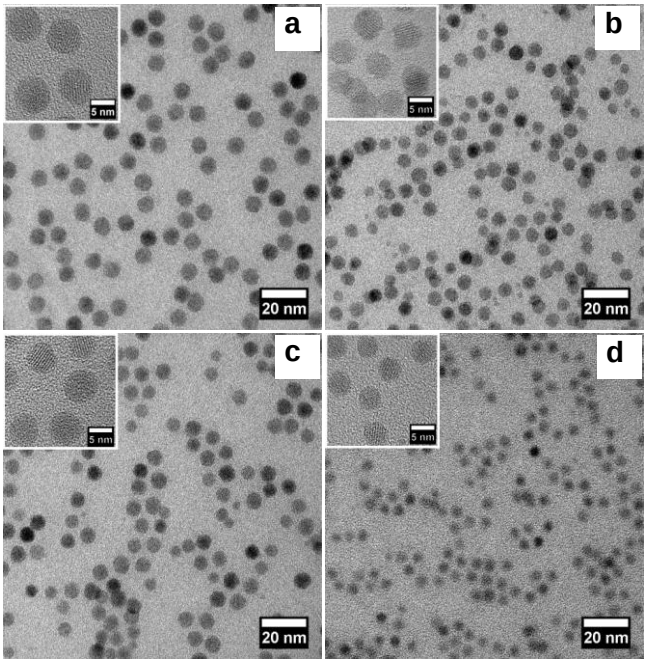

Figure 3.1: TEM images of nearly monodisperse sub-10 nm nanocrystals of (a) β-$NaLaF_4$, (b) β-$NaCeF_4$, (c) β-$NaPrF_4$ and (d) β-$NaNdF_4$ nanocrystals prepared by the reaction of the rare metal oleates with ammonium fluoride in oleylamine/oleic acid/octadecene at 290 °C for 60 min.

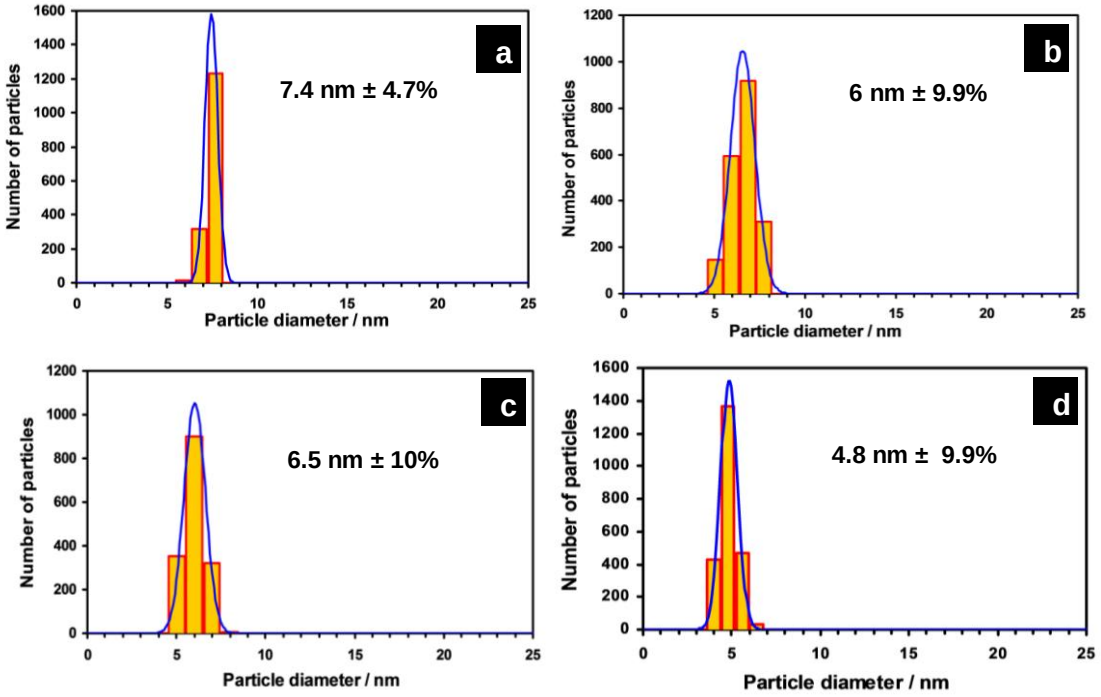

Figure 3.2: Particle size histograms, as derived from TEM images, of (a) β-$NaLaF_4$, (b) β-$NaCeF_4$, (c) β-$NaPrF_4$ and (d) β-$NaNdF_4$ nanocrystals prepared by the reaction of the metal oleates with ammonium fluoride in oleylamine/oleic acid/octadecene at 290 °C for 60 min. The values for the mean particle diameter and the relative standard deviation (in %) are indicated. Blue solid lines indicate Gaussian fits of the corresponding histogram.

In the reaction medium containing oleylamine, Ostwald ripening of these particles is observed to be very slow, as is evident from the above results. To investigate the growth behaviour in the absence of oleylamine, the particles were precipitated with ethanol, washed, and subsequently redispersed in a solvent mixture containing only oleic acid and octadecene. We found that heating at 320 °C for 1 h increases both the mean particle size and the width of the size distribution. The TEM images and the corresponding size histograms are provided in **Figure 3.4**.

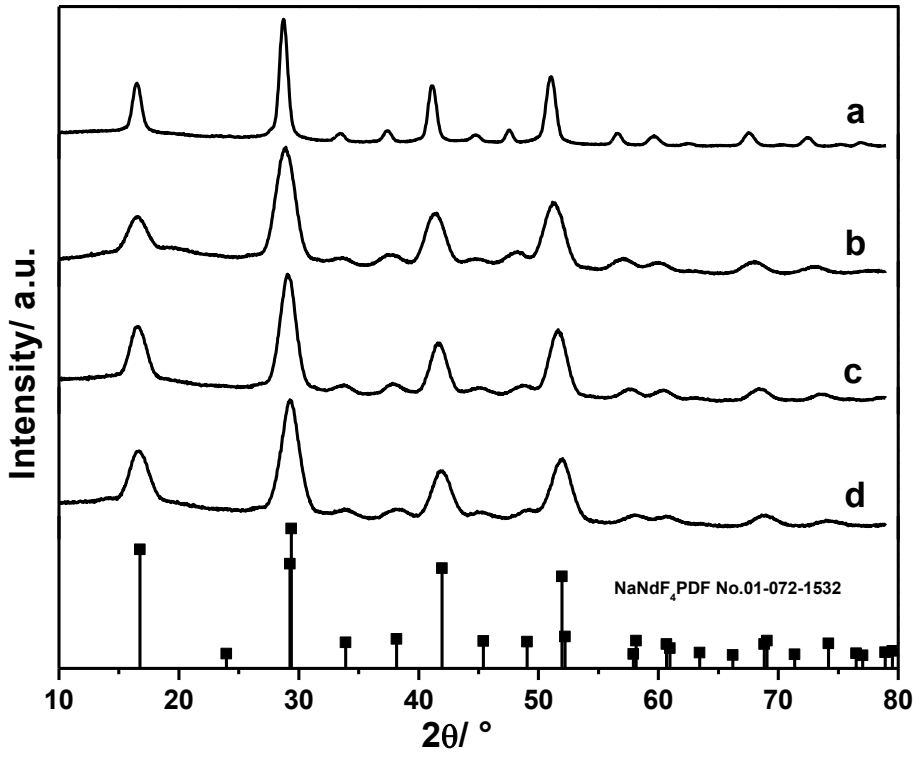

Figure 3.3: XRD data of (a) β-$NaLaF_4$, (b) β-$NaCeF_4$, (c) β-$NaPrF_4$ and (d) β-$NaNdF_4$ nanocrystals prepared by the reaction of the metal oleates with ammonium fluoride in oleylamine/oleic acid/octadecene at 290 °C for 60 min. In all cases the XRD data are in accord with the hexagonal phase of $NaREF_4$.

In the case of $NaCeF_4$, $NaPrF_4$ and $NaNdF_4$ particles, the XRD data display after heating no other phases than the hexagonal β-phase, but a smaller peak width indicates increase in particle size (**Figure 3.5**). This growth behaviour meets the expectations for Ostwald ripening and has already been observed for β-$NaSmF_4$, β-$NaEuF_4$, β-$NaGdF_4$ and β-$NaTbF_4$ nanocrystals [186, 187]. In the case of $NaLaF_4$, however, the diffractogram shows the presence of some LaF_3 already after 60 min of heating at 290 °C. After 60 min of heating at 320 °C, complete decomposition into LaF_3 is observed (**Figure 3.6**). Two conclusions can be drawn from these results. The first is that the β-phase of $NaLaF_4$ is not stable in the more acidic solvent mixture containing no oleylamine. The second conclusion is that Ostwald ripening in the case of $NaCeF_4$, $NaPrF_4$ and $NaNdF_4$ proceeds much faster than in the presence of oleylamine. The reason could be fast protonation of the fluoride ions by oleic acid (H-OA), resulting in faster exchange of "monomers" among particles, according to eq. 3.1:

$$NaREF_4 + 4\ \text{H-OA} \leftrightarrow \text{Na oleate} + RE(OA)_3 + 4\ HF \qquad (3.1)$$

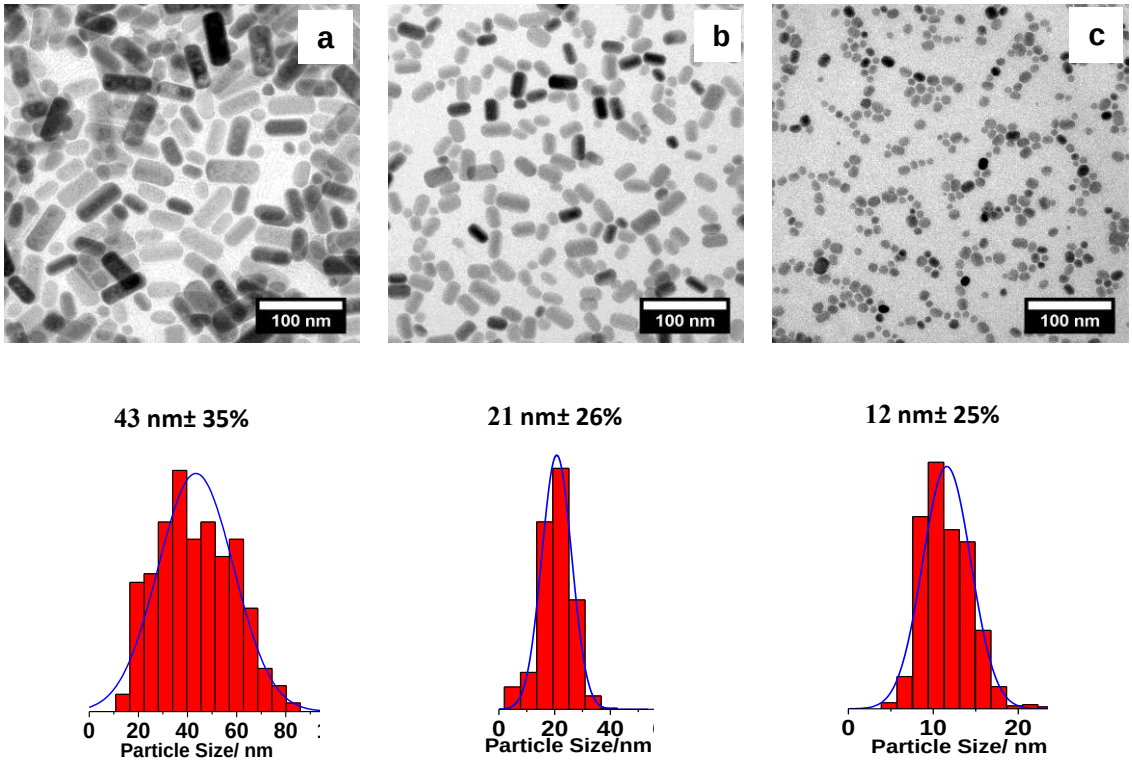

Figure 3.4: TEM images and corresponding particle size histograms of polydisperse (a) β-$NaCeF_4$, (b) β-$NaPrF_4$ and (c) β-$NaNdF_4$ nanocrystals obtained by heating the small β-phase particles shown in figure 3.1 in oleic acid/octadecene at 320 °C for 60 min. Values for the mean particle diameter and the relative standard deviation (in %) are given in the histograms. The blue solid lines indicate Gaussia n fits.

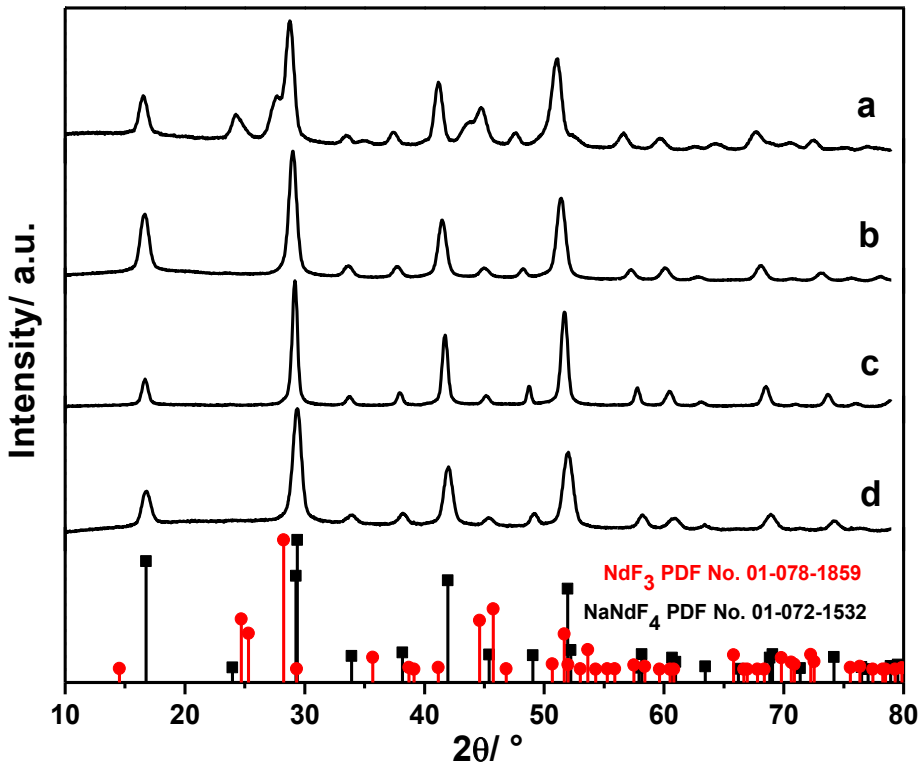

Figure 3.5: XRD data of β-$NaREF_4$ nanocrystals after heating in oleic acid/octadecene at 320 °C for 60 min: a) $NaLaF_4$, b) $NaCeF_4$ c) $NaPrF_4$ and d) $NaNdF_4$. In the case of $NaCeF_4$, $NaPrF_4$, and $NaNdF_4$ the hexagonal β-phase is retained after Ostwald-ripening. $NaLaF_4$ displays partial decomposition into hexagonal phase LaF_3.

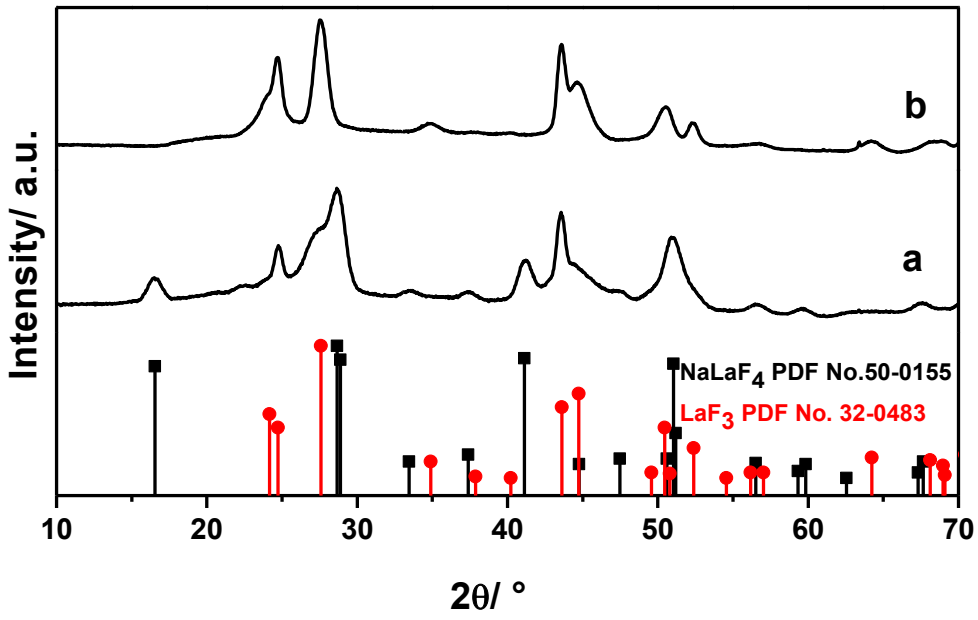

Figure 3.6: XRD data of β-$NaLaF_4$ nanocrystals after heating in oleic acid/octadecene at a) 290 °C and b) 320 °C for 60 min, the latter resulting in complete decomposition into LaF_3 (hexagonal phase).

Ostwald ripening under acidic conditions, therefore, rapidly increases the mean size of $NaCeF_4$, $NaPrF_4$, and $NaNdF_4$ particles but also leads to broadening of the size distribution. To obtain narrow particle size distribution, a high concentration of monomers has to be somehow maintained during particle growth (supersaturation of monomers) [168]. In the case of heavier lanthanides, the latter can be achieved by heating β- phase particles in the presence of a large amount of α-phase particles [187, 186].

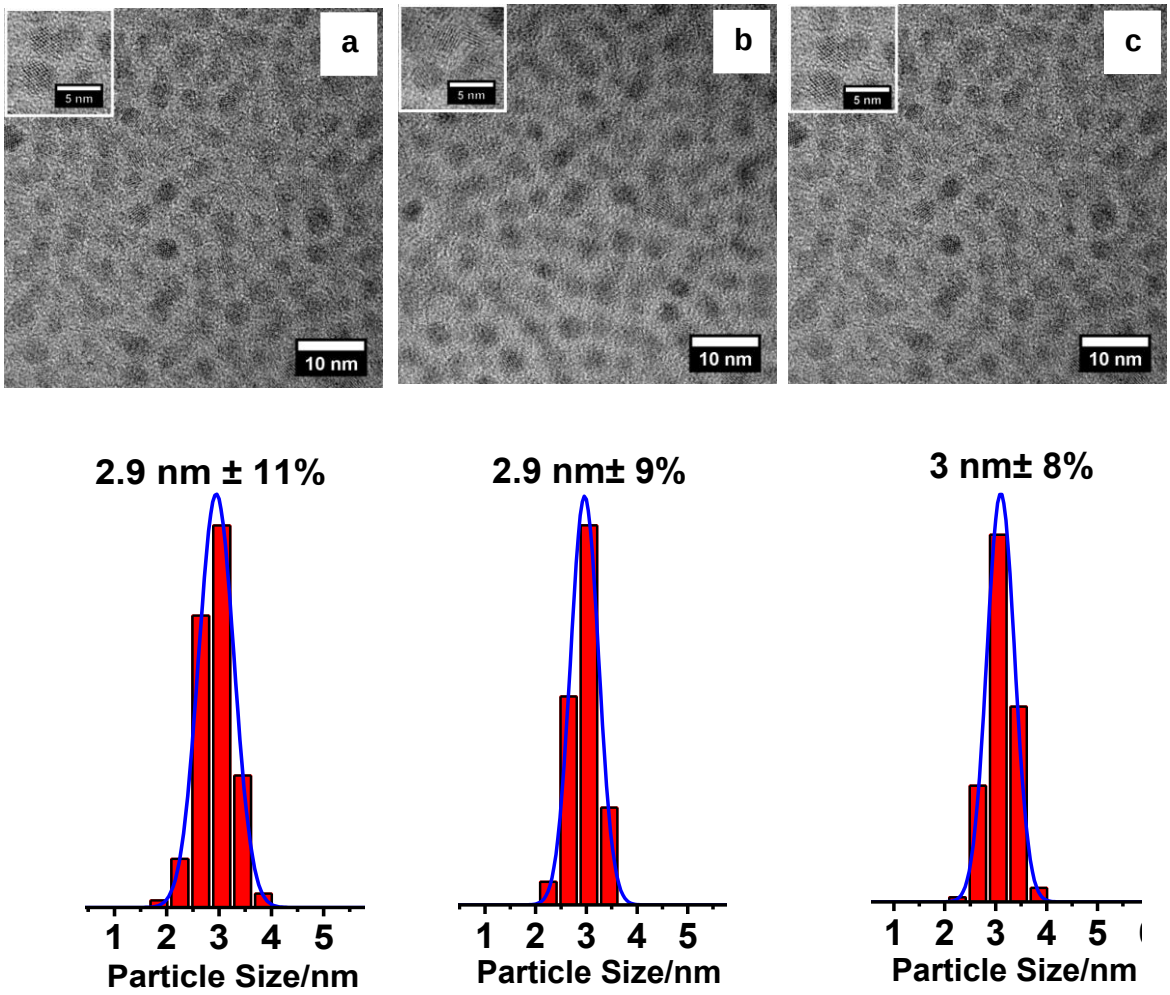

Figure 3.7: TEM images of sub-10 nm nanocrystals of (a) α-$NaCeF_4$, (b) α-$NaPrF_4$ and (c) α-$NaNdF_4$ prepared by the reaction of rare earth oleates with excess sodium fluoride in oleylamine/oleic acid/octadecene solvent. Values for the mean particle diameter and the relative standard deviation (in %) are given in the histograms. The blue solid lines indicate Gaussian fits.

To use this method also in the case of lighter lanthanides, we developed an improved procedure for preparing small particles of the cubic α-phase of these materials. Similar to literature procedures used for the synthesis of $NaSmF_4$, $NaEuF_4$, $NaGdF_4$ and $NaTbF_4$

particles [186, 188], we replaced ammonium fluoride and sodium oleate by excess sodium fluoride to promote the formation of the cubic phase. Additionally we replaced the oleic acid/octadecene solvent by a mixture of oleylamine, oleic acid, and octadecene to lower acidity. This modified procedure allows the preparation not only of α-$NaPrF_4$ and α- $NaNdF_4$ particles but also of α-$NaCeF_4$, which, to our knowledge, has not been reported yet. **Figure 3.7** displays TEM images and corresponding particle size histograms of the resulting nanocrystals after precipitation and washing with ethanol. The XRD data are given in **Figure 3.8**. In all cases, the XRD peaks are well-indexed to the cubic α-phase, even for $NaCeF_4$.

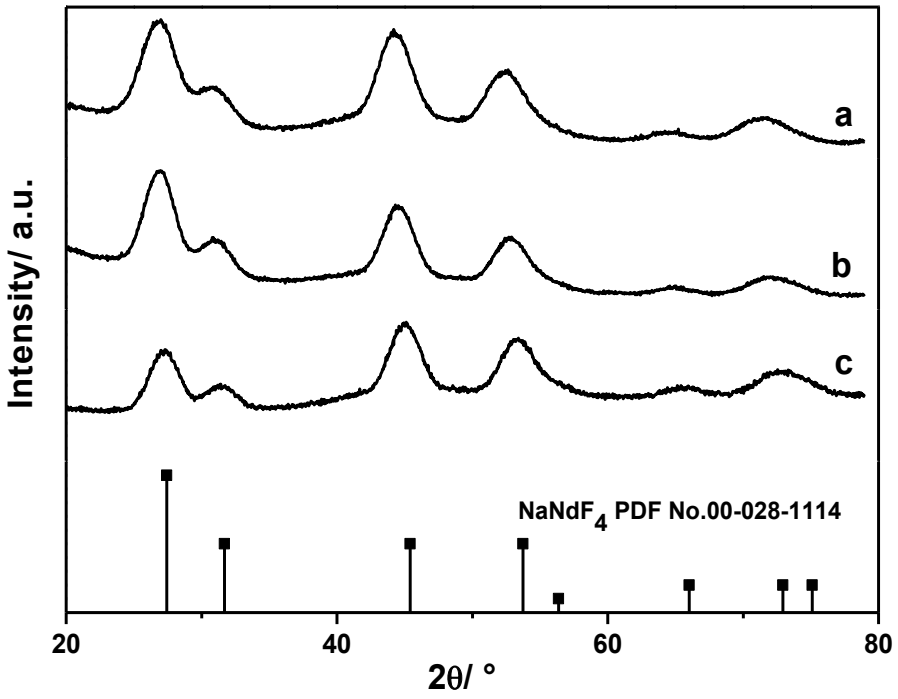

Figure 3.8: XRD data of sub-10 nm nanocrystals, prepared by the reaction of rare earth oleates with excess sodium fluoride in oleylamine/oleic acid/octadecene at 200 °C for 60 min. a) $NaCeF_4$, b) $NaPrF_4$ and c) $NaNdF_4$. In all cases, the cubic α-phase is obtained, even for $NaCeF_4$.

We expected that heating of the α-phase particles in oleic acid/octadecene solvent would lead to Ostwald ripening until particles of the hexagonal β-phase nucleate in solution, as in the case of $NaYF_4$: Yb,Er, $NaSmF_4$, $NaEuF_4$, $NaGdF_4$ and $NaTbF_4$ [224]. The resulting binary mixture of α- and β-phase particles should then show the aforementioned growth behaviour, that is, complete dissolution of all α-phases particles along with fast particle growth and focusing of the size distribution of the β-phase particles [226]. The particles of α- $NaCeF_4$, α-$NaPrF_4$ and α-$NaNdF_4$, however, behave

differently. The TEM images of **Figure 3.9** and the XRD data of **Figure 3.10** show that heating of the purified α- phase particles to 320 °C in oleic acid/octadecene leads mainly to decomposition into lanthanide trifluoride particles. As precipitation of NaF is not observed, we may write as eq. 3.2

$$\alpha\text{-}NaREF_4 \text{ particle } + \text{H-OA} \rightarrow REF_3 \text{ particle} + \text{Na-OA } + \text{HF} \qquad (3.2)$$

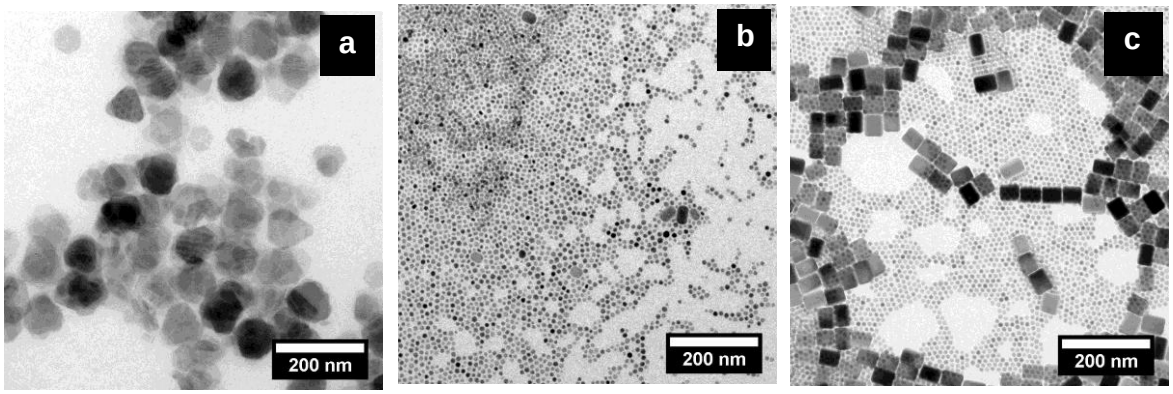

Figure 3.9: TEM images of products obtained by heating (a) α-$NaCeF_4$, (b) α-$NaPrF_4$ and (c) α-$NaNdF_4$ nanocrystals in oleic acid/octadecene at 320 °C for 60 min.

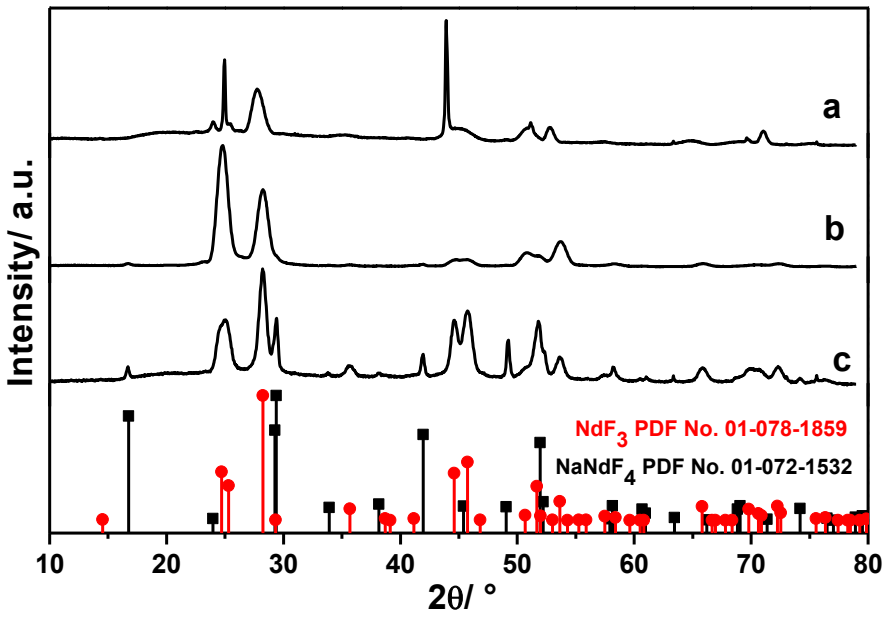

Figure 3.10: XRD data of sub-10nm nanocrystals of the cubic α-phase, after heating in oleic acid/octadecene at 320 °C for 60 min. The data for a) α-$NaCeF_4$, b) α-$NaPrF_4$ and c) α-$NaNdF_4$ indicate complete decomposition into the corresponding lanthanide trifluorides in the case of α-$NaCeF_4$, almost complete decomposition in the case of α-$NaPrF_4$ and partial decomposition in the case of α-$NaNdF_4$.

Complete decomposition is observed for cerium, whereas, in the case of praseodymium, a very small number of β-$NaPrF_4$ particles can be detected among the vast majority of

PrF_3 particles. In the case of α-$NaNdF_4$, partial decomposition is observed, leading to a mixture of small NdF_3 particles and a significant amount of large β-$NaNdF_4$ particles:

α -$NaNdF_4$ (particles) + (1-x) H-OA⟶

$$(1\text{-}x)\ NdF_3 \text{ particles} + x\ \beta\text{-}NaNdF_4 \text{ particles} + (1\text{-}x)\ \text{Na-OA} + (1\text{-}x)\ \text{HF} \qquad (3.3)$$

Note that the large particles of hexagonal phase $NaNdF_4$ in fact display the expected narrow size distribution (Figure 3.9c).

The low stability of the α-$NaCeF_4$ and α-$NaPrF_4$ particles is not unexpected, as the α-phase is missing in the phase diagram of bulk $NaCeF_4$, indicating that bulk α-$NaCeF_4$ is thermodynamically instable [178]. In the case of bulk $NaPrF_4$, the α-phase exists, but only within a narrow range of compositions. For all lanthanides for which the α-phase of $NaREF_4$ exists, the phase is thermodynamically stable only at high temperatures and for sodium-deficient compositions $Na_{1-x}REF_{4-x}$. We therefore investigated the Na/RE ratio of our α-phase materials by X-ray fluorescence analysis (XRF). In the case of nanocrystals, the analysis of the Na/RE ratio is hampered by the fact that the ligand shell of the particles can contain some sodium oleate that cannot be washed off without negatively affecting the dispersibility of the particles. Nevertheless, the Na/RE value of all three cubic materials is significantly smaller than 1 (between 0.3 and 0.5) and 2-3 times lower compared to the corresponding β-phase particles. The high sodium deficiency of the α-phase particles is surprising, as these particles are prepared in the presence of a 6-fold excess of sodium ions (refer to the Experimental Section). In the acidic oleic acid/octadecene solvent mixture, the sodium ions are obviously not easily incorporated into the $Na_{1-x}REF_{4-x}$ lattice, at least not in case of the larger RE-ions, La, Ce, Pr, and Nd. Consequently, only partial conversion to the β-phase is possible.

$$\alpha\text{-}Na_{1-x}REF_{4-x} \rightarrow (1 - x)\ \beta\text{-}NaREF_4 + x\ REF_3 \qquad (3.4)$$

The absence of β-phase particles in figure 3.9a and b indicates, however, that the sodium released by the sodium deficient α-phase particles of $NaCeF_4$ and $NaPrF_4$ is not even sufficient to form any significant number of β-phase particles. We therefore investigated the conversion of the α-phase particles in the presence of additional sodium fluoride in the solvent, since an excess of sodium and fluoride should favour the formation of the reactants on the left-hand side of the reaction 3.4. Thus, α-phase particles of $NaCeF_4$, $NaPrF_4$ or $NaNdF_4$ were redispersed in oleic acid/octadecene, freshly prepared NaF was

added, and the mixture was heated to 320 °C as above. As shown by the XRD data in **Figure 3.11**, complete conversion of the α-phase to the β-phase occurs. TEM images and particle size histograms of the resulting particles are shown in **Figure 3.12**. In all cases, phase-pure β-phase particles with a fairly narrow size distribution are obtained. This result shows how strongly the formation of β-$NaREF_4$ particles is affected by the exchange of sodium ions between the crystal lattice of the particles and the acidic oleic acid/octadecene solvent. In addition, the procedure represents a convenient method to prepare $NaCeF_4$, $NaPrF_4$ or $NaNdF_4$ particles with larger sizes than the sub-10 nm particles shown in figure 3.1.

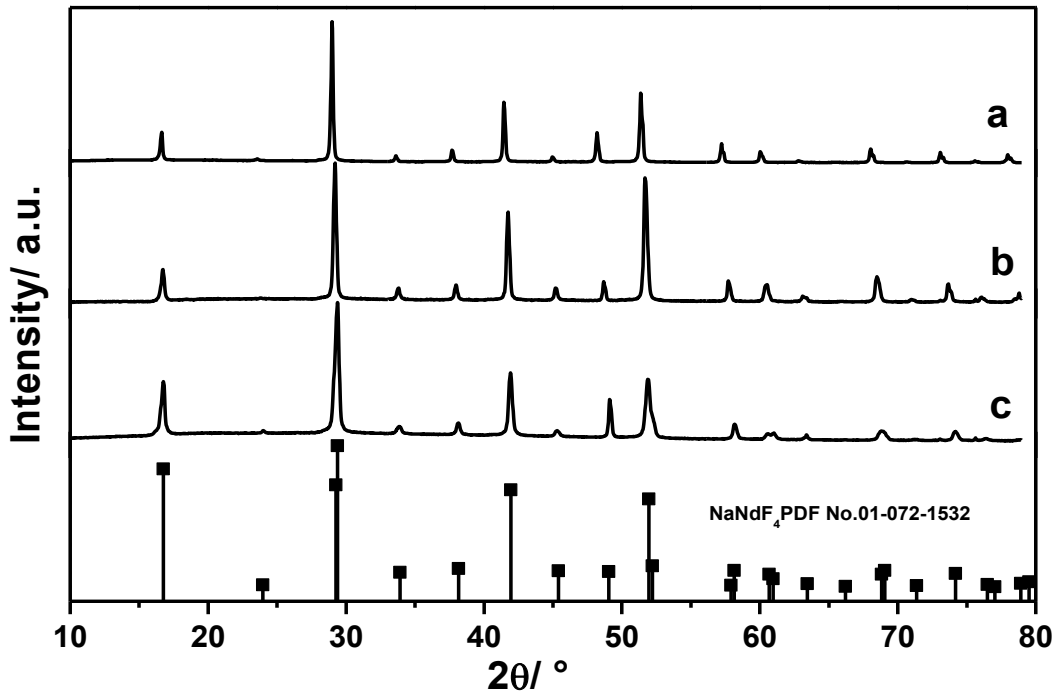

Figure 3.11: XRD data of a) β-$NaCeF_4$, b) β-$NaPrF_4$ and c) β-$NaNdF_4$ obtained by heating sub-10 nm nanocrystals of α-$NaCeF_4$, α-$NaPrF_4$ and α-$NaNdF_4$, respectively, in the presence of sodium fluoride at 320 °C in oleic acid/octadecene for 60 min. The data indicate complete conversion to the α-phase without decomposition into lanthanide trifluorides.

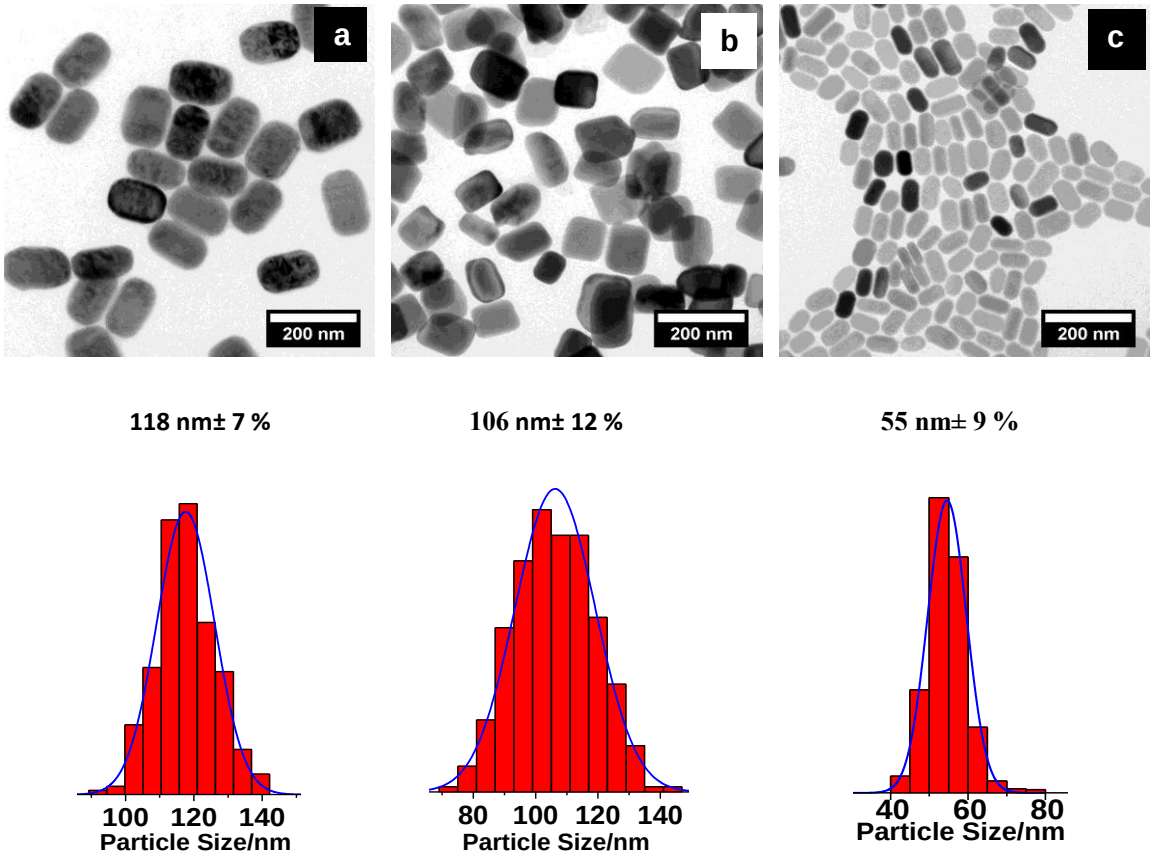

Figure 3.12: TEM images and corresponding particle size histograms of a) β-$NaCeF_4$, b) β-$NaPrF_4$ and c) β-$NaNdF_4$ obtained by heating sub-10 nm nanocrystals of α-$NaCeF_4$, α-$NaPrF_4$ and α-$NaNdF_4$, respectively, in the presence of sodium fluoride in oleic acid/octadecene at 320 °C for 60 min. Values for the mean particle diameter and the relative standard deviation (in %) are given in the histograms. The blue solid lines indicate Gaussian fits.

Nanocrystals of $NaLaF_4$ are very suitable host materials for luminescent rare earth ions such as Ce^{3+}, Pr^{3+} and Nd^{3+} since they have similar ionic radii. Materials doped with $Pr^{3+}$and Nd^{3+} may be used as scintillators [189, 190] and lamp phosphors [191]. In several host materials, Pr^{3+} shows the phenomenon of quantum cutting. These materials may therefore be used as spectral convertor for improving the efficiency of solar cells [79, 78]. Materials doped with, Ce^{3+}/Tb^{3+} are also well established and are used for phosphor applications [80].

To demonstrate the versatility of our new synthesis procedure, we synthesised Ce^{3+} and Pr^{3+} doped β-$NaLaF_4$ as well as Ce^{3+}/Tb^{3+} doped $NaCeF_4$ nanocrystals and characterized them in detail. Nearly monodisperse particles with sizes ranging from 5-8 nm are obtained, as is evident from the TEM images, which are shown in **Figure 3.13**. The XRD pattern corresponding nanocrystals are shown in **Figure 3.14**.

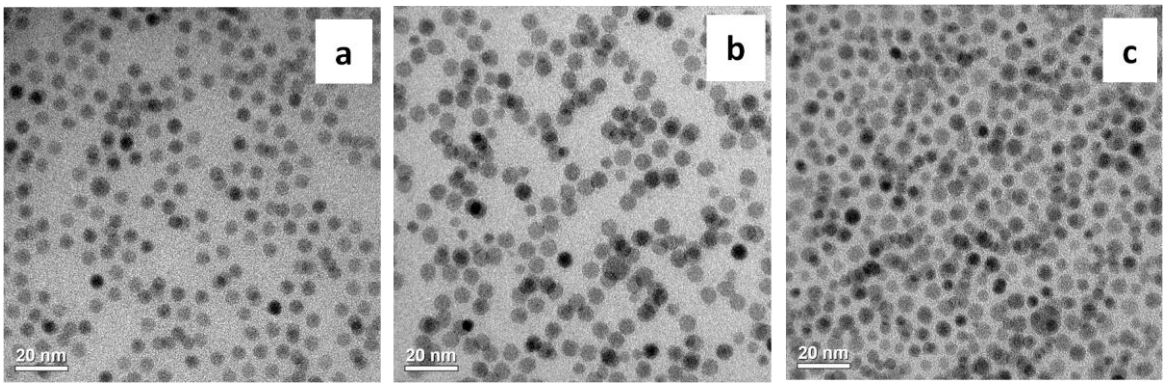

Figure 3.13: TEM images of a) β-$NaLaF_4$:Ce b) β-$NaLaF_4$:Pr and c) β-$NaCeF_4$:Tb nanocrystals prepared by the reaction of the metal oleates with ammonium fluoride in oleylamine/oleic acid/octadecene at 290 °C for 60 min.

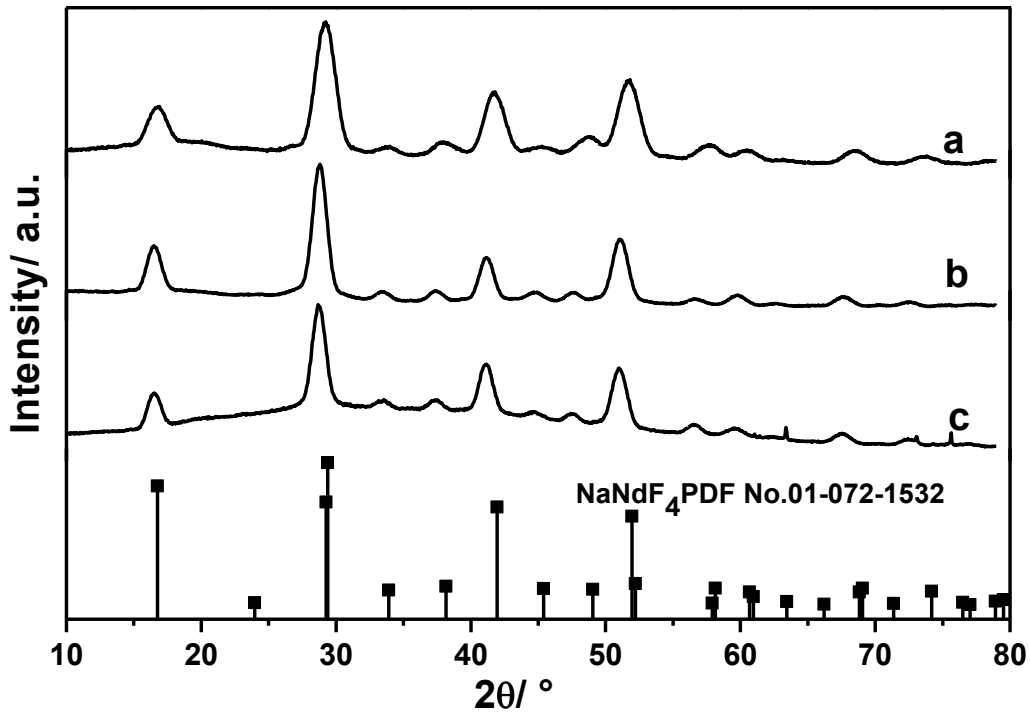

Figure 3.14: XRD data of a) β-$NaCeF_4$:Tb b) β-$NaLaF_4$:Pr and c) β-$NaLaF_4$:Ce nanocrystals prepared by the reaction of the metal oleates with ammonium fluoride in oleylamine/oleic acid/octadecene at 290 °C for 60 min. In all cases the XRD data are in accord with the hexagonal phase of $NaREF_4$.

The optical properties of these RE^{3+} doped $NaLaF_4$ nanocrystals (dispersed in hexane, 1 wt %) were examined using UV-vis absorption and fluorescence spectroscopy. The absorption and emission spectrum (excitation at 243 nm), of $NaCeF_4$:Tb (15%) nanocrystals are dispersed in hexane are shown in **Figure 3.15**. The emission peaks at 490, 544, 584 and 622 nm correspond to the $^5D_4$-^7F_j (J = 6, 5, 4, 3) transitions of Tb^{3+}

ions, respectively. The broad and weak emission band between 290 and 350 nm is due to the d-f transition of Ce^{3+}. Excitation with 254 nm UV light results in clearly visible bright green luminescence, which is consistent with the emission spectrum shown as the most intense peak at 545 nm of the colloidal solution (see digital photograph provided in the inset of the figure). The photoluminescence quantum yield of the sample was measured by comparing the emission intensity with that of the standard Rhodamine 6G dye. For measuring the emission spectra of the samples, the optical density of both, the colloidal dispersion of the nanocrystals and the solution of the dye, was adjusted to 0.1 at the excitation wavelength of 277 nm and all other parameters such as slit width, integration time and step size were kept constant. We obtained a quantum yield of 30%, which is considerably lower than for $CePO_4$:Tb/$LaPO_4$ core/shell nanocrystals (80%) [192]. Of course one should keep in mind that core/shell system displaying enhanced the quantum yield as the optically inactive shell provides passivation of the optically active particle core, which helps to decrease the energy losses on the particle surface. Probably also the quantum yield of these fluoride NCs can be enhanced by forming an optically inactive shell, for instance of $NaLaF_4$ on the optically active $NaCeF_4$:Tb core particles.

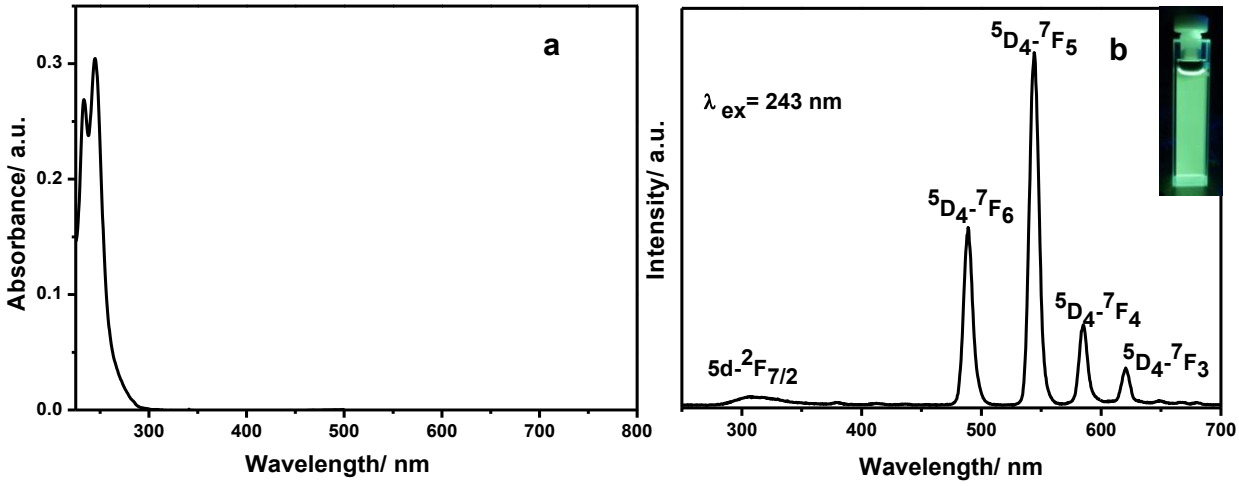

Figure 3.15: Absorption (a) and luminescence emission (b) spectra of $NaCeF_4$:Tb nanocrystals dispersed in hexane (the inset photo shows the green luminescence from the sample).

The excitation and emission spectra of Ce^{3+} doped (5%) $NaLaF_4$ nanocrystals dispersed in hexane were also measured, and the corresponding spectra are shown in **Figure 3.16**. Excitation spectrum recorded at the emission of 310 nm confirms successful doping of

Ce^{3+} into the $NaLaF_4$ matrix as the broad peak observed corresponds to the $^7F_{7/2}$-5d transition of Ce^{3+} . The emission spectrum recorded under 243 nm excitation, consists of a broad peak with maxima at 310 nm as a result of the radiative transition from the 5d state to the $^2F_{7/2}$ level, as already observed for the co-doped sample.

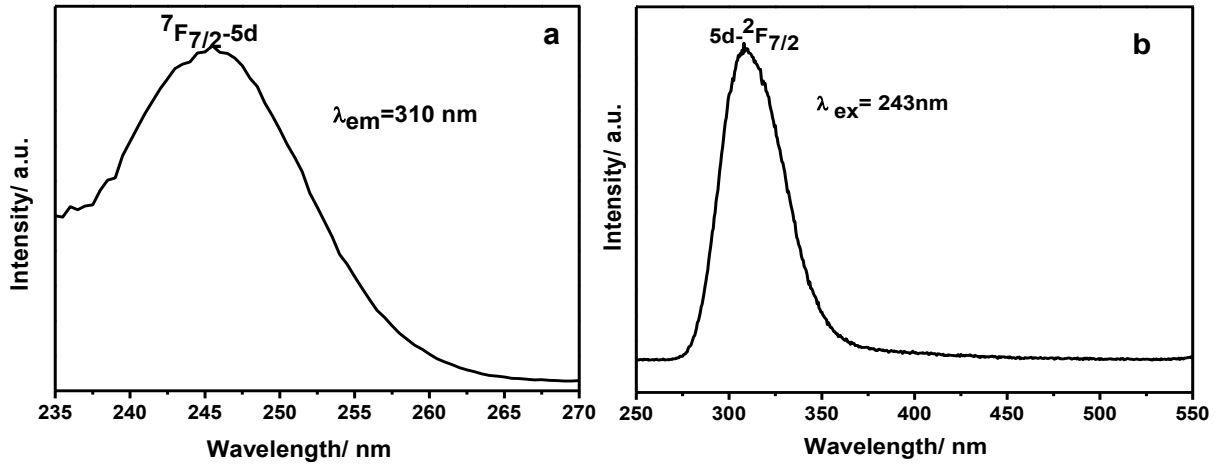

Figure 3.16: Excitation (a) and luminescence emission (b) spectra of $NaLaF_4$: Ce nanocrystals.

Figure 3.17 displays luminescence excitation (λ_{em} = 606 nm) and emission (λ_{ex} = 443 nm) of the 1% Pr^{3+} doped $NaLaF_4$. Excitation at an emission wavelength of 606 nm results in transition from ground state term ^3H to different ^3P excited state levels which are indexed in the spectrum. The emission spectrum consists of several narrow lines in the visible region 470-750 nm and these lines correspond to transitions from the $^3P_0$ and $^1D_2$ levels to the various ^3H and ^3F levels.

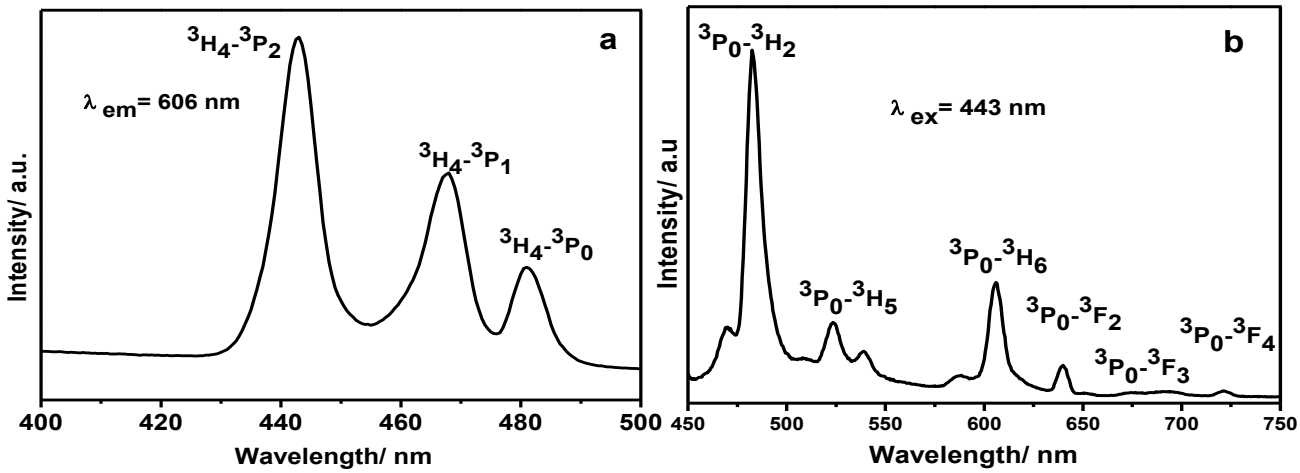

Figure 3.17: Excitation (a) and luminescence emission (b) spectra of $NaLaF_4$: Pr nanocrystals.

3.4. Conclusions

We have investigated the synthesis and Ostwald ripening of $NaLaF_4$, $NaCeF_4$, $NaPrF_4$ and $NaNdF_4$ nanocrystals in oleic acid based solvent mixtures. Sub-10 nm particles of the hexagonal β-phase can be prepared for all four compounds by the reaction of the corresponding metal oleates with ammonium fluoride in oleylamine/oleic acid/octadecene mixtures. In the presence of oleylamine, Ostwald ripening of the particles is very slow. In the absence of oleylamine, that is, when the particles are redispersed and heated in the more acidic oleic acid/octadecene solvent, broadening of the size distribution due to Ostwald ripening takes place in the case of $NaCeF_4$, $NaPrF_4$, and $NaNdF_4$, whereas decomposition to LaF_3 is observed for $NaLaF_4$. Decomposition to the trifluorides is also observed when sub-10 nm particles of the cubic α-phase of $NaNdF_4$, $NaPrF_4$ and $NaCeF_4$ are heated in oleic acid/octadecene solvent. Only in the case of α-$NaNdF_4$, a significant amount of nearly monodisperse β-$NaNdF_4$ particles is formed in addition to small NdF_3 particles. This decomposition of the α-phase particles can be suppressed by the addition of sodium fluoride to the acidic solvent mixture. In this case, Ostwald ripening in connection with the α/β-phase transition leads to the formation of larger β-phase particles with a narrow particle size distribution, similar to the heavier lanthanides. Further, the versatility of the developed process has been demonstrated by doping luminescent rare earth ions containing higher radii, particularly Ce^{3+}, Pr^{3+} and Ce^{3+}/Tb^{3+}.These doped nanocrystals show excellent luminescence properties and we believe that the newly developed process to develop these NCs may facilitate its use in various applications.

Chapter 4

Synthesis and Characterisation of Monodisperse Sub-10 nm Highly Sodium Deficient Cubic Sodium Yttrium Fluoride (α-$NaYF_4$) Nanocrystals

4.1. Introduction

An important peculiarity of sodium rare earth fluoride ($NaREF_4$) is their polymorphism, that is, these materials can either crystallize in the cubic α-phase or the hexagonal β-phase. It has been found that the sodium to rare earth ratio plays a crucial role in the synthesis of these phases. For example, in the case of sodium yttrium fluoride ($NaYF_4$), a very suitable host material for upconverting ions [193, 65, 74], and the sodium to yttrium (Na/Y) ratio should be larger than 0.55, to obtain the α-phase. This is in accord with the bulk phase diagram, where the existence of the α-phase below this ratio is not reported [178]. While the upconversion efficiency of α-phase particles is very low compared to particles of the β-phase, the α-phase is very important from a preparative and mechanistic point of view since it has been found that α-phase particles form at low temperatures as an intermediate product during the synthesis of β-phase particles. The α-phase particles convert to the final β-phase particles only at high temperatures present at later stage of the synthesis [107]. In addition, the number of β-phase seeds that nucleate during Ostwald-ripening of the α-phase particles determines the final size of the β-$NaREF_4$ nanoparticles [187, 184]. It has also been reported that the α/β-phase transition is required to obtain β-$NaYF_4$ particles with narrow size distribution, which is necessary to enable their use in many applications [107]. Hence, many researchers have prepared α-phase $NaYF_4$ separately and used them as a single source precursor for the synthesis of β-phase particles [184] as well as for core/shell particles [194].

In chapter 2 we have already shown that α-$NaREF_4$ (RE = Ce, Pr, Nd) nanoparticles can be prepared which are extremely sodium deficient (Na/RE < 0.55). This motivated us to investigate the existence and stability of NCs of highly sodium deficient α-phase $NaYF_4$ which, to be best of our knowledge, has not been reported before. So the focus of the work presented in this chapter is the synthesis of highly sodium deficient α-phase $NaYF_4$ NCs containing Na^+ and Y^{3+} in a ratio of only 0.1 to 0.55. Furthermore, we discuss how

these highly sodium deficient $NaYF_4$ NCs behave in acidic oleic acid/octadecene solvent, as well as their Oswald ripening and decomposition during heating. Also, we discuss the conversion of highly sodium deficient α-phase $NaYF_4$ to β-$NaYF_4$ particles, and measures required to achieve monodisperse NCs. Our synthetic approach yields not only NCs of highly sodium deficient α-phase $NaYF_4$ but also new insights regarding their existence in the nanoscale regime.

4.2. Experimental Section

Synthesis of yttrium oleate (Y-oleate): For the preparation of Y-oleate, ammonium hydroxide solution (25%) was added slowly to a solution of yttrium chloride that was dissolved in distilled water (1 mmol/1 mL) until no further yttrium hydroxide precipitated. The precipitate was collected by centrifugation and washed with 2M ammonium hydroxide solution until it was free of chloride ions. A standard silver nitrate test was conducted to check the presence of chloride ions. Then a final washing step was conducted with acetone and the precipitate was dried at 80 °C for 2 h. Thereafter, the yttrium hydroxide was dissolved in oleic acid under vacuum at 100 °C on Schlenk line. For 1 mmol of yttrium hydroxide, 6 mL of oleic acid was used and the resulting stock solution of Y-oleate was used in the further reactions.

Synthesis of highly sodium deficient cubic α-$NaYF_4$ nanocrystals: Na-oleate and Y-oleate were dissolved in equal amounts of oleic acid and octadecene (5 ml of each solvent for 1 mmol of Y-oleate). Different amounts of Na-oleate were added in order to vary the Na/Y ratio between 0.1 to 0.55 mmol. The reaction mixture was connected to a Schlenk line apparatus and degassed under vacuum at 100 °C for 60 min. After degassing, ammonium fluoride was added to the solution under nitrogen flow. The amount of NH_4F was chosen such that all Na and Y ions in the system were converted to metal fluorides. Immediately after the addition of NH_4F, the system was cycled three times between vacuum and N_2, applying vacuum for only 5 s in each cycle. The temperature was increased to 240 °C and the reaction mixture was further heated for 60 min under N_2 atmosphere with stirring. After natural cooling to room temperature, the particles were precipitated by the addition of an equal volume of ethanol. Subsequently, the precipitated particles were easily collected by centrifugation. The particles were purified by re-dispersing in hexane (3 mL for 1 mmol) followed by precipitation with ethanol and separation by centrifugation. The purified particles were dried at 80 °C for

14 h in an oven. Five sets of highly sodium deficient cubic α-$NaYF_4$ (Na/Y = 0.1 to 0.55) particles were prepared using an amount of Na-oleate corresponds to 10, 20, 30, 40 and 55% of yttrium oleate respectively.

Synthesis of hexagonal β-$NaYF_4$ nanocrystals: The highly sodium deficient NCs prepared as given above were used as precursors for the preparation of hexagonal β-$NaYF_4$ NCs. For that, equal molar ratios of cubic α-$NaYF_4$, Na-oleate and ammonium fluoride were dissolved in oleic acid and octadecene, and degassed under vacuum at 100 °C for 60 min at a Schlenk line setup. Then, the reaction mixture was heated to 300 °C under N_2 atmosphere under stirring and kept at this temperature for 80 min. Then the solution was cooled down to room temperature and was precipitated by the addition of an equal volume of ethanol. The particles were collected and purified as described above.

4.3. Result and Discussion

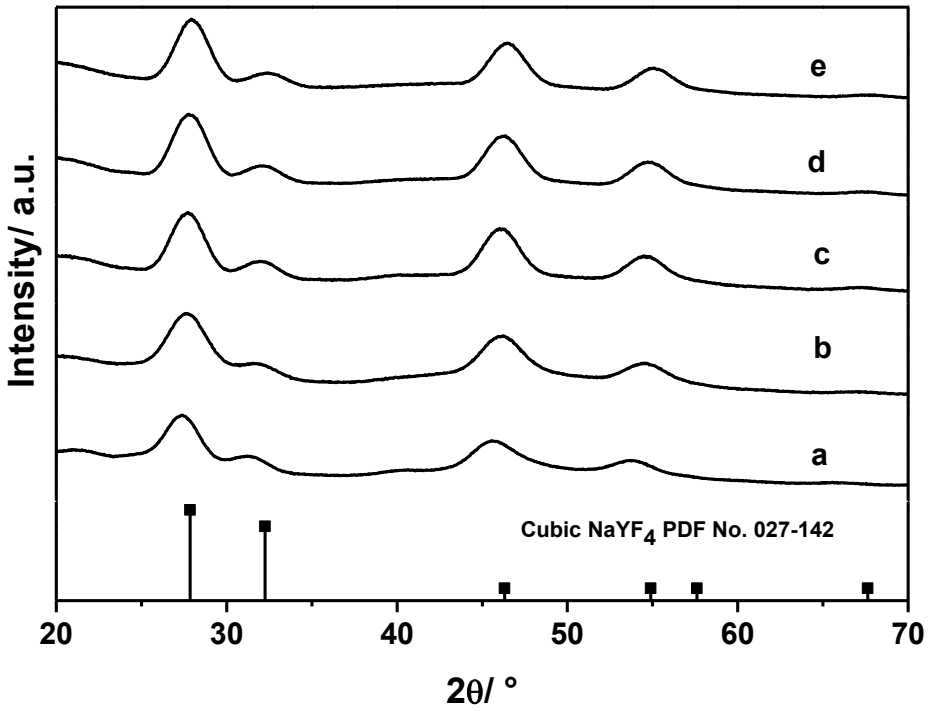

Figure 4.1: XRD data of sodium deficient α-$NaYF_4$ nanocrystals prepared by heating sodium oleate, yttrium oleate and ammonium fluoride in oleic acid and octadecene at 240 °C for 60 min. Different amounts of Na-oleate were used in the synthesis resulting in Na/Y ratios of a) 0.1, b) 0.2, c) 0.3, d) 0.4 and e) 0.55. The diffraction peaks of all the samples are well indexed with the cubic phase of α-$NaYF_4$.

The crystal structure of the as-prepared highly sodium deficient α-$NaYF_4$ NCs was determined by XRD and the corresponding diffractograms are shown in **Figure 4.1**. The diffraction peaks for all five samples (Na/Y ratio between 0.1 and 0.55) are well indexed with the cubic phase of α-$NaYF_4$ [PDF no. 027-0142], which indicates that α-phase $NaYF_4$ with extremely low sodium content have been successfully synthesised. Presumably, the particles obtained are a kinetic product because α-$NaYF_4$ with such low sodium content is not known from the thermodynamic phase diagram.

The broad XRD peaks indicate a very small size of the synthesized particles and the TEM images shown in **Figure 4.2** are well in accord with this observation. As we can see from the micrographs very small $NaYF_4$particles are obtained and the size histogram derived from the TEM images confirm that the average size of particles is in the range of ~ 3-4 nm.

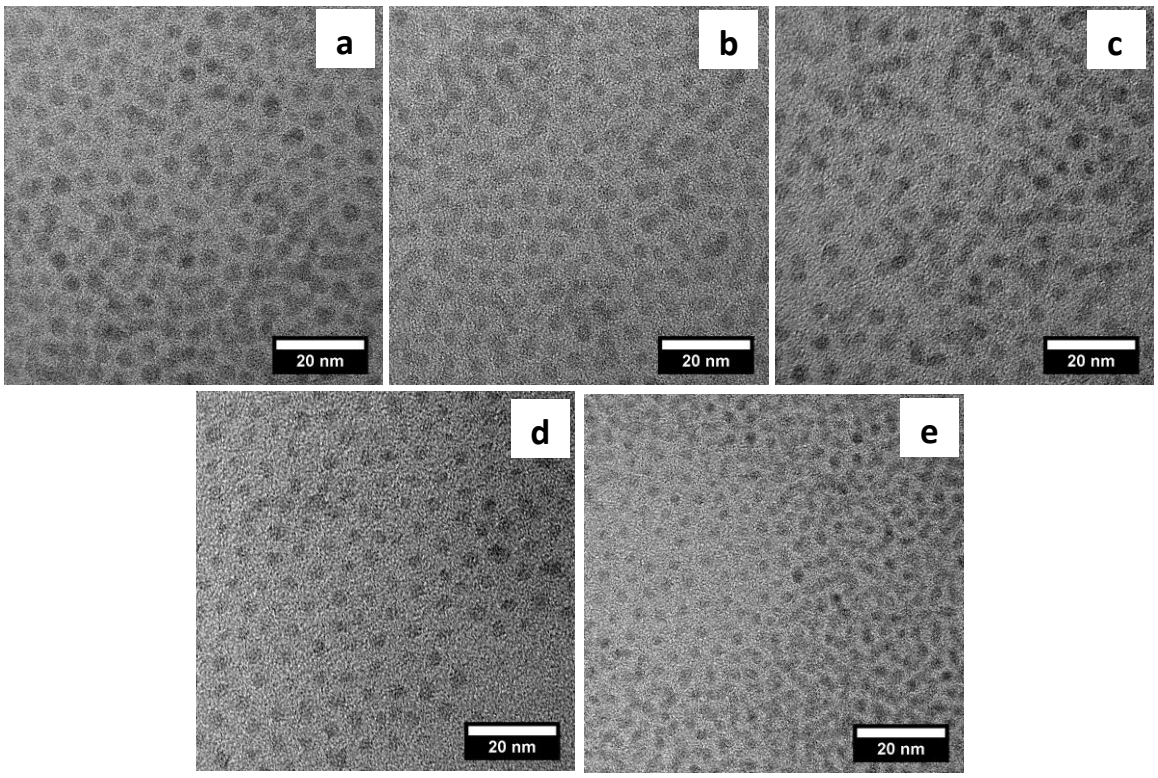

Figure 4.2: TEM images of sodium deficient α-$NaYF_4$ nanocrystals prepared by heating sodium oleate, yttrium oleate and ammonium fluoride in oleic acid and octadecene at 240 °C for 60 min. Different amounts of Na-oleate were used in the synthesis resulting in Na/Y ratios of a) 0.1, b) 0.2, c) 0.3, d) 0.4 and e) 0.55.

The elemental composition of all samples was determined by XRF. All samples were washed three times before the analysis. The Na/Y ratio determined by XRF is plotted in **Figure 4.3** against the Na/Y ratio employed in the synthesis of the α-$NaYF_4$ NCs. The

Na/Y ratios obtained from the XRF analysis are in good agreement with the ratios used in the reactions. The XRF analysis therefore proves the high sodium deficiency of the synthesised α-$NaYF_4$ NCs.

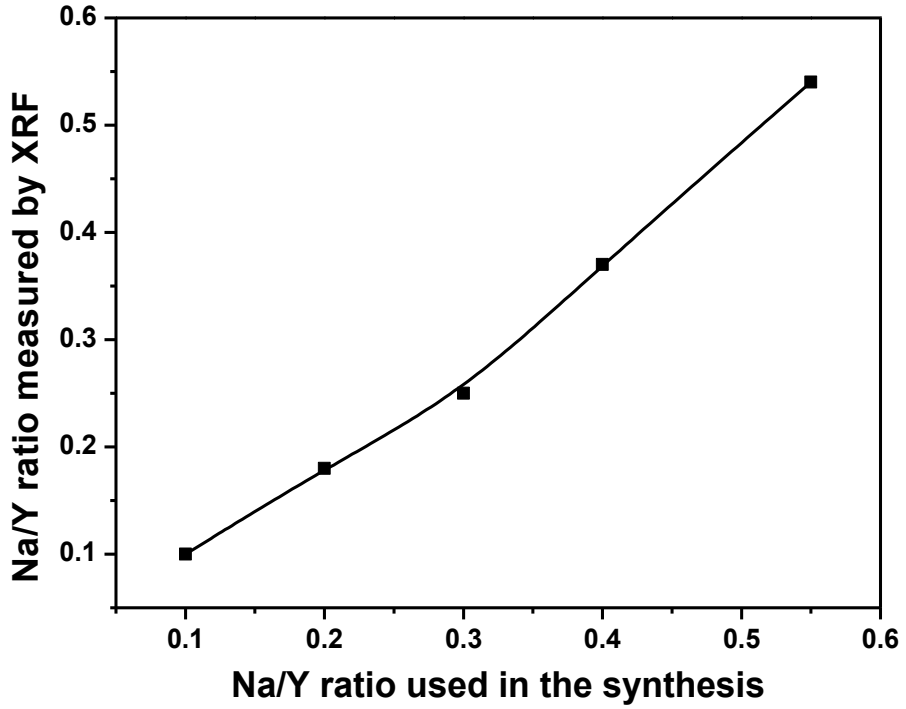

Figure 4.3: XRF data of sodium deficient α-$NaYF_4$ nanocrystals prepared by the reaction of sodium oleate, yttrium oleate and ammonium fluoride in oleic acid and octadecene at 240 °C for 60 min. The Na/Y ratio measured by XRF is plotted against the ratio of Na-oleate and Y-oleate used in the synthesis.

We have studied the growth behavior of these sodium deficient α-$NaYF_4$ NCs by heating (300 °C for 60 min) of the redispersed particles in oleic acid/octadecene solvent. The XRD patterns of the resulting products are shown in **Figure 4.4**. The diffractogram reveals that the NCs with the lowest Na/Y ratios of 0.1 and 0.2 partially decompose to yttrium trifluoride (YF_3) during heating (Figure 4.4a and b). The α-$NaYF_4$ with higher Na/Y ratios of 0.3, 0.4 and 0.55 remain α-phase particles but grow in size, as is evident from the decreased peak width compared to figure 4.1. The heating experiments therefore show that the α-$NaYF_4$ NCs with mild Na-deficiency, i.e. Na/Y ratio=0.3 and 0.4 are stable in acidic condition, whereas the other two samples with extremely high Na-deficiency of Na/Y=0.1 and 0.2 undergo partial decomposition at high temperatures. The decomposition of these particles may be represented by the equation (eq. 4.1).

$$\alpha\text{-}Na_{1-x}YF_{4-x} \rightarrow x\,YF_3 + (1-x)\,\alpha\text{-}NaYF_4 \qquad (4.1)$$

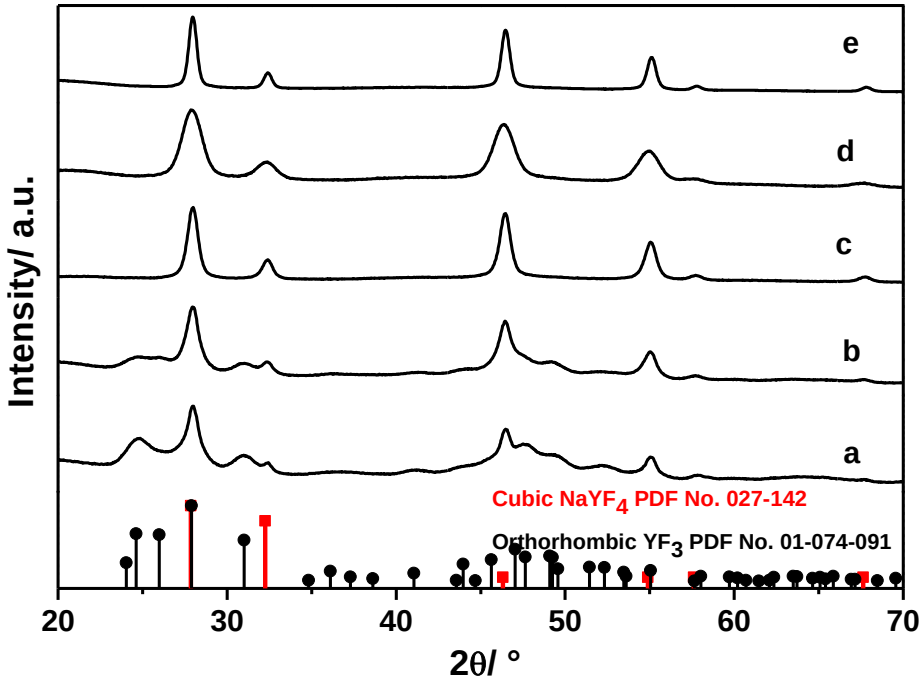

Figure 4.4: XRD data of product particles obtained after heating sodium deficient cubic α-$NaYF_4$ nanocrystals in oleic acid and octadecene at 300 °C for 60 min. Particles with Na/Y ratio of 0.1 (a) and 0.2 (b) undergo partial decomposition into orthorhombic YF_3 while particles with Na/Y ratio of 0.3 (c), 0.4 (d) and 0.55 (e) retain the cubic crystal structure but undergo Ostwald ripening.

The corresponding TEM images are shown in **Figure 4.5**. The partial decomposition to YF_3 (Figure 4.5a and b) observed for particles with Na/Y ratios of 0.1 and 0.2 is well supported by the TEM images because the particles with bipyramidal shape can be assigned to orthorhombic YF_3 and the round shaped particles to remaining cubic α-$NaYF_4$. Compared to the TEM images of the parent particles given in figure 4.2, the particles are larger in size and display a broader size distribution. This indicates that the particles grow in the acidic solvent mixture by Ostwald ripening (Figure 4.5c to e). The narrow XRD peaks in figure 4.4, compared to those of the parent particles (refer Figure 4.1), are also in accord with the particle growth during heat treatment.

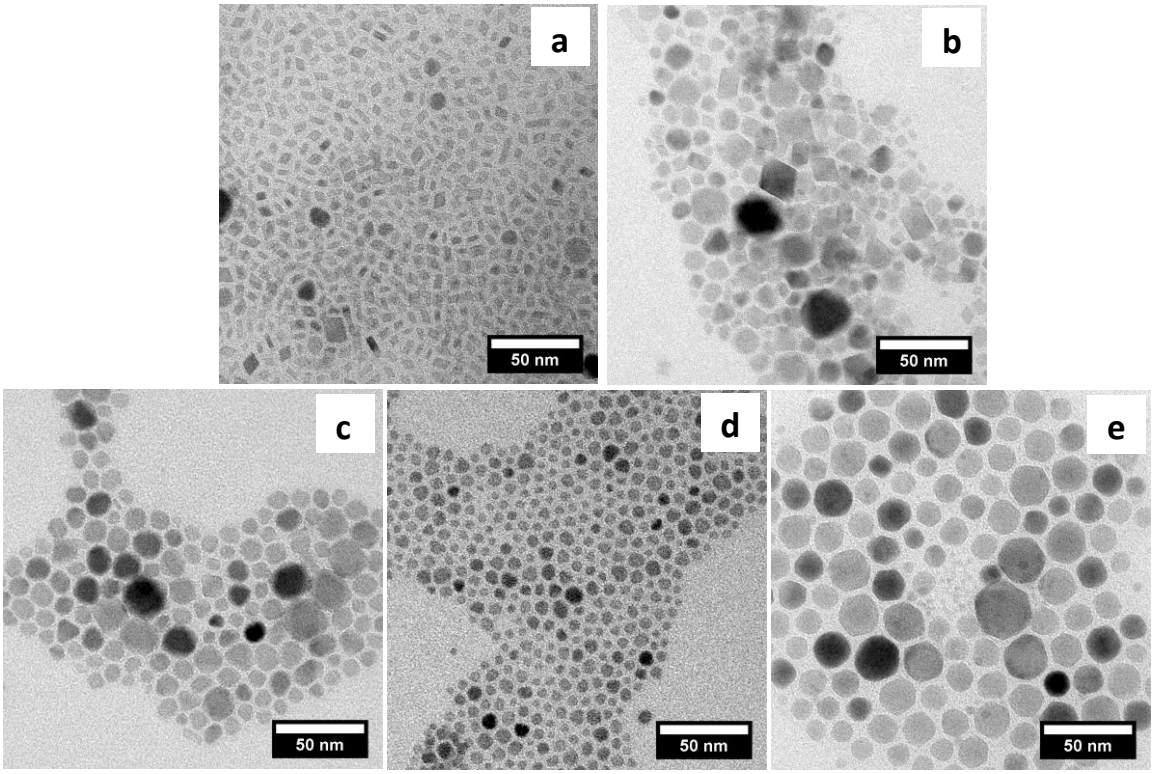

Figure 4.5: TEM images of product particles obtained after heating of sodium deficient cubic α-$NaYF_4$ nanocrystals in oleic acid and octadecene at 300 °C for 60 min. The Na/Y ratio used in the synthesis of sodium deficient α-$NaYF_4$ particles was a) 0.1, b) 0.2, c) 0.3, d) 0.4 and e) 0.55. Micrographs of a and b show bipyramidal shaped YF_3 and round shaped cubic α-$NaYF_4$, whereas c, d and e display round shaped α-$NaYF_4$ nanocrystals.

Interestingly, none of the Na-deficient cubic phase α-$NaYF_4$ NCs convert to the hexagonal β-phase. This observation is well in accord with the literature as only α-$NaYF_4$ particles containing sufficient sodium (Na/Y ratio of 1 or higher) undergo the cubic to hexagonal phase transition whereas sodium deficient [α-$Na_5Y_9F_{32}$ (Na/Y=0.55)] particles do not [195].

We find, however, that the transformation of α-phase to β-phase particles can be achieved even for highly sodium deficient α-$NaYF_4$ NCs by supplying additional sodium and fluoride ions during the conversion. By our new approach we successfully synthesised monodisperse hexagonal β-$NaYF_4$ NCs by adding equimolar amounts (1:1) of Na-oleate and NH_4F to the colloidal solution of redispersed sodium-deficient α-$NaYF_4$ particles and heating this mixture in oleic acid and octadecene at 300 °C for 60 min. The XRD patterns of the products obtained are shown in **Figure 4.6**, and all the diffraction peaks are well indexed with the hexagonal β-$NaYF_4$ crystal structure [PDF No: 016-0334]. The addition of extra sodium and fluoride ions compensate the deficiencies of the

α-phase nanocrystals and allow to form monodisperse hexagonal β-phase particles. This can be represented by the equation 4.2.

$$\alpha\text{-}Na_{1-x}YF_{4-x} + x\,Na^{+} + x\,F^{-} \rightarrow \beta\text{-}NaYF_4 \qquad (4.2)$$

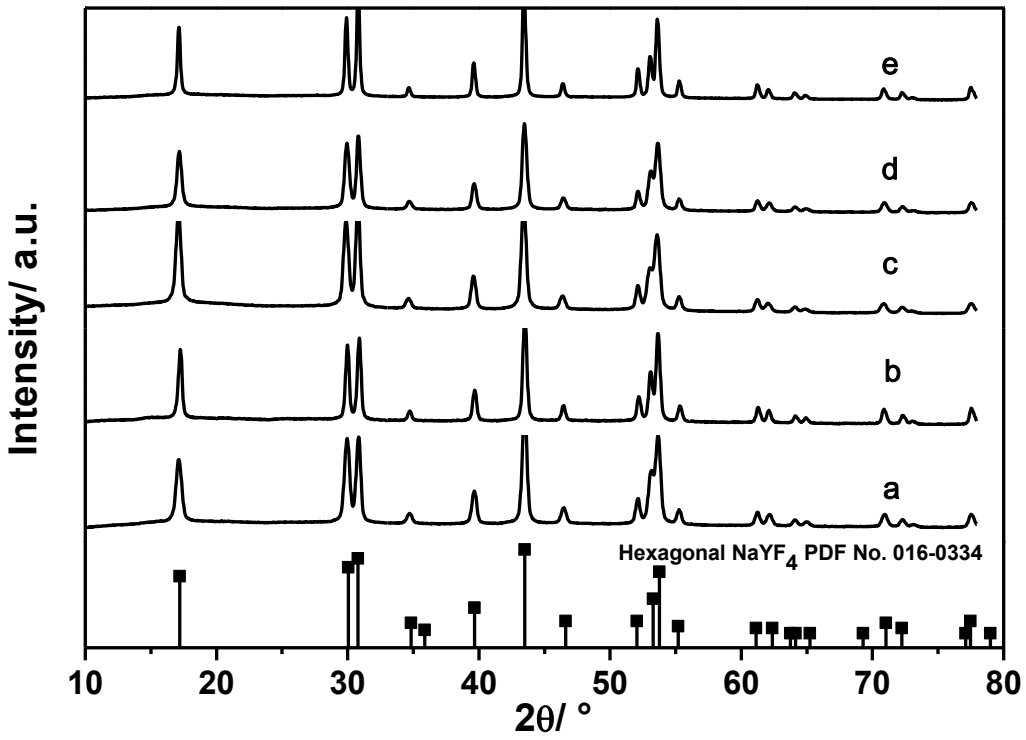

Figure 4.6: XRD data of hexagonal β-$NaYF_4$ nanocrystals obtained after heating sodium deficient cubic α-$NaYF_4$ nanocrystals in the presence of additional Na-oleate and ammonium fluoride in oleic acid and octadecene at 300 °C for 80 min. The Na/Y ratio used in the synthesis of sodium deficient α-$NaYF_4$ nanocrystals was a) 0.1, b) 0.2, c) 0.3, d) 0.4 and e) 0.55 the Na/Y ratio of a) 0.1, b) 0.2, c) 0.3, d) 0.4 and e) 0.55.

The narrow size distribution of the β-phase NCs is clearly visible in their TEM images, which are presented in **Figure 4.7**. The particles display a well-defined elongated morphology. The average particle size and the size histograms of these NCs were calculated from TEM images, and are also shown in figure 4.7. The higher concentration of dissociated sodium and fluoride ions seem to interact differently with the different facets of the nanocrystals, resulting in fast growth in c-direction and an elongated morphology.

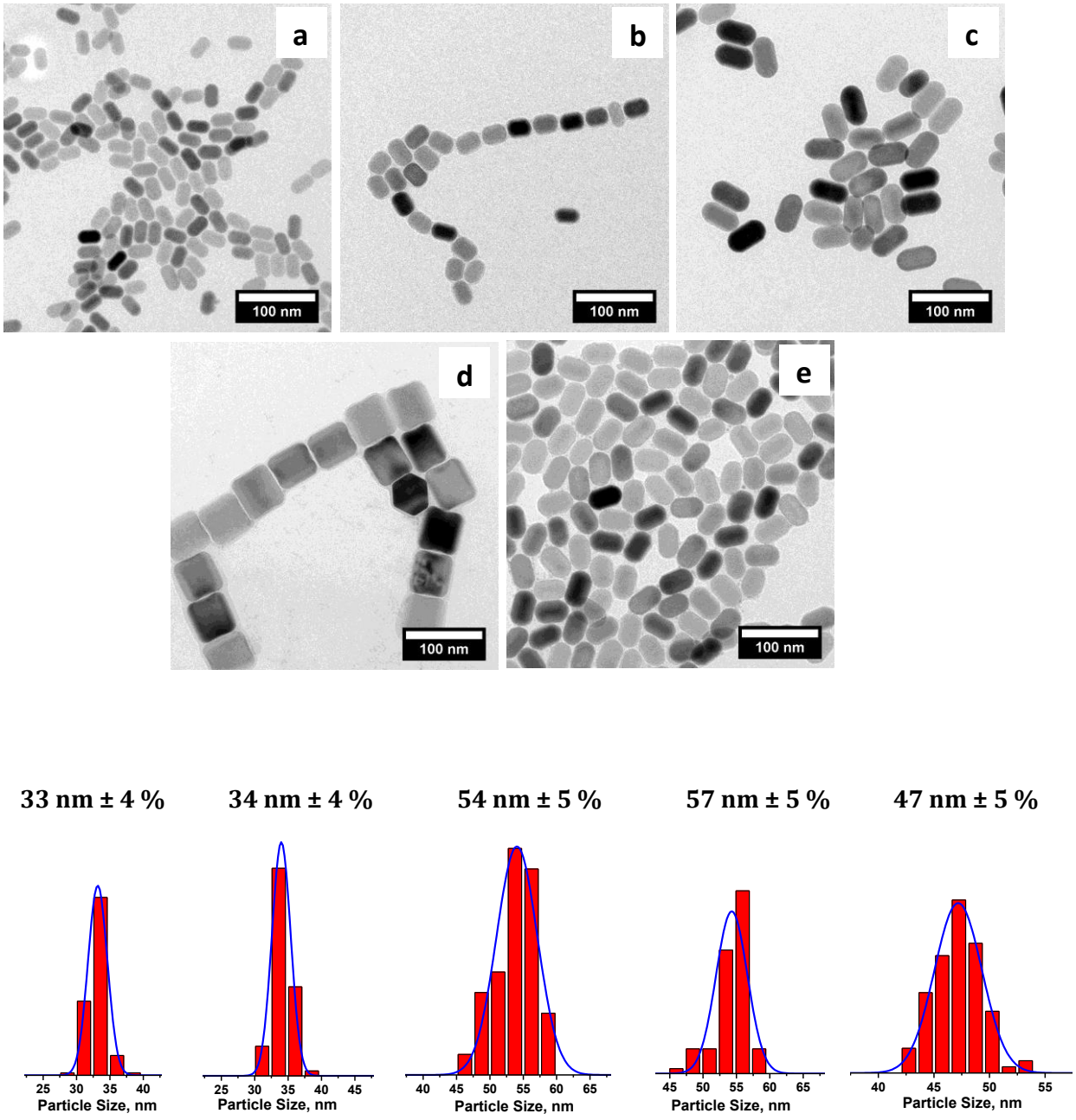

Figure 4.7: TEM images of hexagonal β-$NaYF_4$ nanocrystals obtained after heating of sodium deficient cubic α-$NaYF_4$ nanocrystals in the presence of additional Na-oleate and ammonium fluoride in oleic acid and octadecene at 300 °C for 80 min. The Na/Y ratio used in the synthesis of sodium deficient α-$NaYF_4$ nanocrystals was a) 0.1, b) 0.2, c) 0.3, d) 0.4 and e) 0.55. Values for the mean particle size and the relative standard deviation (in %) are given in the histograms. The blue solid lines indicate Gaussian fits.

4.4. Conclusions

In conclusion, we have successfully synthesised sub-5 nm α-$Na_{1-x}YF_{4-x}$ particles with extremely low sodium content not known from bulk material. Our results show that the ratios of Na/Y in α-$NaYF_4$ nanocrystals have a strong influence on the growth behaviour of the particles in acidic OA/ODE solvent. In all cases Ostwald ripening of the α-$NaYF_4$

particles is observed but this is accompanied by partial decomposition into yttrium trifluoride for the particles with very low Na/Y ratio. Additional supply of sodium as sodium oleate to highly sodium deficient α-$NaYF_4$, sub-5 nm, NCs results in α/β-phase transition during heating and the formation of monodisperse β-phase $NaYF_4$ NCs.

Chapter 5

Synthesis and Characterisation of Monodisperse Sub-10 nm Lithium Rare Earth Fluoride ($LiREF_4$, RE = Y, Gd, Lu) Nanocrystals using Highly Sodium Deficient Cubic α-$NaREF_4$ Nanocrystals

5.1. Introduction

Similar to sodium rare earth fluorides ($NaREF_4$), also lithium rare earth fluorides ($LiREF_4$), display low phonon frequencies. In particular $LiYF_4$, $LiGdF_4$ and $LiLuF_4$ are therefore also considered as suitable host materials for luminescent lanthanide (Ln^{3+}) ions [65]. In contrast to $NaREF_4$, however, the crystal structure of $LiREF_4$ exists only in one phase with tetragonal crystal structure. The optical properties of doped lithium yttrium fluoride ($LiYF_4$) have been extensively investigated for different applications. Bulk $LiYF_4$, doped with Yb^{3+}, Nd^{3+} or Pr^{3+} is widely used as solid state laser material [196, 197]. Nd^{3+} or Tm^{3+} doped $LiLuF_4$ is also used for slab/thin-disk lasers [198]. $LiYF_4$ is also a well known host material for quantum cutting ions, whereby one high energy photon is cut into two lower energy photons, resulting in values for quantum yield of 200%. For example, a quantum yield of 168% has been reported for Yb^{3+}, Pr^{3+} doped bulk $LiYF_4$ [199, 200]. Meijerink and co-workers doped red emitting Eu^{3+} into bulk lithium gadolinium fluoride ($LiGdF_4$) and reported a quantum yield of 200% for the quantum cutting process [68]. Another material, Ce^{3+} doped $LiLuF_4$, gained much attention due to its strong emission in the UV spectral region ranging from 305 to 340 nm. The emission of UV-B and UV-A radiations allow this material to be used as light source for photochemical processes as well as the treatment of skin diseases and cosmetic application. $LiYF_4$ bulk phosphors doped with up-converting ions are also investigated extensively by various groups [201].

Owing to these excellent optical properties, several researchers have been synthesizing and investigating its nanocrystalline counterpart. Er^{3+} doped $LiYF_4$ NCs have been synthesised by Mahalingam and co-workers using a thermal decomposition method [123]. The luminescence of the particles can be excited at 1490 nm, an important wavelength for telecommunication purposes, and the particles also display upconversion (UC) emission. They reported a total UC luminescence quantum yield, which is 4 times higher than that of standard hexagonal $NaYF_4$: Yb, Er NCs under 980 nm. In fact, the standard up-converting ions (Yb/Er or Yb/Tm) used for $NaYF_4$ NCs can

also be used for $LiYF_4$ NCs and show comparable luminescence spectra. In addition, $LiYF_4$ engenders enhanced emission in the deep-UV (294 nm) and NIR region (792 nm) when doped with Yb/Tm ions [122, 123, 202]. The $LiYF_4$ UC emission, particularly in the UV region, has gained much interest in life science, especially for photodynamic therapy [203], markers and imaging [204] applications. The NIR to NIR UC emission of these NCs has been used to study the hydrogel degradation in tissues [202]. It has also been reported that the multicolour emission of Eu^{3+}, Ce^{3+} and Tb^{3+} co-doped $LiYF_4$ core/shell NCs is beneficial not only for multicolour labeling but also for display device applications [205]. Analogous to $LiYF_4$, $LiLuF_4$:Yb,Er/Tm core/shell NCs have also been used as nano bio-probes for biomarkers and bio-imaging [204]. These studies indicate that suitable selection of dopants/sensitizers combination in $LiREF_4$ NCs provides nanomaterials for different applications.

There are only very few reports available on the particle size tuning of monodispersed $LiREF_4$ NCs although particles with well defined size are important to enable their use in many applications. Liu and co-workers synthesised lanthanide doped $LiYF_4$ NCs in high temperature solvents using the corresponding metal chlorides and ammonium fluoride [206]. Further, they were able to control the particle size by changing the ratio of fluoride (F^-) to rare earth ions (RE^{3+}). With increasing F^- to RE^{3+} ratio, they observed a decrease in size from 40 to 12 nm. Another research group, Kim and co-workers, employed Eu^{3+} doping for the alteration of particle size, and 10, 30 and 35% of doping resulted in 8, 10 and 68 nm sized particles respectively [205]. For their synthesis in oleic acid and octadecene solvent, they used the corresponding metal oleates and ammonium fluoride as precursor materials. By a solvothermal technique, Ohishi and co-workers prepared 16 nm to 2 μm sized particles with broader size distribution using different amounts of lithium hydroxide (LiOH) in the reaction [207]. By changing the molar ratio of oleic acid and oleylamine in their solvent mixture, Chen and co-workers succeeded in controlling the particle size of $LiYF_4$:Yb,Er NCs which were prepared by thermal decomposition of the corresponding metal trifluoroacetate [203]. As the acidity of the solvent mixture increases, they found that the size of the particles increases from 8 to 47 nm. The same group also developed a strategy based on successive layer-by-layer (LBL) injection of shell precursors for the synthesis of $LiLuF_4$:Ln/$LiLuF_4$ core/shell UCNCs [204].

The limited literature in this regard may be due to the lack of in-depth knowledge of the respective particle formation mechanism. As discussed in chapter 3, the formation of hexagonal β-$NaYF_4$ NCs occurs through the intermediate formation of cubic α-$NaYF_4$ particles, which is also necessary to obtain monodisperse NCs. We mentioned in the beginning of the chapter, however, that bulk $LiYF_4$ crystallizes in no other phase than the tetragonal phase. Murray and coworkers observed, however, that orthorhombic YF_3 NCs are formed as intermediate product when yttrium-90 labeled $LiYF_4$ NCs are synthesised in OA/OED solvent from YCl_3 and LiF as precursors [208].

While synthesizing Li^+ doped hexagonal $NaYF_4$:Yb,Er [Na_{1-x} Li_xYF_4:Yb/Er] NCs to study the doping effect on its crystal structure and the upconversion emission, Zhang and co-workers observed that the phases formed varied from hexagonal to cubic to tetragonal with an increasing amount of Li^+ [209]. Li and co-workers tried the reverse process, they synthesized Na^+ doped tetragonal $LiYF_4$: Yb,Ln [$Li_{1-x}Na_xYF_4$: Yb/Ln] NCs by thermal decomposition of the corresponding metal trifluoroacetate and tried to control the size of the particles by the degree of sodium doping [210]. They noted that the size of the particles is reduced from 67 to 20 nm when the concentration of sodium is increased from 2 to 30%. The studies further indicated that the tetragonal crystal phase tended to form cubic $NaYF_4$ along with tetragonal $LiYF_4$ if more than 40% of the Li ions are replaced by Na ions.

Though these studies give a first hint on the phase transformations occurring during the formation of $LiYF_4$ NCs, there is no conclusive study how important they are for the synthesis of the particles. So in the work presented in this chapter we demonstrate a new approach where we provide purified NCs as intermediate precursor particles for the formation of $LiYF_4$, $LiLuF_4$ and $LiGdF_4$ NCs. For this, we use the highly sodium deficient cubic α-$NaYF_4$ NCs which we derived from the study presented in chapter 3, along with additional molecular precursors. In the same way, orthorhombic YF_3 NCs were separately prepared and investigated as precursor particles. We are able to confirm that the formation of $LiYF_4$ and $LiLuF_4$ occurs through an intermediate phase. The composition of this intermediate phase depends on the ions available in the reaction mixture. The formation of intermediate particles is also confirmed by another set of studies, where molecular precursors for Na^+, Y^{3+}, Li^+ and Lu^{3+} ions instead of precursor particles are used. Using these methods we successfully synthesised highly monodisperse sub-10 nm $LiYF_4$ as well as $LiLuF_4$ NCs. Our effort to synthesise the

corresponding $LiGdF_4$ NCs was unsuccessful, which is also discussed in the chapter. Furthermore, we extended our new approach to the synthesis of upconverting $LiYF_4$:Yb, Er core and core/shell NCs and these results are also presented in the chapter.

5.2. Experimental Section

Synthesis of lithium oleate (Li-oleate): Lithium hydroxide monohydrate ($LiOH.H_2O$) and oleic acid were combined in a molar ratio of 1:3. The suspension was heated at a Schlenk line at 100 °C under vacuum until a clear solution was obtained. This solution was used as stock solution for further reactions.

Synthesis of yttrium oleate (Y-oleate), lutetium oleate (Lu-oleate) and gadolinium oleate (Gd-oleate): A detailed synthesis procedure for Y-oleate is given in chapter 4, section 4.2. The same procedure was also adopted for the synthesis of Lu-oleate and Gd-oleate, where $LuCl_3.6H_2O$ and $GdCl_3.6H_2O$ were used as starting materials.

Synthesis of $LiYF_4$ nanocrystals using sodium deficient cubic α-$NaYF_4$ precursor particles: The preparation of sodium deficient cubic α-$NaYF_4$ (Na/Y ratio=0.1, 0.2, 0.3 and 0.4) NCs was described in detail in chapter 4. $LiYF_4$ NCs were prepared by using these NCs as precursor particles. For a typical synthesis, equimolar amounts of sodium deficient cubic α-$NaYF_4$, Li-oleate and ammonium fluoride (1:1:1) were used. Li-oleate and sodium deficient cubic α-$NaYF_4$ were dissolved in oleic acid and octadecene solvent (5 mL of each for 1 mmol of Li-oleate). The solution was degassed on a Schlenk line apparatus by applying vacuum (1 mbar) for 60 min at 100 °C under vigorous stirring. After degassing, ammonium fluoride was added to the solution under nitrogen flow. Immediately after the addition of NH_4F, the system was cycled three times between vacuum and N_2, applying vacuum for only 5 s in each cycle. Afterwards the reaction mixture was heated at 300 °C for 90 min under nitrogen flow. Then the system was cooled down to room temperature and the NCs dispersed in the solution were precipitated with the addition of an equal amount of ethanol and separated by centrifugation. The particles were purified from the insoluble by-products by redispersing the precipitate in hexane (1 mL of hexane per 1 mmol of NCs), centrifuged the suspension for 30 s. The particles were precipitated from the clear supernatant solution with twice the amount of ethanol. Then the nanocrystals were separated by centrifugation.

Tetragonal $LiLuF_4$ NCs were prepared in an analogous way. The sodium deficient cubic α-$NaLuF_4$ NCs required in this case, were prepared by the same method as described in chapter 4 for the synthesis sodium deficient cubic α-$NaYF_4$ NCs.

Synthesis of $LiYF_4$ nanocrystals using molecular precursors: Here we used lithium oleate, sodium oleate and yttrium oleate as precursors instead of cubic nanocrystals. Equimolar amounts of yttrium oleate and lithium oleate were combined with oleic acid and octadecene (5 mL of each solvent per 1 mmol of rare earth oleate). An appropriate amount of sodium oleate was added to obtain a Na/Y ratio of 0.1, 0.2, 0.3 or 0.4. The solution was degassed on a Schlenk line apparatus by applying vacuum (1 mbar) for 60 min at 100 °C under vigorous stirring. After degassing, ammonium fluoride was added to the solution under nitrogen flow. The amount of ammonium fluoride was calculated to be sufficient to convert all lithium, sodium and yttrium ions into fluoride. Immediately after the addition of NH_4F, the system was cycled three times between vacuum and N_2, applying vacuum for only 5 s in each cycle. Then the reaction mixture was heated at 300 °C for 90 min under nitrogen flow. After that the system was cooled down to room temperature and the NCs dispersed in the solution were precipitated with the addition of an equal amount of ethanol and separated by centrifugation. The particles were further purified by the washing steps described above.

$LiLuF_4$ and $LiGdF_4$ NCs were prepared analogously by using separately prepared oleates of lutetium and gadolinium as precursors.

Synthesis of small orthorhombic YF_3 nanocrystal precursor: For the preparation of small YF_3 NCs, yttrium oleate and tetramethylammonium fluoride tetrahydrate [TMAF, $(CH_3)_4NF{\cdot}4H_2O$] were used as starting materials. A stock solution of TMAF was prepared by dissolving TMAF in a solvent mixture consisting of two volume parts of octadecene, one part of oleic acid and one part of oleylamine (for 1 mmol TMAF per 10 mL of solvent mixture) in a three-necked round bottom flask. To remove water and dissolved oxygen, the dispersion was degassed on a vacuum Schlenk line for 60 min at 50 °C and for another 60 min at 100 °C under vigorous stirring. Subsequently, the turbid suspension was cycled three times between vacuum and nitrogen atmosphere, and the solution thereafter kept under nitrogen flow at 100 °C. In a separate setup, yttrium oleate was dissolved in oleic acid and octadecene (5 mL of each of the solvent for 1 mmol of yttrium oleate) in a three-necked round bottom flask. The solution further degassed for 60 min

at 100 °C under vacuum and strong stirring. Afterwards, the solution was cycled three times between vacuum and nitrogen atmosphere and TMAF stock solution was added to the yttrium oleate solution using a syringe under N_2 flow. The amount of TMAF added corresponds to three times the molar amount of yttrium oleate. Then the reaction mixture was heated at 220 °C for 60 min under nitrogen flow. After cooling down to room temperature, the obtained clear yellowish solution was mixed with an equal amount of ethanol to precipitate the small YF_3 particles, which were separated by centrifugation. Purification of the samples was carried out as described above. The samples were dried at 80 °C for 14 h before they were used for further reactions.

An analogous procedure was used to prepare small orthorhombic LuF_3 NCs.

Synthesis of $LiYF_4$ nanocrystals using small orthorhombic YF_3 nanocrystal precursors: $LiYF_4$ NCs were prepared by using small YF_3 NCs as precursor material along with equimolar amounts of Li-oleate and ammonium fluoride. For a typical synthesis, equimolar amounts of YF_3 and Li-oleate were dissolved in oleic acid and octadecene (5 mL of each solvent for 1 mmol of YF_3). The solution was degassed for 60 min at 100 °C on a vacuum Schlenk line apparatus under vigorous stirring. Thereafter, the ammonium fluoride was added to the solution under N_2 flow and the solution was cycled between vacuum and N_2 for three times. Then the reaction mixture was heated at 300 °C for 60 min under nitrogen flow. The solution was allowed to cool down to room temperature and followed by the addition of an equal amount of ethanol to precipitate the $LiYF_4$ NCs, which were collected by centrifugation. The particles were further purified by the washing steps described above.

$LiLuF_4$ NCs were synthesized similarly by using small orthorhombic LuF_3 NCs as precursor.

Synthesis of $LiYF_4$ nanocrystals using molecular precursors without sodium: For the synthesis of $LiYF_4$ NCs, molecular precursors such as Li-oleate, Y-oleate and ammonium fluoride were used. In a typical synthesis, equimolar amounts of Y-oleate and Li-oleate were dissolved in oleic acid and octadecene (5 mL of each solvent for 1 mmol of Y-oleate) in a three-necked round bottom flask. The solution was degassed for 60 min at 100 °C on a vacuum Schlenk line apparatus under vigorous stirring. Thereafter, the stoichiometric amount of ammonium fluoride was added to the solution under N_2 flow and the solution was cycled between vacuum and N_2 for three times. Then

the reaction mixture was heated at 300 °C for 90 min under nitrogen flow. The solution was allowed to cool down to room temperature and followed by the addition of an equal amount of ethanol to precipitate the $LiYF_4$ NCs, which were collected by centrifugation. The particles were further purified by the washing steps described above.

The same method was used to prepare $LiLuF_4$ and $LiGdF_4$ NCs, using the corresponding oleates.

Synthesis of $LiYF_4$:Yb,Er/$LiYF_4$ core/shell nanocrystals: First $LiYF_4$:Yb,Er core NCs were prepared by using corresponding sodium deficient cubic α-$NaYF_4$:Yb,Er (Na/Y=0.2) NCs as precursor particles as described above. For the synthesis of core/shell NCs, 0.5 mmol of the core particles were combined with 5 mL of oleic acid and 5 mL of octadecene along with 3 mmol of Li-oleate and 3 mmol of Y-oleate in a three-necked round bottom flask. The solution was degassed for 60 min at 100 °C on a vacuum Schlenk line apparatus under vigorous stirring. Thereafter, 12 mmol of ammonium fluoride was added to the solution under N_2 flow and the solution was cycled between vacuum and N_2 for three times. Then the reaction mixture was heated at 300 °C for 40 min under N_2 flow. The solution was allowed to cool down to room temperature and followed by the addition of an equal amount of ethanol to precipitate the NCs, which were collected by centrifugation. The particles were further purified by the washing steps described above. The purification step was repeated for 3 times. NCs were dried at 80 °C for 14 h and powdered well for the luminescence measurements.

5.3. Results and Discussion

XRD patterns of tetragonal $LiYF_4$ NCs are shown in **Figure 5.1**. The particles were prepared in oleic acid/octadecene solvent using highly sodium deficient (N/Y ratio of 0.1, 0.2, 0.3 and 0.4) sub-5 nm sized cubic α-$NaYF_4$ NCs as precursor particles along with Li-oleate and ammonium fluoride. The diffractograms a, b and c shown in the figure belong to particles that were synthesised from cubic α-$NaYF_4$ NCs having N/Y ratio of 0.1, 0.2 and 0.3 respectively. The diffractograms show that the cubic NCs are completely transformed into tetragonal $LiYF_4$ since the reflections are well indexed with the corresponding standard powder diffraction data [PDF no: 01-077-0816]. However, when cubic α-$NaYF_4$ NCs with a Na/Y ratio of 0.4 were used as precursor, the respective diffractogram (Figure 5.1d) indicates that $LiYF_4$ is formed along with some cubic $NaYF_4$ [PDF no: 01-077-2042]. It is important to note that the XRD patterns do not give any

indication of the presence of YF_3 or other phases, except the presence of cubic $NaYF_4$ when the precursor NCs have a Na/Y ratio higher than 0.3.

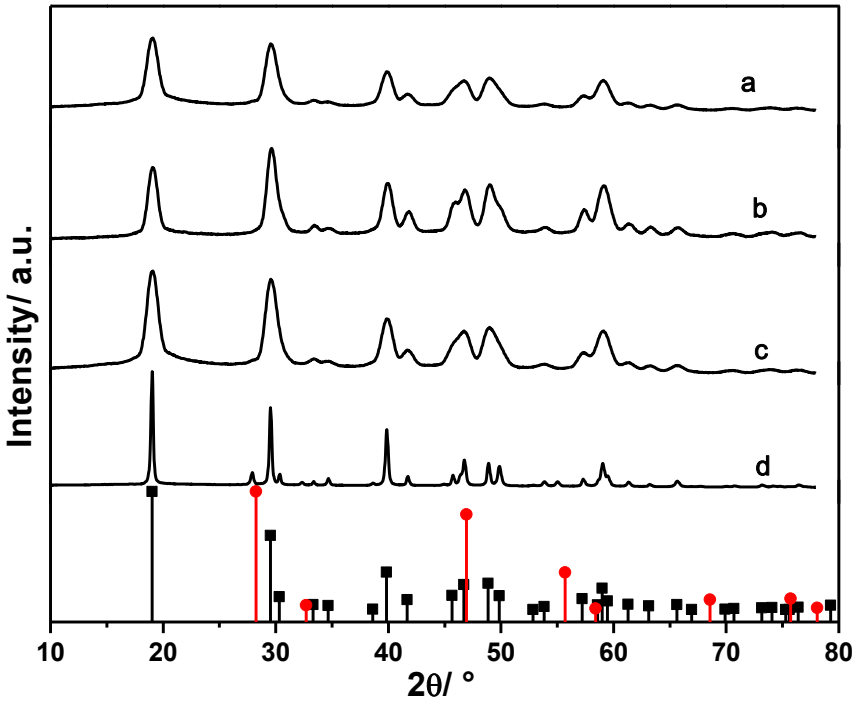

Figure 5.1: XRD data of nanocrystals obtained by the reaction of sodium deficient cubic α-$NaYF_4$ with Li-oleate and ammonium fluoride in oleic acid and octadecene at 300 °C for 90 min. The Na/Y ratio used in the synthesis of sodium deficient α-$NaYF_4$ particles was a) 0.1, b) 0.2, c) 0.3, d) 0.4 and e) 0.55. The reflections of a, b and c are indexed with the tetragonal phase of $LiYF_4$ whereas the reflections of d) indicate with tetragonal phase of $LiYF_4$ and cubic phase of α-$NaYF_4$.

The former samples were also analyzed through TEM and the corresponding micrographs are shown in **Figure 5.2**. It is clearly visible from the micrographs that the particles formed are monodisperse with an average size of equal to or less than 100 nm. When cubic α-$NaYF_4$ NCs with a N/Y ratio of 0.4 used as precursor, $LiYF_4$ particles with characteristic, bipyramidal shape are formed along with smaller spherical particles (Figure 5.2d). The observation is well corroborated with the XRD diffractogram provided in figure 5.1d. From the width of the XRD reflexes, the round shaped, polydispersed, particles with an average size range of 12-35 nm can be assigned to cubic α-$NaYF_4$ NCs and the larger particles with an average size of 100 nm to tetragonal $LiYF_4$. The XRD peaks of cubic α-$NaYF_4$ NCs (refer Figure 5.1d) are more narrow than those of the parent particles, (refer Figure 4.1, in chapter 4) proving that the cubic particles grow during the synthesis. Due to their high sodium deficiency, however, the particles remain

in the cubic phase, as we also observed in the studies presented in chapter 4 and are not converting into the corresponding hexagonal phase.

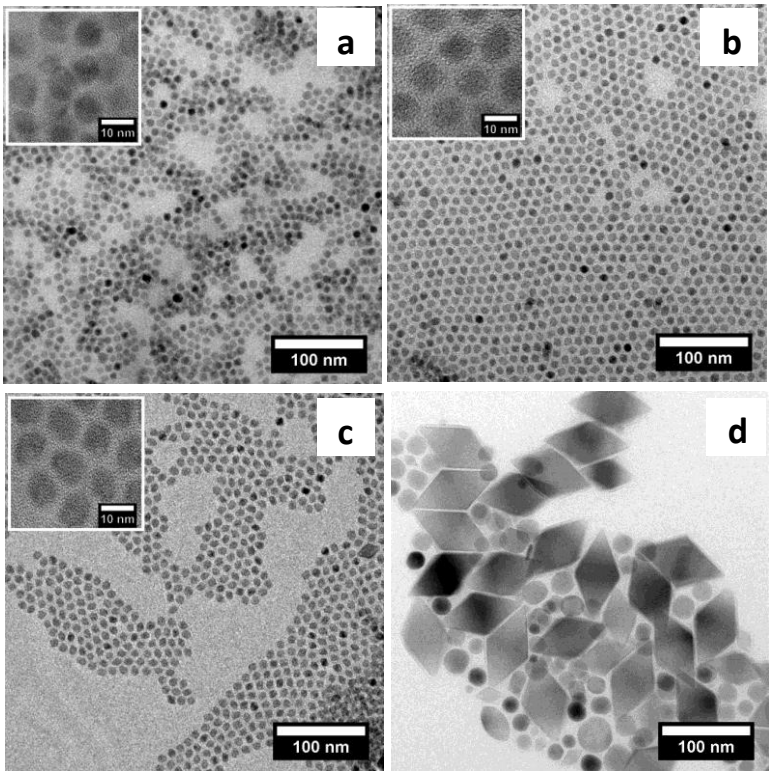

Figure 5.2: TEM images of nanocrystals obtained by the reaction of sodium deficient cubic α-$NaYF_4$ with Li-oleate and ammonium fluoride in oleic acid and octadecene at 300 °C for 90 min. The Na/Y ratio used in the synthesis of sodium deficient α-$NaYF_4$ particles was a) 0.1, b) 0.2, c) 0.3, d) 0.4 and e) 0.55. Samples a, b and c contain only tetragonal $LiYF_4$ whereas sample (d) consist of mixture of tetragonal $LiYF_4$ and cubic α-$NaYF_4$.

Further, XRF analysis was carried out to check the presence of sodium, if any, in the $LiYF_4$ NCs. The data provided in **Figure 5.3** shows that a small amount of sodium is evident, and the amount is similar in all NCs. The form of the sodium present in these NCs is difficult to assign. It may be contained as Na-oleate in the organic ligand layer or it may exist as sodium ions doped into the $LiYF_4$ matrix as $Li_{1-x}Na_xYF_4$. Doped phases such as tetragonal $Li_{1-x}Na_xYF_4$ and cubic/hexagonal $Na_{1-x}Li_xYF_4$ have been reported, as we mentioned in the introduction [210, 209]. However, here we could not detect any change or shift in the XRD reflections of our $LiYF_4$ samples as expected. If a significant amount of Li^+ ions are replaced against larger Na^+ ions, detailed and in-depth study using different analytical tools and mathematical calculations is required to investigate the influence of Na doping on the lattice parameters, which is at this point out of scope of the thesis. What we want to stress as a point here, however, is that the highly sodium deficient

cubic α-$NaYF_4$ NCs can be used as precursor particles to form monodisperse sub-10 nm sized tetragonal $LiYF_4$ NCs. This raises the question whether these cubic particles are always formed as intermediate product, when $LiYF_4$ particles are prepared from the molecular precursors.

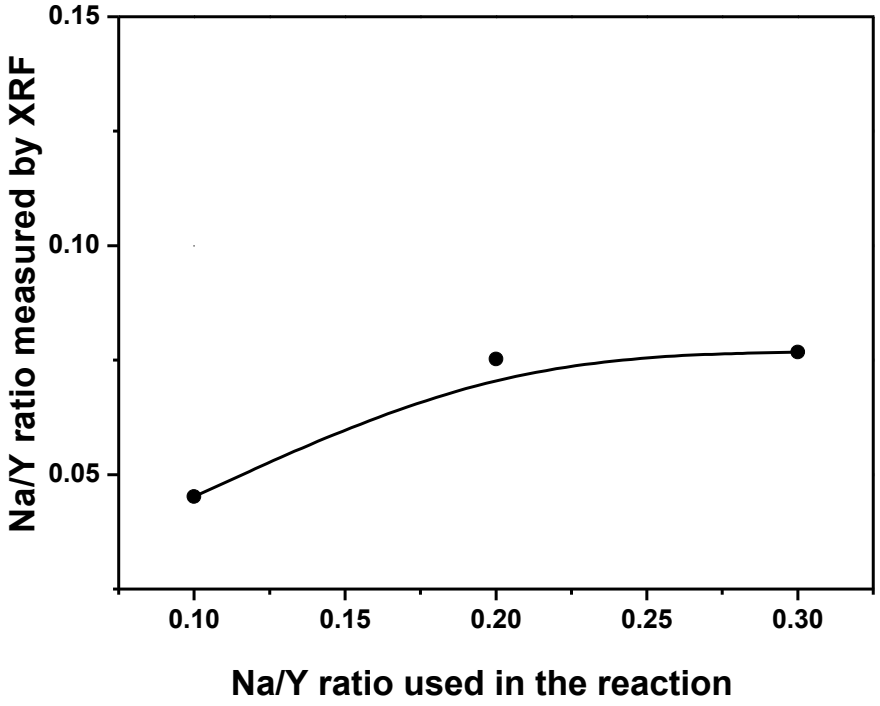

Figure 5.3: Sodium content of $LiYF_4$ nanocrystals prepared by the reaction of sodium deficient cubic α-$NaYF_4$ nanocrystals with Li-oleate and ammonium fluoride in oleic acid and octadecene at 300 °C for 90 min. The sodium to yttrium ratio of the $LiYF_4$ nanocrystals was measured by XRF. The ratio is plotted against the ratio of Na/Y that was present in the synthesis of α-$NaYF_4$ precursor particles.

We therefore repeated the above reactions with the corresponding molecular precursors instead of sodium deficient cubic α- $NaYF_4$ NCs. To keep the Na/Y ratio to the above values of 0.1, 0.2, 0.3 and 0.4, an appropriate amount of Na-oleate was used along with Y-oleate, Li-oleate and ammonium fluoride in oleic acid/octadecene solvent. Also, we kept all other parameters the same as in the other synthesis and a detailed synthesis procedure is described in section 5.2. XRD and TEM images of the final particles derived from these reactions are given in **Figure 5.4** and **5.5** respectively. The XRD analysis already indicates that the $LiYF_4$ particles formed are similar to those formed when we use NCs as precursor. Again all peaks are well indexed with the corresponding $LiYF_4$ standard patterns, also plotted with the figure. Well faceted highly monodisperse tetragonal $LiYF_4$ NCs are obtained, as is clearly evident from the micrographs presented

in figure 5.5. The average size of the NCs is found to be increasing with the Na/Y ratio. The $LiYF_4$ NCs synthesised with a Na/Y ratio of 0.1 have an average size of 10 nm, which is similar to the particle size obtained with the corresponding cubic NCs precursor particles. Higher Na/Y ratios of 0. 2 and 0.3 yield the particle size of 16 and 32 nm respectively. As we mentioned in the introduction part of the chapter, size tuning of $LiYF_4$ particles was studied by doping different cations [210, 209, 207]. Among them, Li and co-workers successfully reduced the size of tetragonal $LiYF_4$: Yb, Ln NCs from 67 to 20 nm by doping with sodium ions [$Li_{1-x}Na_xYF_4$:Yb/Ln] using doping concentration between 2 and 30% [210]. However, here we have noticed an increase in size as the amount of sodium increases. This is the opposite to what Li et.al reported. We feel that, as we mentioned above, the variation of size with the sodium content is difficult to explain at this point with the data available. Nevertheless, it is clear that the presence of sodium affects the nucleation of the $LiYF_4$ particles and, therefore, their final size.

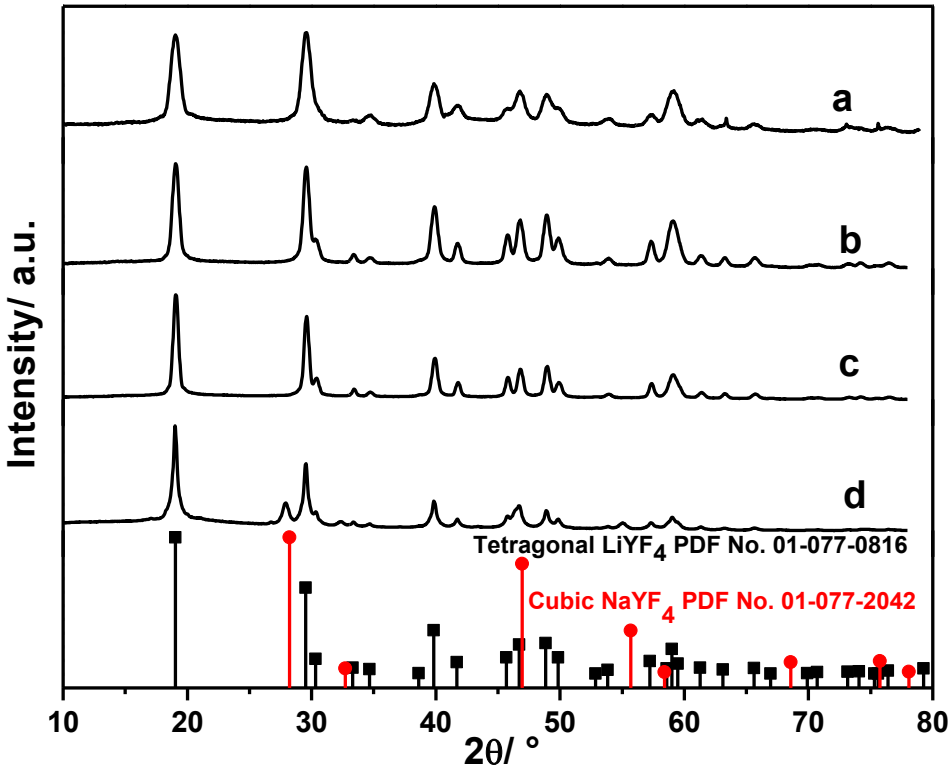

Figure 5.4: XRD data of $LiYF_4$ nanocrystals prepared by the reaction of the molecular precursors Li-oleate, Na-oleate, Y-oleate and ammonium fluoride in oleic acid and octadecene at 300 °C for 90 min. The sodium oleate used in the synthesis corresponded to Na/Y ratios of a) 0.1, b) 0.2, c) 0.3 and d) 0.4. Nanocrystals of tetragonal $LiYF_4$ were obtained in the case of Na/Y ratios of 0.1, 0.2 and 0.3 (a, b and c). In the case of a Na/Y ratio of 0.4, mixture of tetragonal $LiYF_4$ and cubic $NaYF_4$ is formed (d).

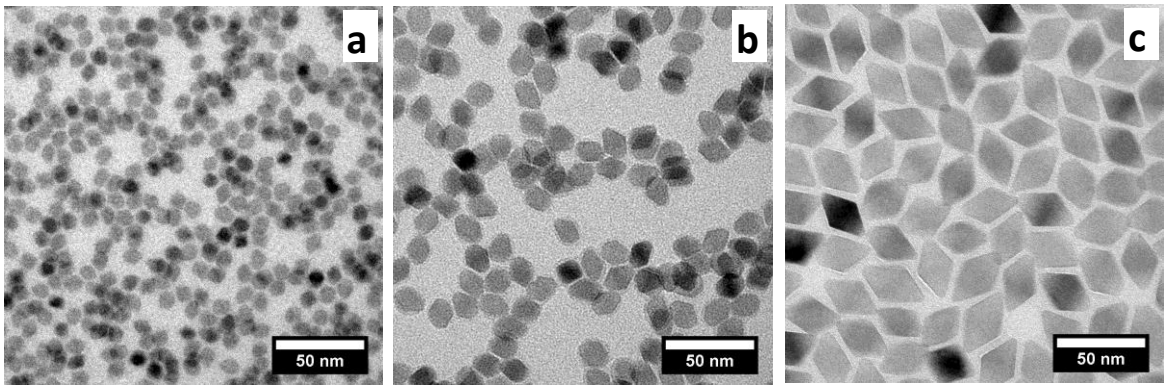

Figure 5.5: TEM images of $LiYF_4$ NCs prepared by the reaction of the molecular precursors Li-oleate, Na-oleate, Y-oleate and ammonium fluoride in oleic acid and octadecene at 300 °C for 90 min. The sodium oleate was chosen to obtain a Na/Y ratio of a) 0.1, b) 0.2 and c) 0.3 in the synthesis.

It is clear from the above two sets of experiments with different precursors, one with sodium deficient cubic $NaYF_4$ NCs and another with corresponding molecular precursors, $LiYF_4$ NCs with similar sizes formed. The question now is whether in the presence of sodium, cubic α-$NaYF_4$ is formed as an intermediate phase before $LiYF_4$ NCs are observed. This was investigated by a temperature and time dependent reaction study, where molecular precursors with a Na/Y ratio of 0.2 are heated at different temperatures in oleic acid/octadecene solvent. For that, the molecular precursors dissolved in the solvent mixture were heated at temperature above 270 °C for 30 min. During the reaction, the samples were withdrawn at different time and temperature. The products were purified and analyzed with XRD. The XRD data shown in **Figure 5.6** confirms that small cubic α-$NaYF_4$ NCs are formed as an intermediate product at lower temperatures, as is evident from the diffractogram of the sample that was drawn when the temperature reached 280 °C (280 °C/0 min, Figure 5.6a). The stronger broadened reflections indicate that the particles are very small, probably less than 5 nm. During further heating to 300 °C, these small cubic α-$NaYF_4$ particles are slowly converted to tetragonal $LiYF_4$. We think that, when dissolution of these small cubic α-$NaYF_4$ particles occurs at high temperatures, the availability of the Li^+ ions in solution helps to form stable nuclei of $LiYF_4$. These nuclei further grow to NCs by using monomers available in the solution during the dissolution of the α-phase particles at high temperatures. As we described in the above sections, a study has already been published by Li et. al., where sodium oleate used in the preparation of doped $LiYF_4$:Yb, Ln ($Li_{1-x}Na_xYF_4$: Yb/Ln) NCs. There it was noted that, when the doping concentration of sodium increases, the bipyramidal shape of the $LiYF_4$ particles is gradually changing, but not the crystal

structure, and above 40% a two products, $LiYF_4$ along with α-$NaYF_4$, were obtained [210]. However, as such this result gives no clear indication of the presence of any intermediate phase. In our studies, however, it was confirmed that cubic α-$NaYF_4$ particles are formed as an intermediate product during the reaction, which undergoes dissolution and in presence of Li-oleate recrystallises as tetragonal $LiYF_4$ NCs.

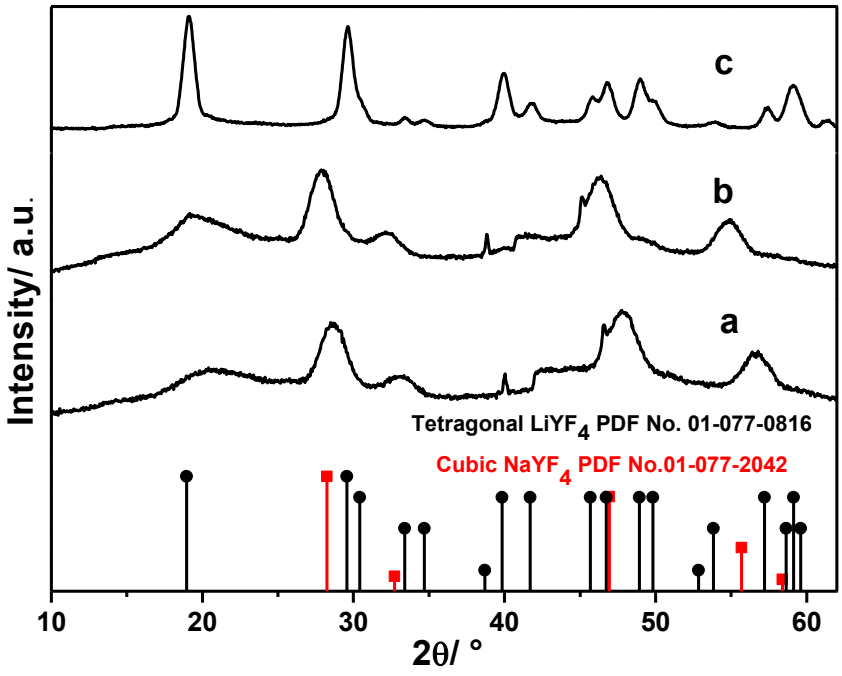

Figure 5.6: XRD data of nanocrystals that formed intermediately during the reaction of the molecular precursors Na-oleate, Li-oleate, Y-oleate, and ammonium fluoride in oleic acid and octadecene at different temperatures and time. Small nanocrystals of cubic α-$NaYF_4$ are formed as an intermediate phase at 280 °C/0 min (a), a mixture of cubic α-$NaYF_4$ and tetragonal $LiYF_4$ particles is formed at 300 °C/0 min (b). After 30 min at 300 °C the intermediately formed cubic α-$NaYF_4$ particles are completely converted to tetragonal $LiYF_4$ at 300 °C/30 min(c).

As we mentioned in the introduction, Murray and co-workers detected the intermediate formation of orthorhombic YF_3 when they prepared $LiYF_4$ from the molecular precursors, YCl_3 and commercially available LiF [208]. Our diffractograms given above, however, do not indicate the formation of YF_3 as intermediate. We therefore also investigated the formation of intermediate phases when $LiYF_4$ NCs are prepared in the absence of sodium ions. For that, we have prepared small orthorhombic YF_3 NCs precursor particles using a synthesis procedure presented in section 5.2. It is clear from the corresponding XRD presented in **Figure 5.7** that very small YF_3 are formed presumably of the orthorhombic phase. The reflections are very broad in accord with

the TEM micrograph of the particles presented in the right part of the figure showing sub-5 nm particles.

These YF_3 NCs were then combined with Li-oleate and ammonium fluoride to produce $LiYF_4$ in a mixture of oleic acid and octadecene at 300 °C for 60 min. It is clearly evident from the respective XRD provided in **Figure 5.8** that the YF_3 NCs used as precursor are completely converted into tetragonal $LiYF_4$. The obtained products consist of well faceted tetragonal $LiYF_4$ NCs with an average size of 12 nm, as is obvious from the micrograph presented on the right side of the figure (right, Figure 5.8.).

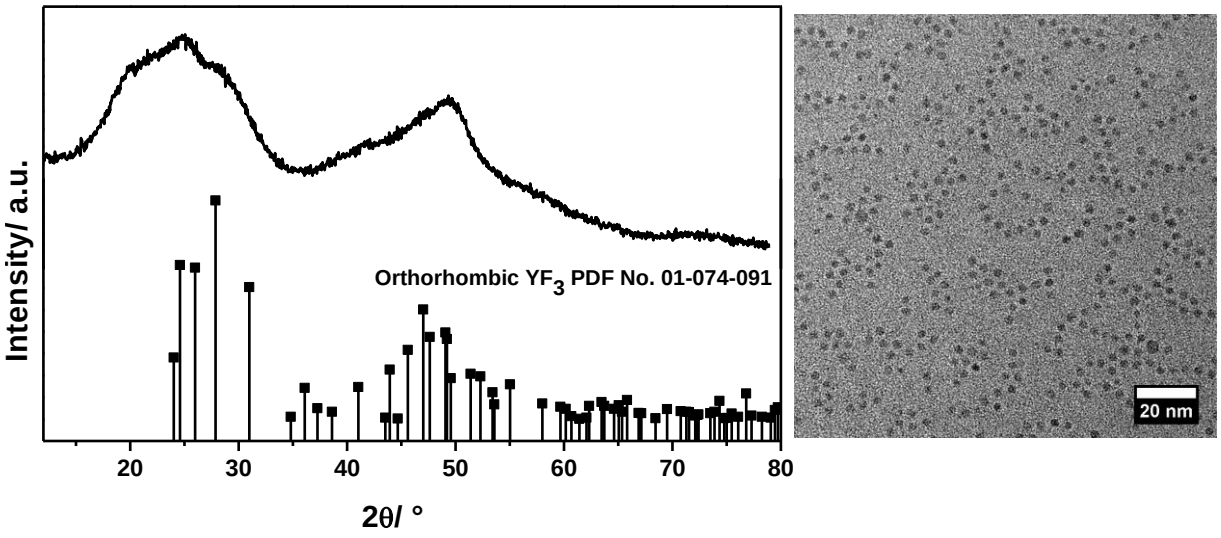

Figure 5.7: XRD data (left) and TEM image (right) of YF_3 nanocrystals prepared by the reaction of Y-oleate and tetramethylammonium fluoride tetrahydrate in oleic acid and octadecene at 220 °C for 60 min. The diffraction peaks are in accord with the orthorhombic phase of YF_3 and an average particle size of 2-3 nm.

The formation of $LiYF_4$ NCs is further studied by using the corresponding molecular precursors, i.e. Y-oleate instead of YF_3 NCs precursor particles, along with Li-oleate and ammonium fluoride. The XRD diffractogram and TEM microgram of the obtained particles are shown in **Figure 5.9**. All XRD peaks of samples are well indexed with the corresponding standard of $LiYF_4$. The TEM image shows that the samples consist in fact of well faceted $LiYF_4$ NCs with an average size of 12 nm, which is comparable to the size of the particles obtained with YF_3 particles as precursor.

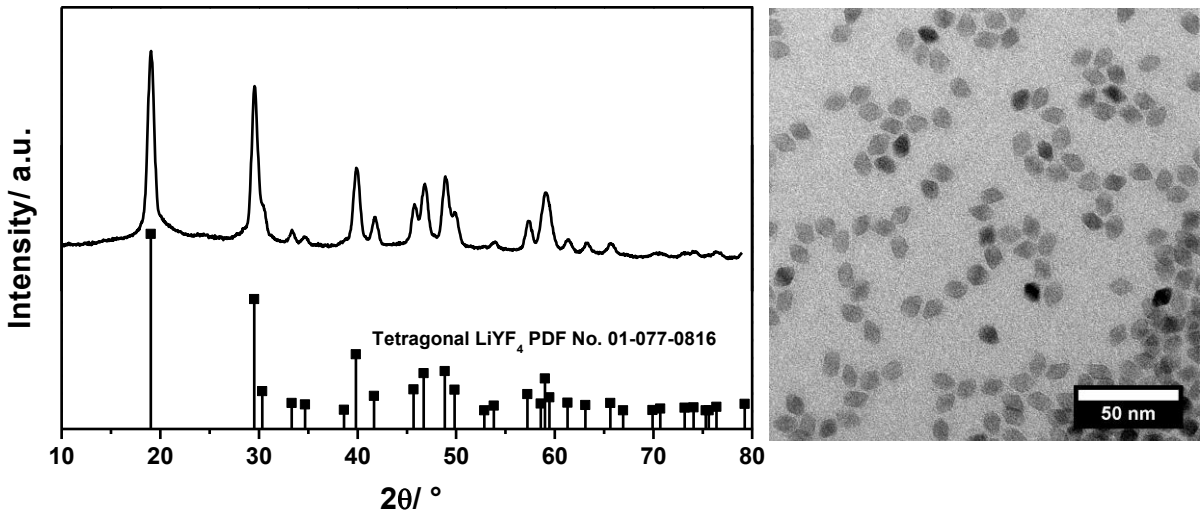

Figure 5.8: XRD data (left) and TEM image (right) of $LiYF_4$ nanocrystals prepared by the reaction of small YF_3 nanocrystals with Li-oleate and ammonium fluoride in oleic acid and octadecene at 300 °C for 60 min. The diffraction peaks were in accord with the tetragonal phase of $LiYF_4$ and an average particle size of 12 nm.

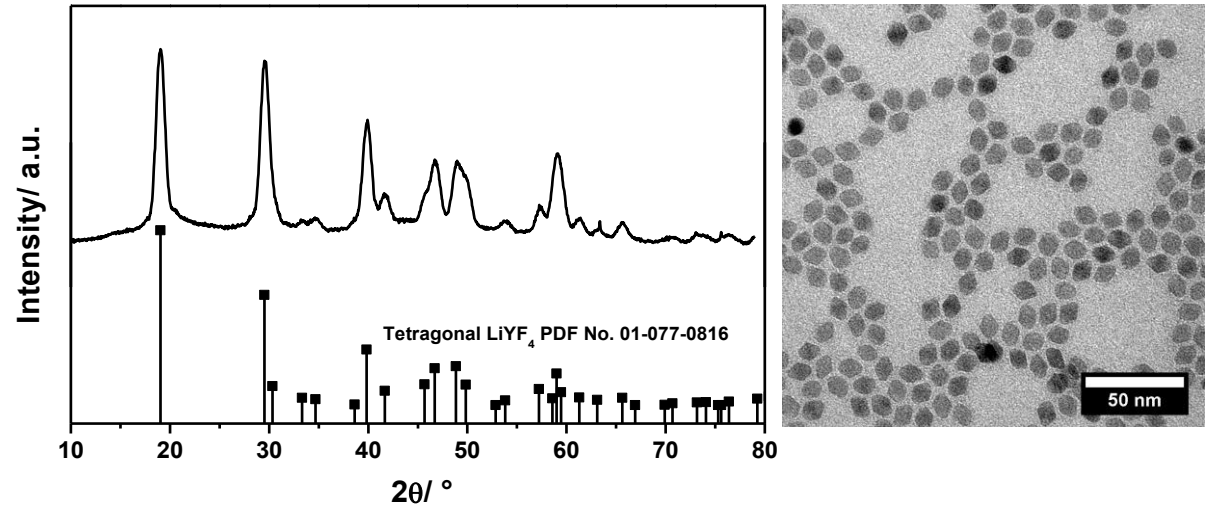

Figure 5.9: XRD data (left) and TEM image (right) of $LiYF_4$ nanocrystals prepared by the reaction of the molecular precursors Li-oleate, Y-oleate and ammonium fluoride in oleic acid and octadecene at 300 °C for 90 min. The diffraction peaks are indexed with the tetragonal phase of $LiYF_4$ and an average particle size of 12 nm.

This way indicates that YF_3 is formed as intermediate phase in this synthesis of $LiYF_4$ NCs when sodium is absent. This becomes more evident by a temperature and time dependent reaction study, where the molecular precursors were heated at different temperatures in oleic acid/octadecene solvent and samples were drawn at different times and temperatures. Each purified product was analyzed with XRD; the corresponding diffractograms are shown in **Figure 5.10**. Clearly orthorhombic YF_3 is

formed as an intermediate product, as is evident from the XRD analysis of the sample drawn immediately after a temperature of 300 °C was reached (300 °C/0 min, Figure 5.10a). The unmatched sharp peaks presented in the diffractogram (see asterix), are caused by a small amount of LiF formed by the reaction of Li-oleate and NH_4F. When we analyzed the XRD data of the samples drawn at low temperature, than 300 °C, we could find that intermediate phases or particles had not started to form.

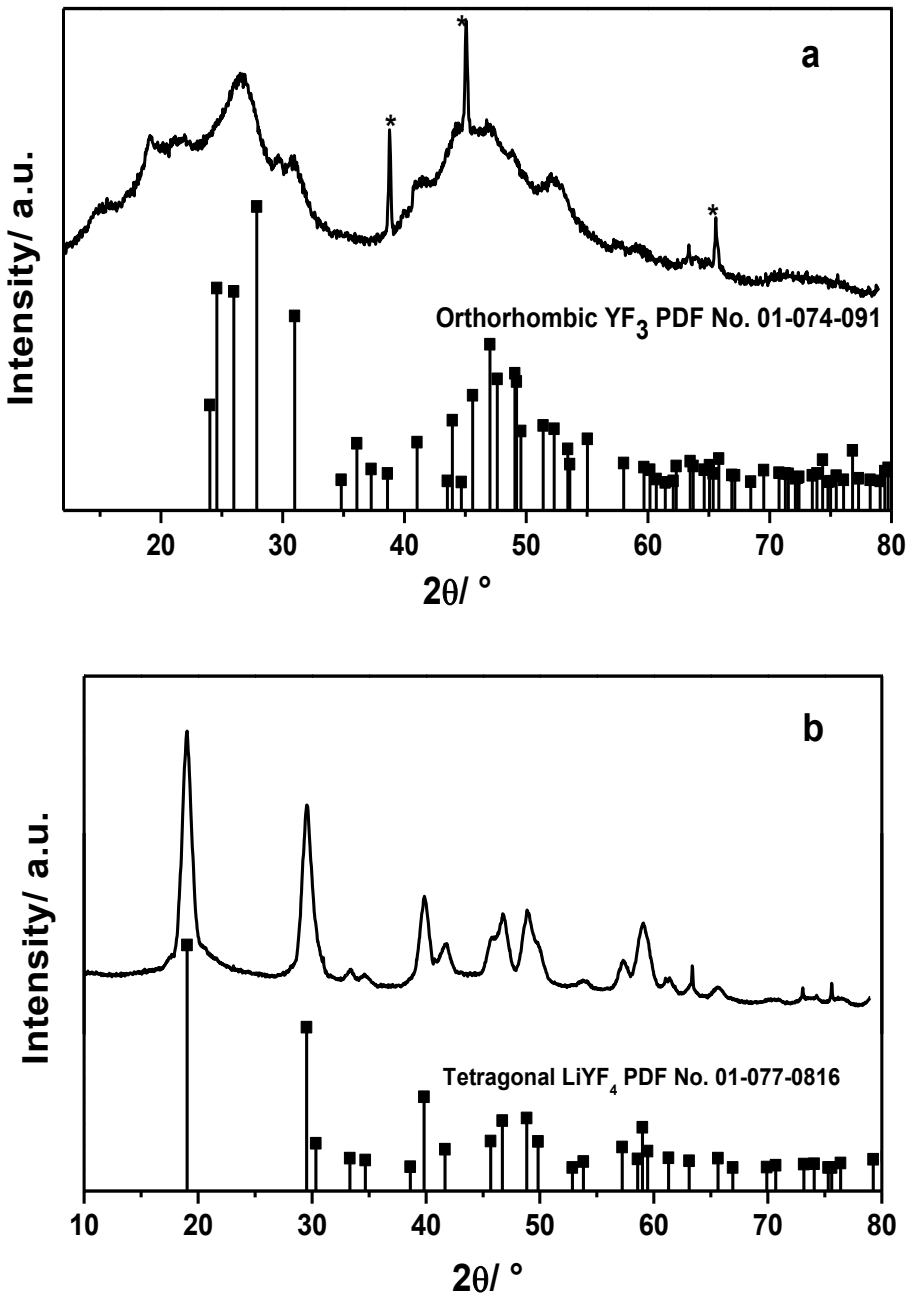

Figure 5.10: XRD data of nanocrystals formed at different time during the reaction of the molecular precursors Li-oleate, Y-oleate and ammonium fluoride in oleic acid and octadecene at 300 °C. Small particles of orthorhombic YF_3 are formed as intermediate product at 300 °C (a) but these particles are completely converted to tetragonal $LiYF_4$ at after 30 min (b)(* = LiF peaks).

The above study, with sodium deficient α-$NaYF_4$ particles and YF_3 particles as well as the corresponding molecular precursors give clear evidence that $LiYF_4$ NCs are formed through an intermediate nanocrystalline phase and the nature of the intermediate phase is determined by the metal ions available in the reaction mixture. That is, if sodium ions are present in the mixture, α-$NaYF_4$ particles are formed as intermediate phase whereas YF_3 particles are formed in the absence of sodium ions.

In the next step, we investigated whether these findings also apply to the isomorphous materials $LiLuF_4$ and $LiGdF_4$. For that, we first prepared sodium deficient (Na/Lu=0.3) cubic α-$NaLuF_4$ NCs as precursor particles as per the synthesis procedure presented in the experimental section 5.2. The XRD data and the TEM image of the precursor NCs are shown in **Figure 5.11**. The XRD pattern display well defined reflexes, which are well indexed with the standard pattern of cubic α-$NaLuF_4$ [PDF No: 027-072]. The broadness of the diffraction peaks indicate that the synthesised particles are very small, in accord with the TEM micrograph showing a mean particle size of less than 5 nm.

Now we used these NCs as precursor particles for the synthesis of tetragonal $LiLuF_4$ according to a procedure described in the experimental section 5.2. The diffractogram and the TEM image of the resulting tetragonal $LiLuF_4$ NCs are shown in **Figure 5.12**. The particles were prepared by using the sodium deficient sub-5 nm sized cubic α-$NaLuF_4$ NCs as precursor particles along with Li-oleate and ammonium fluoride in oleic acid and octadecene solvent. The XRD analysis shows that the cubic α-$NaLuF_4$ precursor particles are completely transformed into the tetragonal phase of $LiLuF_4$, and the reflections are well indexed with the corresponding standard data of $LiLuF_4$ [PDF no: 00-027-1251]. Also, monodisperse particles with an average size of 12 nm are observed in the TEM micrograph presented on the right side of the figure.

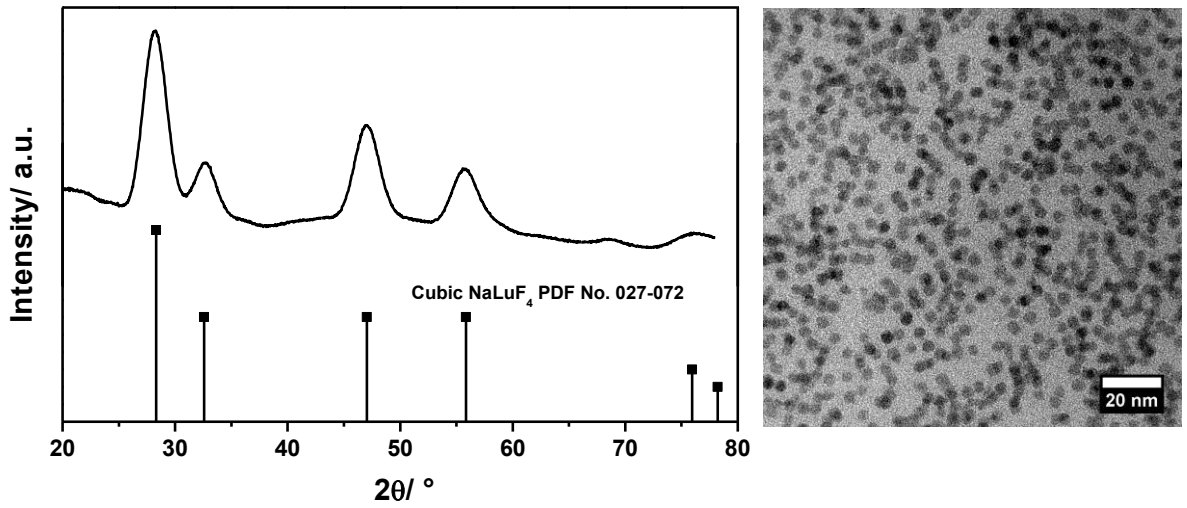

Figure 5.11: XRD data (left) and TEM image (right) of sodium deficient cubic α-$NaLuF_4$ nanocrystals (Na/Y ratio=0.3) prepared by the reaction of Lu-oleate, Na-oleate and ammonium fluoride in oleic acid and octadecene at 240 °C for 90 min. The diffraction peaks are in accord with the orthorhombic phase of LuF_3 and an average particle size of 3-4 nm.

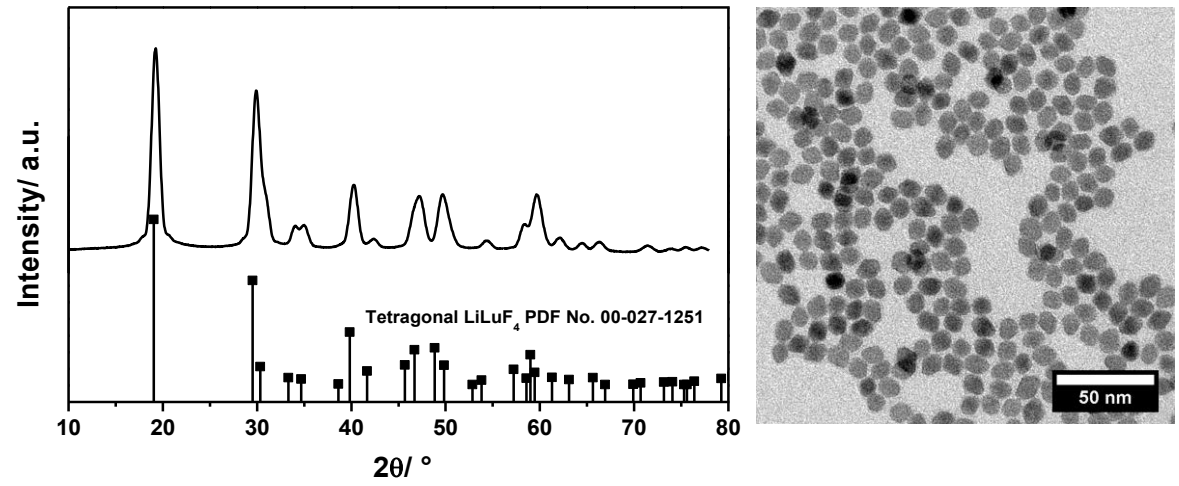

Figure 5.12: XRD data (left) and TEM image (right) of $LiLuF_4$ nanocrystals prepared by the reaction of sodium deficient α-$NaLuF_4$ particles with Li-oleate and ammonium fluoride in oleic acid and octadecene at 300 °C for 60 min. The diffraction peaks are indexed with the tetragonal phase of $LiLuF_4$ and an average particle size of 12 nm.

To check the presence of α-$NaLuF_4$ as intermediate particles during the formation of $LiLuF_4$ NCs, we repeated the above reactions with the corresponding molecular precursors. Thus, Na-oleate and Lu-oleate were combined in a molar ratio to 0.3 and heated at 300 °C in oleic acid and octadecene solvent for 60 min along with Li-oleate and ammonium fluoride. The XRD and the TEM image of the particles derived from the reaction are provided in **Figure 5.13**. The XRD analysis shows that all the peaks are well

matched with the corresponding standard data of $LiLuF_4$, which is also plotted with the diffractogram. In fact, well faceted highly monodisperse tetragonal $LiLuF_4$ NCs are obtained, as is clearly evident from the micrograph. The average size of the NCs is 12 nm and, hence, very similar to the size obtained with α-$NaLuF_4$ particles as precursor.

The above two sets of experiments show that $LiYF_4$ and $LiLuF_4$ particles behave similar insofar as sodium containing intermediate phases, α-$NaYF_4$ and α-$NaLuF_4$, are formed in both cases in presence of sodium oleate. In the next step we studied the formation of $LiLuF_4$ particles in the absence of sodium. For that, we have prepared small orthorhombic LuF_3 precursor particles as in the synthesis procedure presented in section 5.2. The purified products of this synthesis were analyzed by XRD and TEM as shown in **Figure 5.14**. It is clear from the XRD that very small LuF_3 are formed, as the reflections are very broad. The width of the XRD peaks is too broad to identify the crystal phase with certainty but the pattern is at least not in contradiction to the orthorhombic phase of LuF_3. Then TEM results are well correlated with these observations, as the size of the particles is less than 5 nm.

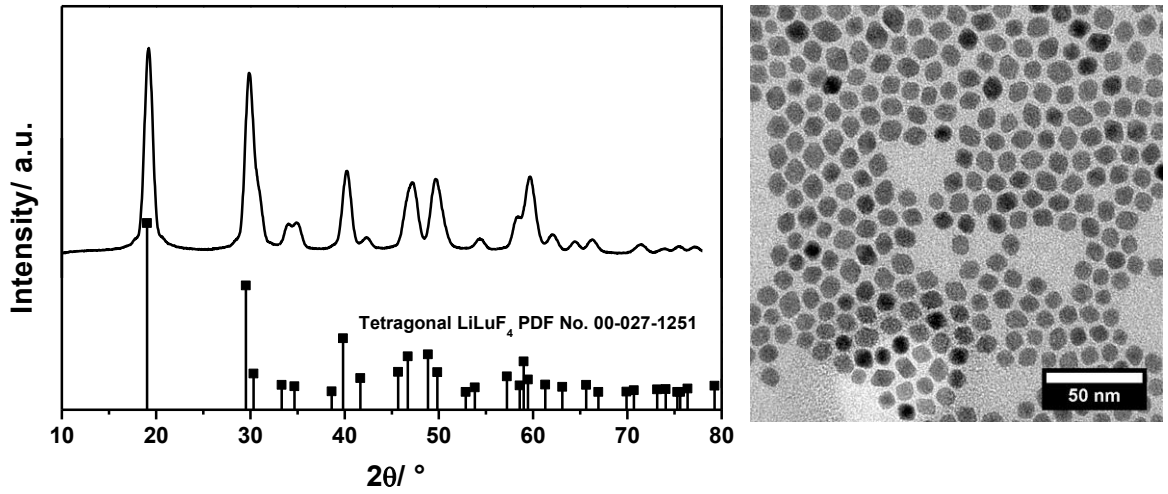

Figure 5.13: XRD data (left) and TEM image (right) of $LiLuF_4$ nanocrystals prepared by the reaction of the molecular precursors, Li-oleate, Na-oleate, Lu-oleate and ammonium fluoride in oleic acid and octadecene at 300 °C for 90 min. Na-oleate and Y-oleate were used in a molar ratio of 0.3. The diffraction peaks are indexed with the tetragonal phase of $LiLuF_4$ and an average particle size of 12 nm.

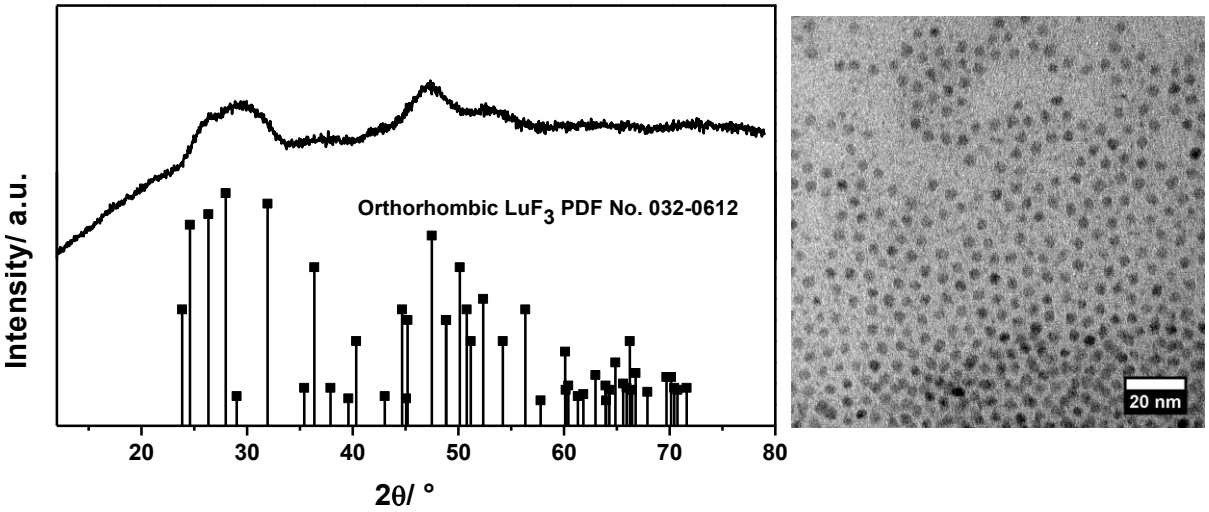

Figure 5.14: XRD data (left) and TEM image (right) of LuF_3 nanocrystals prepared by the reaction of Lu-oleate and tetramethylammonium fluoride tetrahydrate in oleic acid and octadecene at 220 °C for 60 min. The diffraction peaks are indexed with the orthorhombic phase of LuF_3 and an average particle size of 3-4 nm.

The small LuF_3 NCs obtained were used along with Li-oleate and ammonium fluoride to produce $LiLuF_4$ in oleic acid and octadecene at 300 °C. It is clearly visible from the corresponding XRD provided in **Figure 5.15** that the LuF_3 NCs are completely converted into tetragonal $LiLuF_4$. The obtained particles are well faceted tetragonal $LiLuF_4$ NCs with an average size of 12 nm, as is evident from the micrograph and the XRD data (Figure 5.15).

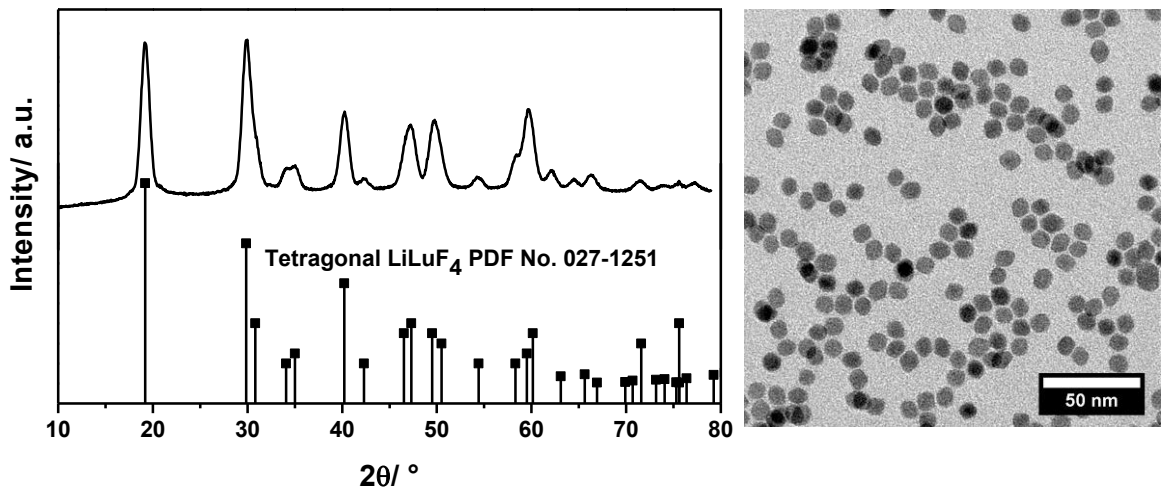

Figure 5.15: XRD data (left) and TEM image (right) of $LiLuF_4$ nanocrystals prepared by heating small LuF_3 nanocrystals with Li-oleate and ammonium fluoride in oleic acid and octadecene at 300 °C for 60 min. The diffraction peaks are indexed with the tetragonal phase of $LiLuF_4$ and an average particle size of 12 nm.

Finally $LiLuF_4$ NCs were also prepared by using the corresponding molecular precursors, i.e. in the presence of Lu-oleate instead of LuF_3 NCs precursor particles, along with Li-oleate and ammonium fluoride. The XRD diffractogram and the TEM micrograph of the particles obtained are shown in **Figure 5.16**. All reflections from the particles are well indexed with the corresponding standard data of $LiLuF_4$, which is also drawn in the figure. Again, well faceted tetragonal $LiLuF_4$ NCs with an average size of 12 nm are obtained. This size is identical to the size obtained with the precursor particles.

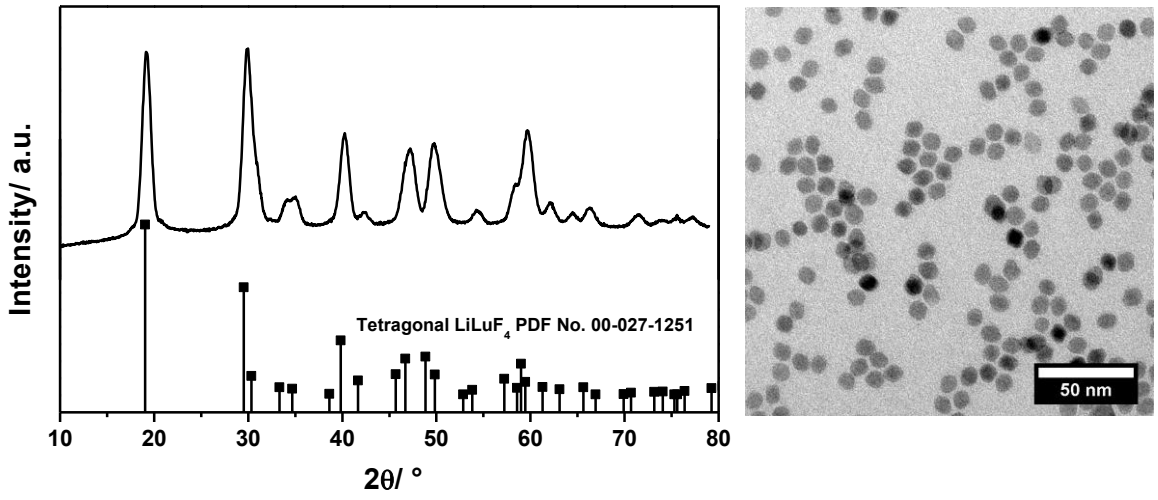

Figure 5.16: XRD data (left) and TEM image (right) of $LiLuF_4$ nanocrystals prepared by heating the molecular precursors Li-oleate, Lu-oleate and ammonium fluoride in oleic acid and octadecene at 300 °C for 90 min. The diffraction peaks are indexed with the tetragonal phase of $LiLuF_4$ and an average particle size of 12 nm.

It is clear from these results that NCs of $LiLuF_4$ also behave similar to $LiYF_4$ NCs as both can be formed through an intermediate phase. The composition of this intermediate phase depends on the metal ions available in the reaction mixture. Further, we checked whether this principle is extendable to $LiGdF_4$, one of the best host materials for quantum cutting ions. $LiGdF_4$ is believed to be difficult to prepare as nanocrystalline material and no researcher has reported corresponding nanoparticles yet [211]. Unfortunately, our efforts to synthesise $LiGdF_4$ NCs were also ineffective and the reaction of the molecular precursors, Li-oleate and Gd-oleate with ammonium fluoride, resulted in the formation of GdF_3 particles. The corresponding XRD data and a TEM image are shown in **Figure 5.17**. We also tried to convert these NCs into $LiGdF_4$ by heating them in the presence of Li-oleate and NH_4F. However, it was unsuccessful. Since it has been reported that sodium deficient α-$NaGdF_4$ NCs (Na/Gd ratio below 0.4) cannot

be prepared, we did not attempt to prepare $LiGdF_4$ NCs via highly sodium deficient α-$NaGdF_4$ [212].

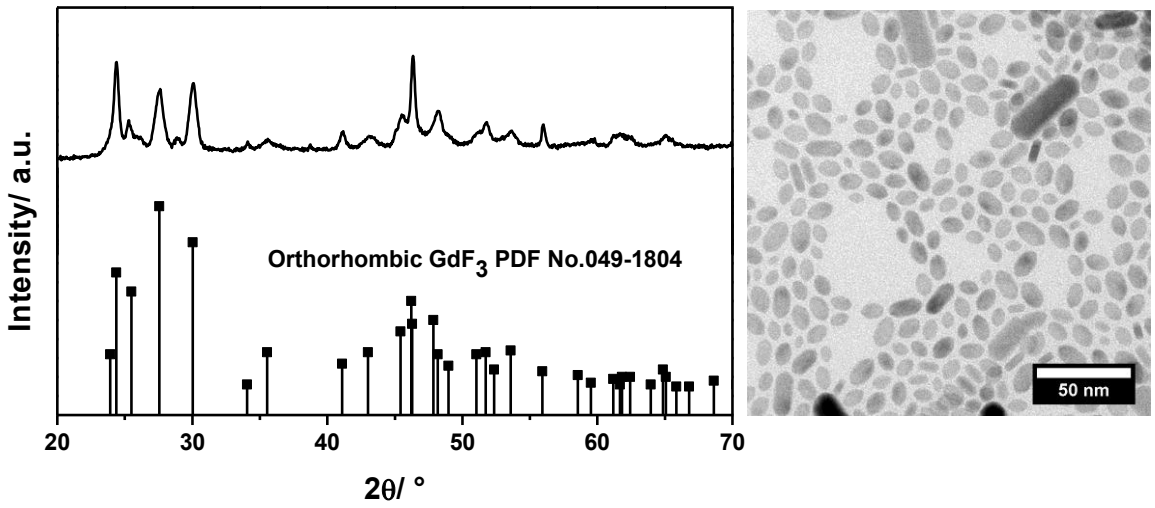

Figure 5.17: Attempt to synthesise $LiGdF_4$ nanocrystals by heating the molecular precursors Li-oleate, Gd-oleate and ammonium fluoride in oleic acid and octadecene at 300 °C for 90 min. The XRD data (left) shows that orthorhombic GdF_3 nanocrystals are formed instead of tetragonal $LiGdF_4$. The corresponding the TEM image is shown on the right.

Further, we used our new approach based on sodium deficient cubic α-$NaREF_4$ NCs as precursor to synthesise optically active $LiYF_4$ NCs, that is, upconverting ions (Yb/Er) doped monodisperse sub-15 sized tetragonal $LiYF_4$. Using these as core particles, an optically inactive shell of $LiYF_4$ was deposited onto the $LiYF_4$:Yb,Er core particles as core/shell NCs ($LiYF_4$:Yb,Er/$LiYF_4$). The XRD diffractogram and the TEM micrograph of the core and the core/shell particles are shown in **Figure 5.18**.

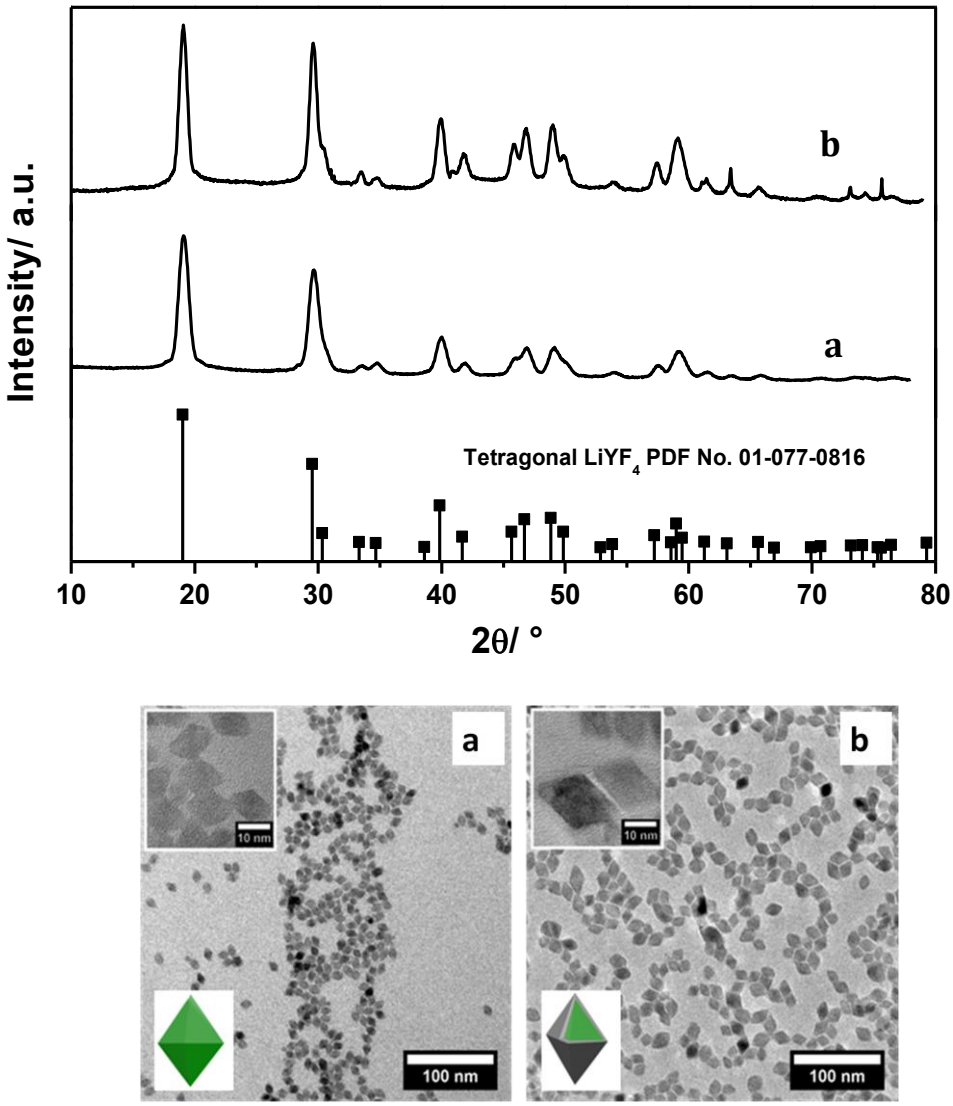

Figure 5.18: XRD data (top) and TEM images (bottom) of a) $LiYF_4$:Yb,Er core and b) $LiYF_4$:Yb,Er/$LiYF_4$ core/shell nanocrystals. The diffraction peaks of both core and core/shell nanocrystals are in accord with the tetragonal phase of $LiYF_4$. The core particles have an average size of 12 nm which increases to 20 nm after the shell formation. A schematic illustration of the core and the core/shell NCs are shown in the left bottom of each micrograph.

The optical properties of the NCs revealed that, NCs of $LiYF_4$ also act as an effective host material for upconverting ions. The $LiYF_4$:Yb,Er core particles and the precursor of the $LiYF_4$ shell were employed in a molar ratio of 1 to 6. The shell should therefore increase the volume of the particle by a factor of 7 or the size by a factor of $7^{1/3}$= 1.9, resulting in an expected increase from 12 nm of the core particles to 23 nm of the core/shell particles. The TEM images in figure 5.18 show a somewhat smaller increase in size from 12 to 20 nm indicating that not all of the $LiYF_4$ material was deposited as shell. The corresponding luminescence spectra in **Figure 5.19**, nevertheless, show that the shell

enhances the luminescence intensity of the particles by a factor of 35 (Excitation of 980 nm with 1 W/cm^2). This clearly shows that the energy loss processes at the particle surface are strongly reduced by the inert $LiYF_4$ shell.

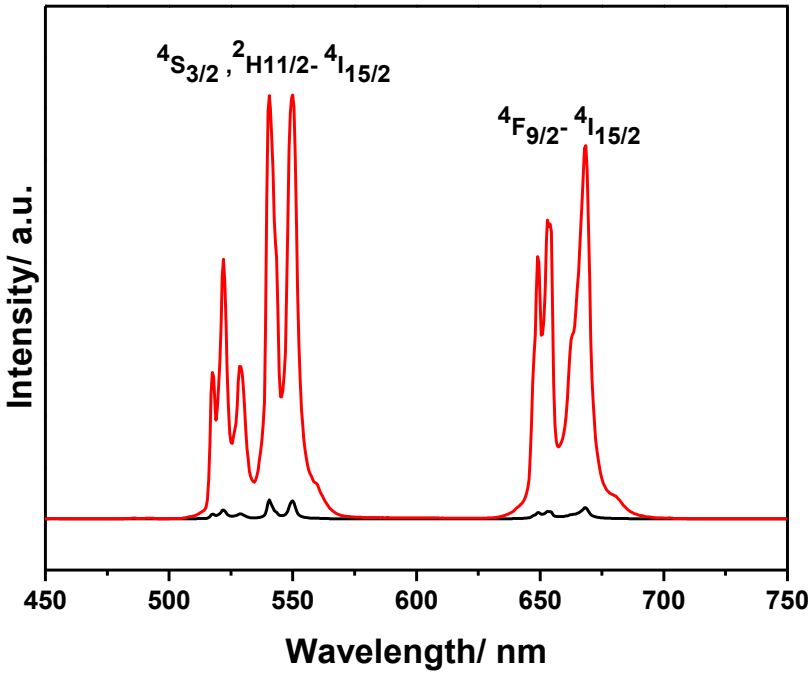

Figure 5.19: Luminescence spectra of $LiYF_4$:Yb,Er upconversion core (black) and $LiYF_4$:Yb,Er/$LiYF_4$ core/shell nanocrystals (red). The inert $LiYF_4$ shell enhances the luminescence intensity of the core particles by a factor of 35.

5.4. Conclusions

We have successfully developed a new approach to prepare monodisperse sub-10 nm sized $LiYF_4$ NCs using sodium deficient α-$NaYF_4$ NCs as precursor particles. The synthesis of NCs of $LiYF_4$ was also conducted with yttrium trifluorid NCs, YF_3, as precursor as well as molecular precursors. Also, we have successfully used the new approach to study intermediate phases formation during the synthesis of $LiYF_4$ NCs. Our studies confirm that $LiYF_4$ NCs are formed through an 'available intermediate phase' having a composition which is determined by the available cations in the reaction mixture. Moreover, we found that our approach is readily extendable to the isomorphous system $LiLuF_4$. However, our efforts to synthesise the corresponding $LiGdF_4$ NCs by these methods were unsuccessful. To demonstrate that also the synthesis of core/shell particle is feasible with our approach, upconversion particles with $LiYF_4$:Yb,Er/$LiYF_4$ core/shell structure were successfully prepared. The shell enhances the luminescence intensity by a factor of 35.

Summary

Main topics of this thesis are the synthesis and the characterization of monodisperse sub-10 nm sized alkali metal rare earth fluoride nanocrystals. In particular, nanocrystals of $NaREF_4$ (RE = La, Ce, Pr, Nd) and $LiREF_4$ (RE = Y, Gd, Lu) were studied, because their synthesis is hampered by instable polymorphs, decomposition reactions and the lack of conclusive information about the growth mechanism. In Chapter 1, a short introduction on nanoparticles, rare earth elements and rare earth fluoride nanocrystals is provided with special emphasis on the synthesis of alkali metal rare earth fluoride nanocrystals. Also, a detailed description of the aims of this work is given in this chapter. The theory for the formation of monodisperse nanocrystals and a short description on different analytical techniques used for the characterisation of the synthesised nanocrystals are given in Chapter 2.

Chapter 3 deals with the synthesis and characterisation of monodisperse sub-10 nm sized sodium rare earth fluoride nanocrystals of the lighter rare earths, $NaREF_4$ (RE = La, Ce, Pr, Nd). Synthesis procedures for the preparation of both polymorphs, hexagonal and cubic, of $NaLaF_4$, $NaCeF_4$, $NaPrF_4$ and $NaNdF_4$ nanocrystals are presented in detail. It is worthwhile to mention that some of these polymorphs are not reported in the thermodynamic phase diagrams of the bulk materials. Obviously, these materials are obtained as metastable compounds due to the low synthesis temperatures (200-300 °C). A detailed study on Ostwald ripening, size focusing and decomposition effects of these nanocrystals are also addressed in this chapter. It is found that Ostwald ripening of the β-phase of these nanomaterials is slow in basic reaction medium, whereas it is more pronounced in acid medium. As expected, Ostwald ripening leads to a broad size distribution. The stability of the cubic polymorphs was studied by heating the α-$NaREF_4$ nanocrystals in oleic acid/octadecene mixture at 300 °C, and it is found that these nanocrystals undergo decomposition into the corresponding trifluorides, REF_3. However, by supplying additional sodium fluoride, the decomposition can be avoided and the α-phase is effectively converted to its hexagonal polymorph with narrow size distribution. Further, the versatility of this procedure has been demonstrated by also preparing doped, especially Ce^{3+}, Pr^{3+} and Ce^{3+}/Tb^{3+} doped $NaREF_4$ nanocrystals, which show excellent luminescence properties.

It is known that the amount of sodium in sodium rare earth fluorides ($NaREF_4$) plays an important role in their phase stability, their phase transition from cubic to hexagonal, and their final size distribution. The phase diagram of $NaYF_4$ bulk material shows that the cubic phase of $NaYF_4$ (α-$NaYF_4$) is stable only at high temperatures and that its composition can be varied from $NaYF_4$ to α-$Na_5Y_9F_{32}$, i.e., Na/Y ratios from 1 to 0.55. In this thesis, however, extremely sodium deficient α-$NaYF_4$ nanocrystals (Na/Y ratio down to 0.1) with sizes of less than 10 nm could be prepared through a synthesis method presented in Chapter 4. The material is metastable at room temperature as is the cubic α-phase in general. The stability of these sodium deficient α-$NaYF_4$ nanocrystals were also studied by further heating in oleic acid/octadecene mixture at 300 °C. It is observed that the nanocrystals having Na/Y ratios of 0.3, 0.4 and 0.55 undergo classic Ostwald ripening, which leads to polydisperse nanocrystals. However, nanocrystals with Na/Y ratios smaller than 0.3 undergo partial decomposition into yttrium trifluoride, YF_3. Again, these highly sodium deficient α-phase $NaYF_4$ nanocrystals could be converted to the corresponding monodisperse β-phase particles by providing additional sodium compounds during the conversion.

In Chapter 5, approaches to synthesise monodisperse sub-10 nm lithium rare earth fluoride ($LiREF_4$, RE = Y, Gd and Lu) nanocrystals which are based on different precursor materials are described. Nanocrystals of highly sodium deficient cubic α-$NaYF_4$ (described in chapter 4), orthorhombic YF_3 nanocrystals (size less than 5 nm) or corresponding molecular precursors (Li-oleate, Na-oleate, Y-oleate and ammonium fluoride) were used as starting material for the preparation of tetragonal $LiYF_4$ nanocrystals in oleic acid and octadecene mixture. When highly sodium deficient α-$NaYF_4$ nanocrystals (Na/Y ratio 0.1, 0.2 and 0.3) were used as precursor particles, the formation of monodisperse sub-10 nm tetragonal $LiYF_4$ nanocrystals is observed, while precursor particles with a higher Na/Y ratio of 0.4 resulted in a mixture of tetragonal $LiYF_4$ and cubic α-$NaYF_4$ nanocrystals. When molecular precursors such as Na-oleate, Li-oleate, Y-oleate and ammonium fluoride were employed, cubic α-$NaYF_4$ nanocrystals are formed first as intermediate product which converts to tetragonal $LiYF_4$ particles at higher temperatures. Tetragonal $LiYF_4$ nanocrystals with a size of 12 nm are also obtained when small nanocrystals of orthorhombic YF_3 were used as precursor particles along with Li-oleate and ammonium fluoride. Such orthorhombic YF_3 particles are also formed at low temperatures as intermediate products if the corresponding molecular

precursors were used. So this approach provides new insights into the formation of intermediate phases during the synthesis of nanocrystals, which were not clear from previous studies. This thesis confirms that $LiYF_4$ nanocrystals are formed through an 'available intermediate phase' and formation of this 'available phase' is determined by the cations available in the reaction mixture. The same approach was successfully carried out for the preparation of tetragonal $LiLuF_4$ nanocrystals. The new approach can also be used for the synthesis of core/shell nanocrystals as demonstrated by the preparation of $LiYF_4$:Yb,Er/$LiYF_4$ upconversion nanocrystals. This core/shell nanocrystals show a 35 times enhancement in luminescence compared to the corresponding core particles. Finally, unsuccessful trials to synthesise $LiGdF_4$ nanocrystals are also mentioned in this chapter.

We believe that the newly developed synthesis methods and our studies on the formation intermediate phase may further facilitate research in the area.

References

[1] F. Antonii, „Panacea Aurea-Auro Potabile," *Hamburg: Bibliopolio Frobeniano,* 1618.

[2] E. Drexler, „There's Plenty of Room at the Bottom, Richard Feynman," *Pasadena,* 29 December 1959.

[3] L. Murr, *Microsc.Microana,* Vol. 13, p. 1118, 2007.

[4] A. Vaughan, *IEEE Elec. Insul. Mag.,* Vol. 4, p. 24, 2008.

[5] E. Roduner, *Chem. Soc. Rev.,* Vol. 35, p. 583, 2006.

[6] I. Freestone, N. l. Meeks, M. Sax and C. Higgitt, *Gold Bulletin,* Vol. 40, p. 270, 2007.

[7] R. P. Feynman, *J. Microelectromechanical Syst.,* Vol. 1, p. 60, 1992.

[8] R. Nagarajan and T. Alan Hatton, ''Nanoparticles: Synthesis, Stabilization, Passivation, and Functionalization'' *New York: American Chemical Society,* 2008.

[9] H. Gleiter and P. Marquardt, Vol. 75, p. 263, 1984.

[10] S. K. Ghosh and T. Pal, *Chem. Rev.,* Vol. 107, p. 4797, 2007.

[11] R. Birringer, H. Gleiter, H.-P. Klein, P. Marquardt, *Phys. Lett. A, Vol.* 2102, p. 365, 1984.

[12] K. B. Mogensen and K.Kneipp, *J. Phys. Chem. C,* Vol. 118, p. 28075, 2014.

[13] A. L. Stepanov, A. N. Golubev, S. I. Nikitin and Y. N. Osin, *Rev. Adv. Mater. Sci.,* Vol. 38, p. 160, 2014.

[14] Ö. Metin, V. Mazumder, S. Özkar and S. Sun, *J. Am. Chem. Soc.,* Vol. 132, p. 1468, 2010.

[15] M. R. Decan, S. Impellizzeri, M. L.Marin and J. C. Scaiano, *Nat.Comm.,* p. DOI: 10.1038/ncomms5612, 2014.

[16] B. I. Lemon and R. M. Crooks, *J. Am. Chem. Soc.,* Vol. 122, p. 12886, 2000.

[17] M. Gao, S. Kirstein and H. Möhwald, *J. Phys. Chem. B,* Vol. 102, p. 8360, 1998.

[18] J. Yang, H. I. Elim, Q. Zhang, J. Y. Lee, and W. Ji, *J. Am. Chem. Soc.,* Vol. 128, p. 11921, 2006.

[19] Y. W. Cao and U. Banin, *J. Am. Chem. Soc.,* Vol. 122, p. 9692, 2000.

[20] R. Xie, D. Battaglia and X. Peng, *J. Am. Chem. Soc.,* Vol. 129, p. 15432, 2007.

[21] S. Laurent, D. Forge, M. Port, A. Roch, C. Robic, L.V. Elst and R. N. Muller, *Chem. Rev.,* Vol. 108, p. 2064, 2008.

[22] Y. P. Wang, Y. T. Liao, C. H. Liu, J. Yu, J. C. Chen and K. C. Wu, *Biointerphases,* Vol. 10, p. 021005, 2015 .

[23] M. J. Bowers, J. R. McBride and S. J. Rosenthal, *J. Am. Chem. Soc.,* Vol. 127, p. 15378, 2005.

[24] J. M. Phillips , M. E. Coltrin, M. H. Crawford, A. J. Fischer, M. R. Krames, R. Mueller-Mach, G. O. Mueller, Y. Ohno, L. E. S. Rohwer, J. A. Simmons and J. Y. Tsao, *Laser and Photon. Rev.,* Vol. 1, p. 307, 2007.

[25] P. Kamat, *J. Phys. Chem. C,* Vol. 112, p. 18737, 2008.

[26] V. Subramanian, E. E. Wolf and P. V. Kamat, *J. Am. Chem. Soc.,* Vol. 126, p. 4943, 2004.

[27] L. Tarpani, D. Ruhlandt, L. Latterini, D. Haehnel, I. Gregor, J. Enderlein and A. I Chizhik, *Nano Letters,* Vol. 16, p. 4312, 2016.

[28] Z. R. Tian, J. A. Voigt, J. Liu, B. Mckenzie, M. J. Mcdermott, M. A. Rodriguez, H. Konishi and H. Xu, *Nat. Mater.,* Vol. 2, p. 821, 2003.

[29] Q. Xu, D. Jiang, T. Wang, S. Meng and M. Chen, *RSC Adv.,* Vol. 6, p. 55039, 2016.

[30] S. Anantharaj, P. E. Karthik, B. Subramanian and S. Kundu, *ACS Catal.,* Vol. 6, p. 4660, 2016.

[31] L. Weller, V. V. Thacker, L. O. Herrmann, E. A. Hemmig, A. Lombardi, U. F. Keyser and J. J. Baumberg, *ACS Photonics,* Vol. 3, p. 1589, 2016.

[32] E. L. Hu, D. T. Shaw, Nanostructure Science and Technology, Springer Netherlands, 1999.

[33] S. R. Taylor and S. M. Mclennan, The continental curst: its composition and evolution, Blackwell, Oxford, 1985.

[34] J. Hedrick, U. S. Geological Survey, Rare Earths, 2007.

[35] J. Hedrick, in *REE Handbook - The ultimate guide to Rare Earth Elements*, p. http://www.reehandbook.com/definition.html.

[36] Qi. Dai, M. E. Foley, C. J. Breshike, A. Lita and G. F. Strouse, *J. Am. Chem. Soc.,* Vol. 133, p. 15475, 2011.

[37] C. R. Ronda , T. Justel and H. Nikol, *J. Alloys Compd.,* Vol.2275-277, p. 669, 1998.

[38] C. C. Lin, W. -T. Chen, C. Chu, K. -W. Huang, C. -W. Yeh, B.-M. Cheng and R. -S. Liu, *Light: Science and Applications,* Vol. 5, p. e16066, 2016.

[39] S. Tanabe, *Int. J. Appl. Glass Sci.,* Vol. 6, p. 305, 2015.

[40] Z. Shan, D. Chen, Y. Yu, P. Huang, H. Lin and Y. Wang, *J. Mater. Sci.,* Vol. 45, p. 2775, 2010.

[41] B. Rohrig, *ACS Chem. Mater.,* p. 10, April/May 2015.

[42] R. F. Mendes, P. Silva, M. M. Antunes, A. A. Valente and F. A. Almeida Paz, *Chem. Commun.,* Vol. 51, p. 10807, 2015.

[43] A. Asati, S. Santra, C. Kaittanis, S. Nath and J. M. Perez, *Angew. Chem. Int. Ed.,* Vol. 48, p. 2308, 2009.

[44] A. E. C. Palmqvist, M. Wirde and M. Muhammed, *Nano Struc. Mater.,* Vol. 11, p. 995, 1999.

[45] E. T. C. Vogt and B. M. Weckhuysen, *Chem. Soc. Rev.,* Vol. 44, p. 7342, 2015.

[46] D. Wallace, *Am.Cheml Soc.,* Vol. Chapter 6 , p. 101, 1981.

[47] H. Hattori, *Chem. Rev.,* Vol. 95, p. 537, 1995.

[48] K. Rajesh, P. Shajesh, O. Seidel, P. Mukundan and K. G. K. Warrier, *Adv. Funct. Mater.,* Vol. 17, p. 2007, 1682.

[49] B. Zhu, X. Liu, Z. Zhu and R. Ljungberg, *Int. J. Hydrogen Energ.,* Vol. 33, p. 3385, 2008.

[50] G. A. Sotiriou, M. Schneider and S. E. Pratsinis, *J. Phys. Chem. C,* Vol. 115, p. 1084, 2011.

[51] C. -C. Huang, T. -Y. Liu, C. -H. Su, Yi. -W. Lo, J. -H. Chen and C.- S. Yeh, *Chem. Mater. ,* Vol. 20, p. 3840, 2008.

[52] W. Mao, M. Wilde, T. Chikada, S. Ogura, K. Fukutani, T. Terai and H. Matsuzaki, *J. Phys. Chem. C,* Vol. 120, p. 15147, 2016.

[53] J. Miyawaki, S. Matsumura, R. Yuge, T. Murakami, S. Sato, A. Tomida, T. Tsuruo, T. Ichihashi, T. Fujinami, H. Irie, K. T. S. Iijima, K. Shiba and M. Yudasaka, *J. Phys. Chem. C,* Vol. 120, p. 15147, 2016.

[54] G. Bühler and C. Feldmann, *Angew. Chem. Int. Ed.,* Vol. 45, p. 486, 2006.

[55] Y. P. Fang, A. W. Xu, R. Q. Song, H. X. Zhang, L. P. You, J. C. Yu and H. Q. Liu, *J. Am. Chem. Soc.,* Vol. 125, p. 16025, 2003.

[56] J. A. Dorman, J. H. Choi, G. Kuzmanich and J. P. Chang, *J. Phys. Chem. C,* Vol. 116, p. 12854, 2012.

[57] J. K. Marsh, *Nature,* Vol. 163, p. 998, 1949.

[58] A. W. Wylie, *Nature,* Vol. 160, p. 830, 1947.

[59] S. H. Ahmed, O. S. Helaly and M. S. Abd El-Ghany, *Int.J.Inor.Bio.ic Chem. ,* Vol. 5, p. 1, 2015.

[60] M. D. Regulacio, N. Tomson and S. L. Stoll, *Chem. Mater.,* Vol. 17, p. 3114, 2005.

[61] M. Abdesselem, M. Schoeffel, I. Maurin, R. Ramodiharilafy, G. Autret, O. Clément, P. L. Tharaux, J. P. M. Abdesselem, M. Schoeffel, I. Maurin, R. Ramodiharilafy, G. Autret, O. Clément, P. L. Tharaux, J. P. Boilot, T. Gacoin, C. Bouzigues and A. Alexandrou, *ACS Nano,* Vol. 8, p. 11126, 2014.

[62] J. R. Gambino and C. J. Guare, *Nature,* Vol. 198, p. 1084, 1963.

[63] S. Heer, K. Kömpe, H. U. Güdel and M. Haase, *Adv. Mater.,* Vol. 16, p. 2102, 2004.

[64] F. Wang and X.Liu , *Chem. Soc. Rev.,* Vol. 38, p. 976, 2009.

[65] H. Schäfer and M. Haase, *Angew. Chem., Int. Ed. ,* Vol. 50, p. 5808, 2011.

[66] K. W. Krämer, D. Biner, G. Frei, H.U.Güdel and M. P. Hehlen, *Chem. Mater.,* Vol. 16, p. 1244, 2004.

[67] N. J. J. Johnson, A. Korinek, C. Dong and F. C. J. M. van Veggel, *J. Am. Chem. Soc.,* Vol. 134, p. 11068, 2012.

[68] R. T. Wegh, H. Donker, K. D. Oskam and A. Meijerink, *Science,* Vol. 283, p. 663, 1999.

[69] P. Ghosh, S. Tang and A. V. Mudring, *J. Mater. Chem.,* Vol. 21, p. 8640, 2011.

[70] X. P. Chen, X. Y. Huang and Q. Y. Zhang, *J. Appl. Phys.,* Vol. 106, p. 063518, 2009.

[71] L. Xu, S.Y. Zhang and J. Q. Xu, *Laser Phys. Lett.,* Vol. 7, p. 303, 2010.

[72] L. Aarts, B. M. van der Ende and A. Meijerink, *J. Appl. Phys.,* Vol. 106, p. 023522, 2009.

[73] N. J. J. Johnson, W. Oakden, G. J. Stanisz, R. S. Prosser and F. C. J. M. van Veggel, *Chem. Mater.,* Vol. 23, p. 3714, 2011.

[74] B. Y. Park, J. H. Kim, K. T. Lee, K. S. Jeon, H. B. Na, J. H. Yu, H. M. Kim, N. Lee, S. H. Choi, S. Baik, H. Kim, S. P. Park, B. Park, Y. W. Kim, S. H. Lee, S. Y. Yoon, I. C. Song, W. K. Moon, Y. D. Suh and T. Hyeon, *Adv. Mater.,* Vol. 21, p. 4467, 2009.

[75] L. Xu, S. Y. Zhang and J. Q. Xu, , *Laser Phys. Lett.,* Vol. 7, p. 303, 2010.

[76] S. Baldell, *Nat. Photonics,* Vol. 5, p. 75, 2011.

[77] H. Zhu, X. Chen,L. M. Jin, Q. J. Wang, F. Wang and S. F. Yu, *ACS Nano ,* Vol. 7, p. 11420, 2013.

[78] M. van der Ende, L. Aarts and A. Meijerink, *Phys. Chem. Chem. Phys.,* Vol. 11, p. 11081, 2009.

[79] T. Trupke, M. A. Green and P. Würfel, *J. Appl. Phys,* Vol. 92, p. 4117, 2002.

[80] A. A. Ansari, A. K. Parchur, B. Kumar and S. B. Rai, *J. Fluoresc.,* Vol. 26, p. 1151, 2016.

[81] L. Aarts, B. M. van der Ende and A. Meijerink, *J. Appl. Phys.,* Vol. 106, p. 023522,

2009.

[82] L.M. Yao, J. Zhou, J.L. Liu , W. Feng and F.Y. Li, *Adv Funct Mater.,* Vol. 22, p. 2667, 2012.

[83] Q. Liu, J. Peng , L. Sun and F. H. Li, *ACS Nano,* Vol. 5, p. 8040, 2011.

[84] H. S. Mader and O. S. Wolfbeis, *Anal. Chem.,* Vol. 82, p. 5002, 2010.

[85] R. Alia, S. M. Saleha, R. J. Meiera, H .A. Azabb, I. I. Abdelgawadc and O. S. Wolfbeis, *Sensors and Actuators B: Chemica,* Vol. 150, p. 126, 2010.

[86] C. Liu, Z. Wang, H. Jiaa and Z. Li, *Chem. Commun.,* Vol. 47, p. 4661, 2011.

[87] P. Zhang, S. Rogelj, K. Nguyen and D. Wheeler, *J. Am. Chem.Soc.,* Vol. 128, p. 12410, 2006.

[88] C. Wang, X. Lia and F. Zhang, *Analyst,* Vol. 141, p. 3601, 2016.

[89] B. Zhou, B. Shi, D. Jin and X. Liu, *Nat. Nanotechnol.,* Vol. 10, p. 924, 2015.

[90] C. Chen, C. Li and Z. Shi, *Adv. Sci.,* Vol. 3, p. 1600029, 2016.

[91] F. Wang, D. Banerjee, Y. Liu, X. Chenc and X. Liu, *Analyst,* Vol. 135, p. 1839, 2010.

[92] J. Zhou, Z. Liu and F. Y. Li, *Chem. Soc. Rev.,* Vol. 41, p. 1323, 2012.

[93] M. González-Béjar, L. Francés-Soriano and J. Pérez-Prieto, *Front Bioeng Biotechnol.,* Vol. 4, p. 47, 2016.

[94] W. Zheng, P. Huang, D. Tu, E. Ma, H. Zhuab and X. Che, *Chem. Soc. Rev.,* Vol. 44, p. 1379, 2015.

[95] X. Wu, Li. Xu, W. Ma, L. Liu, H. Kuang, N. A. Kotovand and C. Xu, *Adv. Mater.,* Vol. 28, p. 5907, 2016.

[96] H. Guo, N. M. Idris and Y. Zhang, *Langmuir,* Vol. 27, p. 2854, 2011.

[97] J. Shi, F. Tian, J. Lyu and M. Yang, *J. Mater. Chem.,* Vol. 3, p. 6989, 2015.

[98] A. Bagheri, H. Arandiyan, C. Boyer and M. Lim, *Adv. Sci.,* Vol. 3, p. 1500437, 2016.

[99] S. He, K. Krippes, S. Ritz, Z. Chen, A. Best, H. Butt, V. Mailänderab and S. Wu, *Chem. Commun.,* Vol. 51, p. 431, 2015.

[100] J. Liu, W. Bu, L. Pan and J. Shi, *Angew. Chem. Int. Ed.,* Vol. 52, p. 4375, 2013.

[101] N. J. J. Johnson, W. Oakden, G. J. Stanisz, R. S. Prosser and F. C. J. M. van Veggel, *Chem. Mater.,* Vol. 23, p. 3714, 2011.

[102] G. Chen, T. Y. Ohulchanskyy, W. C. Law, H. Ågrenb and P. N. Prasad, *Nanoscale ,* Vol. 3, p. 2003, 2011.

[103] H. Guo, Z. Li, H. Qian, Y. Hu and I. N. Muhammad, *Nanotechnology ,* Vol. 21, p. 125602, 2010.

[104] F. Chen, W. Bu, S. Zhang, X. Liu, J. Liu, H. Xing, Q. Xiao, L. Zhou, W. Peng, L. Wang and J. Shi, *Adv. Funct. Mater. ,* Vol. 21, p. 4285, 2011.

[105] A. Hischemöller, J. Nordmann, P. Ptacek, K. Mummenhoff and M. Haase, *J. Biomed. Nanotechnol.,* Vol. 5, p. 278, 2009.

[106] J. Nordmann, S. Buczka, B. Voss, M. Haase and K. Mummenhoff, *J. Mater. Chem. B,* Vol. 3, p. 144, 2015.

[107] H. X. Mai, Y. W. Zhang, R. Si, Z. G. Yan, L. S. Sun, L. P. You and C. H. Yan, *J. Am. Chem. Soc.,* Vol. 128, p. 6426, 2006.

[108] S. Bertaina, S. Gambarelli, A. Tkachuk, I. N. Kurkin, B. Malkin, A. Stepanov and B. Barbara, *Nature Nanotechnology,* Vol. 2, p. 39, 2007.

[109] Y. W. Zhang, X. Sun, R. Si, L. P. You and C. H. Yan, *J. Am. Chem. Soc.,* Vol. 127, p. 3260,

2005.
[110] X. Sun, Y. W. Zhang, Y. P. Du, Z. G. Yan, R. Si, L. P. You and C. H. Yan, *Chem.–Eur. J.,* Vol. 13, p. 2320, 2007.
[111] G. S. Yi and G. M. Chow, Adv. Funct. Mater., Vol. 16, p. 2324, 2006.
[112] J. C. Boyer, F. Vetrone, L. A. Cuccia and J. A. Capobianco, *J. Am. Chem. Soc.,* Vol. 128, p. 7444, 2006.
[113] J.N. Shan, W.J. Kong, R. Wei, N. Yao and Y.G. Ju, *J. Appl. Phys.,* Vol. 107, p. 054901, 2010.
[114] J. N. Shan and Y. G. Ju, *Appl. Phys. Lett.,* Vol. 91, p. 123103, 2007.
[115] J. N. Shan, M. Uddi, R. Wei, N. Yao and Y. G. Ju, *J. Phys. Chem. C,* Vol. 2114, p. 2452, 2010.
[116] J. N. Shan and Y. G. Ju, *Nanotechnology,* Vol. 20, p. 275603, 2009.
[117] H. Zhang, Y. J. Li, Y. C. Lin, Y. Huang and X. F. Duan, *Nanoscale,* Vol. 3, p. 963, 2011.
[118] R. Naccache, F. Vetrone, V. Mahalingam, L. A. Cuccia and J. A. Capobianco, *Chem. Mater.,* Vol. 21, p. 717, 2009.
[119] N. Bogdan, F. Vetrone, R. Roy and J. A. Capobianco, *J. Mater. Chem.,* Vol. 20, p. 7543, 2010.
[120] G. Y. Chen, T. Y. Ohulchanskyy, R. Kumar, H. Agren and P. N. Prasad, *ACS Nano,* Vol. 4, p. 3163, 2010.
[121] Q. Q. Zhan, J. Qian, H. J. Liang, G. Somesfalean, D. Wang, S. L. He, Z. G. Zhang and S. Andersson-Engels, *ACS Nano,* Vol. 5, p. 3744, 2011.
[122] V. Mahalingam, F. Vetrone, R. Naccache, A. Speghini and J. A. Capobianco, *Adv. Mater.,* Vol. 21, p. 4025, 2009.
[123] V. Mahalingam, R. Naccache, F. Vetrone and J. A. Capobianco, *Chem.–Eur. J.,* Vol. 15, p. 9660, 2009.
[124] V. Mahalingam, F. Vetrone, R. Naccache, A. Speghini and J. A. Capobianco, *J. Mater. Chem.,* Vol. 19, p. 3149, 2009.
[125] Y. Wei, F.Q. Lu, X. R. Zhang and D. P. Chen, *Chem. Mater.,* Vol. 18, p. 5733, 2006.
[126] C. H. Liu, H. Wang, X. R. Zhang and D. P. Chen, *J. Mater. Chem.,* Vol. 19, p. 489, 2009.
[127] C. H. Liu, H. Wang, X. Li and D. P. Chen, *J. Mater. Chem.,* Vol. 19, p. 3546, 2009.
[128] J. N. Shan, X. Qin, N. Yao and Y. G. Ju, *Nanotechnology,* Vol. 18, p. 445607, 2007.
[129] Y. Wei, F. Q. Lu, X. R. Zhang and D. P. Chen, *Chem. Mater.,* Vol. 18, p. 5733, 2006.
[130] C. H. Liu, H. Wang, X. R. Zhang and D. P. Chen, *J. Mater. Chem.,* Vol. 19, p. 489, 2009.
[131] Z. Li and Y. Zhang, *Angew. Chem. Int. Ed.,* Vol. 45, p. 7732, 2006.
[132] C. Burda, X. B. Chen, R. Narayanan and M. A. El-Sayed, *Chem.Rev.,* Vol. 105, p. 1025, 2005.
[133] J. Yang, C. M. Zhang, C. Peng,C. X. Li, L. L. Wang, R. T. Chai and J. Lin, *Chem.–Eur. J.,* Vol. 15, p. 4649, 2009.
[134] J. Yang, C.M. Zhang, C. X. Li, Y. N. Yu and J. Lin, *Inorg. Chem.,* Vol. 47 , p. 7262, 2008.
[135] J. Yang, C. K. Lin, Z. L. Wang and J. Lin, *Inorg. Chem.,* Vol. 45, p. 8973, 2006.
[136] Y. D. Yin and A. P. Alivisatos, *Nature,* Vol. 437, p. 664, 2005.
[137] A. R. Tao, S. Habas and P. D. Yang, *Small,* Vol. 4, p. 310, 2008.
[138] X. Wang, J. Zhuang, Qi. Peng and Y. Li, *Nature,* Vol. 437, p. 121, 2005.
[139] J. L. Zhuang, L. F. Liang, H. H. Y. Sung, X. F. Yang, M. M. Wu, I. D. Williams, S. H. Feng

and Q. Su, *Inorg. Chem,* Vol. 46, p. 5404, 207.

[140] M. F. Zhang, H. Fan, B. J. Xi, X. Y. Wang, C. Dong and Y. T. Qian, *J. Phys. Chem. C,* Vol. 111, p. 6652, 2007.

[141] X. Liang, X. Wang, J. Zhuang, Q. Peng and Y. D. Li, *Inorg. Chem.,* Vol. 46, p. 6050, 2007.

[142] Y. J. Sun, Y. Chen, L. J. Tian, Y. Yu, X. G. Kong, J. W. Zhao and H. Zhang, *Nanotechnology,* Vol. 18, p. 275609, 2007.

[143] J. W. Zhao, Y. J. Suan, X. G. Kong, L. J. Tian, Y. Wang, L. P. Tu, J. L. Zhao and H. Zhang, *J. Phys. Chem. ,* Vol. 112, p. 15666, 2008.

[144] R. X. Yan and Y. D. Li , *Adv. Funct. Mater.,* Vol. 15, p. 763, 2005.

[145] J. L. Lemyre and A. M Ritcey, *Chem. Mater.,* Vol. 17, p. 3040, 2005.

[146] M. He, P. Huang, C. Zhang, F. Chen, C. Wang, J. Ma, R. He and D. Cui , *Chem. Commun.,* Vol. 47, p. 9510, 2011.

[147] P. Li, Q. Peng and Y. Li, *Adv. Mater.,* Vol. 21, p. 1945, 2009.

[148] L. Wang, P. Li and Y. Li, *Adv. Mater.,* Vol. 19, p. 3304, 2007.

[149] D. Xu, C. Liu, J. Yan, S. Yang and Y. Zhang, *J. Phys. Chem. C,* Vol. 119, p. 6852, 2015.

[150] L. Wang, W. Qin, Z. Liu, D. Zhao, G. Qin, W. Di and C. He, *Opt. Express,* Vol. 20, p. 7602, 2012.

[151] W. Jiang, B. Y. S. Kim, J. T. Rutka and W. C. W. Chan, *Nat. Nanotechnol.,* Vol. 3, p. 145, 2008.

[152] J. Ladol, H. Khajuria, S. Khajuria and H. N. Sheikh, *Bull. Mater. Sci. ,* Vol. 39, p. 943, 2016.

[153] F. Zhang, J. Li, J. Shan, L. Xu and D. Zhao, *Chem. Eur. J. ,* Vol. 15, p. 11010, 2009.

[154] F. Shi, J. Wang, X. Zhai, D. Zhao and W. Qin, *Cryst. Eng. Comm.,* Vol. 13, p. 3782, 2011.

[155] F. Zhang, Y. Wan, T. Yu, F. Zhang, Y. Shi, S. Xie, Y. Li, L. Xu, B. Tu and D. Zhao, *Angew. Chem. Int. Ed,* Vol. 46, p. 7976, 2007.

[156] F. Wang, Y. Han, C. S. Lim, Y. Lu, J. Wang, J. Xu, H. Chen, C. Zhang, M. Hong and X. Liu, *Nature,* Vol. 463, p. 1061, 2010.

[157] J. W. Stouwdam and F. C. J. M. van Veggel, *Nano Lett.,* Vol. 2, p. 733, 2002.

[158] Z. Li and Y. Zhang, *Angew. Chem., Int. Ed.,* Vol. 45, p. 7732, 2006.

[159] F. Wang, D. K. Chatterjee, Z. Li, Y. Zhang, X. Fan and M. Wang, *Nanotechnology,* Vol. 17, p. 5786, 2006.

[160] S. Sivakumar, F. C. J. M van Veggel and M. Raudsepp, *J. Am. Chem. Soc.,* Vol. 127, p. 12464, 2005.

[161] V. Sudarsan, S. Sivakumar, C. J. M. van Veggel and M. Raudsepp, *Chem. Mater.,* Vol. 17, p. 4736, 2005.

[162] S. Sivakumar, J.-C. Boyer, E. Bovero and F. C. J. M. van Veggel, *J. Mater. Chem.,* Vol. 19, p. 2392, 2009.

[163] Y. Wei Y, F. Q. Lu , X. R. Zhang and D. P. Chen, *J Alloys Compd.,* Vol. 455, p. 376, 2008.

[164] H. Q. Wang and T. Nann, *ACS Nano,* Vol. 3, p. 3804, 2009.

[165] V. K. LaMer and R. H. Dinegar, *J.Am.Chem.Sco.,* Vol. 72, p. 4847, 1950.

[166] N. T. K. Thanh, N. Maclean and S. Mahiddine, *Chem. Rev.,* Vol. 114, p. 7610, 2014.

[167] C. Wagner, *Z. Elektrochem.,* Vol. 65, p. 581, 1961.

[168] T. Sugimoto, *Adv. Colloid. Interface. Sci.,* Vol. 28, p. 165, 1987.

[169] I. M Lifshitz and V.V. Slyozov, *J. Phys. Chem. Solids,* Vol. 19, p. 35, 1961.

[170] P. Laurencot, *SIAM J. Math. Anal.,* Vol. 34, p. 257, 2002.

[171] D. Talapin, A. Rogach, M. Haase and H. Weller, *J. Phys.Chem. B,* Vol. 105, p. 12278, 2001.

[172] Y. Yin and A. P. Alivisatos, *Nature,* Vol. 437, p. 664, 2005.

[173] W. Ostwald, M. Bodenstein, K. Clusius, K. F. Bonhoeffer and H. Falkenhagen, *Zeitschrift für physikalische Chemie, The University of California: Akademische Verlagsgesellschaft Geest and Portig,* 1900.

[174] T. Vossmeyer, L. Katsikas, M. Giersig, I. Popovic, K. Diesner, A. Chemseddine, A. Eychmueller and H. Wellerr, *J. Phys. Chem.,* Vol. 98, p. 7665, 1994.

[175] C. B. Murray, D. J. Norris and M. G. Bawendi, *J. Am. Chem. Soc.,* Vol. 115, p. 1993, 8706.

[176] H. Reiss, *J. Chem. Phys.,* Vol. 19, p. 482, 1951.

[177] X. Peng, J. Wickham and A. P. Alivisatos, *J. Am. Chem. Soc.,* Vol. 120, p. 5343, 1998.

[178] R. E. Thoma, H. Insley and G. M. Hebert, *Inorg. Chem.,* Vol. 5, p. 1222, 1966.

[179] J. H. Zeng, Z. H. Li, J. Su, L. Wang, R. Yan and Y. Li, *Nanotechnology,* Vol. 17, p. 3549, 2006.

[180] J. Shan, X. Qin, N. Yao and Y. Ju, *Nanotechnology,* Vol. 18, p. 445607, 2007.

[181] S. Li, T. Xie, Q. Peng and Y. Li , *Chem. Eur. J.,* Vol. 15, p. 2512, 2009.

[182] X. Wu, Q. Zhang, X. Wang, H. Yang and Y. Zhu, *Eur. J. Inorg. Chem.,* Vol. 2011, p. 2158, 2011.

[183] S. Zeng, G. Ren, C. Xu and Q. Yang, *Cryst. Eng. Comm.,* Vol. 13, p. 1384, 2011.

[184] B. Voß, J. Nordmann, A. Uhl, R. Komban and M. Haase, *Nanoscale,* Vol. 5, p. 806, 2013.

[185] J. Park, K. An, Y. Hwang, J. Park, H. Noh, J. Kim, J. Park, N. Hwang and T. Hyeon, *Nat. Mater.,* Vol. 3, p. 891, 2004.

[186] R. Komban, P. J. Klare, B. Voss, J. Nordmann, H. J. Steinhoff and M. Haase, *Angew. Chem., Int. Ed.,* Vol. 51, p. 6506, 2012.

[187] B. Voss and M. Haase, *ACS Nano,* Vol. 7, p. 11242, 2013.

[188] C. Liu, Hui Wang, X. Zhanga and D. Chen, *J. Mater. Chem.,* Vol. 19, p. 489, 2009.

[189] A. Srivastava, *J. Lumin.,* Vol. 129, p. 1419, 2009.

[190] M. Nikl, A. Yoshikawa, A. Vedda and T. Fukuda, *J. Cryst. Growth,* Vol. 292, p. 416, 2006.

[191] H. Höppe, *Angew. Chem., Int. Ed.,* Vol. 48, p. 3572, 2009.

[192] K. Kömpe, H. Borchert, J. Storz, A. Lobo, S. Adam, T.s Möller and M. Haase, *Angew. Chem. Int. Ed.,* Vol. 42, p. 2003, 2003.

[193] X. D. Zhang, X. Jin, D. F. Wang, S. Z. Xiong and X. H. Geng, *Phys. Status Solid C,* Vol. 7, p. 1128, 2010.

[194] T. Rinkel , A. N. Raj, S. Dühnen, M. Haase , *Angew Chem Int Ed Engl. ,* Vol. 55, p. 1164, 2016.

[195] T. Rinkel, J. Nordmann, A. N. Raj and M. Haase, *Nanoscale,* Vol. 6, p. 14523, 2014.

[196] J. Hu, H. Xia, H. Hu, Y. Zhang, H. Jiang and B. Chen, *J. Appl. Phys.,* Vol. 112, p. 073518, 2012.

[197] Z. P. Cai, B. Qu, Y. J. Cheng, S. Y. Luo, B. Xu, H. Y. Xu, Z. Q. Luo, P. Camy, J. L. Doualan, and R. Moncorgé, *Opt. Exp.,* Vol. 22, p. 31722, 2014.

[198] G. Stoeppler, D. Parisi, M. Tonelli and M. Eichhorn, *Opt. Lett.,* Vol. 37, p. 1163, 2012.

[199] P. W. Metz, F. Reichert, F. Moglia, S. Müller, D.-Timo Marzahl, C. Kränkel and G. Huber, *Opt. Lett.,* Vol. 39, p. 3193, 2014.

[200] J. X. Hu, H. P. Xia, H. Y. Hu, Y. P. Zhang, H. C. Jiang and B. J. Chen, *J. Appl. Phys.,* Vol. 112, p. 073518, 2012.

[201] R. Martín-Rodríguez and A. Meijerink, *J. Luminesc.,* Vol. 147, p. 147, 2014.

[202] G. Jalani, R. Naccache, D. H. Rosenzweig, S. Lerouge,L. Haglund, F. Vetrone and M. Cerruti, *Nanoscale,* Vol. 7, p. 11255, 2015.

[203] M. Wang, Z. Chen,W. Zheng, H. Zhu, S. Lu , E. Ma, D. Tu, S. Zhou, M. Huang and X. Chen, *Nanoscale,* Vol. 6, p. 8274, 2014.

[204] P. Huang, Wei Zheng, S. Zhou, D. Tu, Z. Chen, H. Zhu, R. Li, E. Ma, M. Huang and X. Chen, *Angew. Chem. Int. Ed.,* Vol. 53, p. 1252, 2014.

[205] S. Y. Kim,Y-H. Won and H. S. Jang, *Sci. Report.,* Vol. 5, p. 7866, 2014.

[206] J. Wanga, F. Wanga, J. Xub, Y. Wangb, Y. Liuc, X. Chenc, H. Chen and X. Liu, *Comptes Rendus Chimie,* Vol. 13, p. 731, 2010.

[207] X. Xue, S. Uechi, R. N. Tiwari, Z. Duan, M. Liao, M. Yoshimura, T. Suzuki and Y. Ohishi, *Optical Materials Express,* Vol. 3, p. 989, 2013.

[208] T. Paik, A.-Marie Chacko, J. L. Mikitsh, J. S. Friedberg, D. A. Pryma and C. B. Murray, *ACS Nano,* Vol. 9, p. 8718, 2015.

[209] Q. Dou and Y. Zhang, *Langmuir,* Vol. 27, p. 13236, 2011.

[210] D. Yang, Y. Dai, P. Ma, X. Kang, M. Shang, Z. Cheng, C. Li and J. Lin, *J. Mater. Chem.,* Vol. 22, p. 20618, 2012.

[211] M. Banski, M. Afzaal, D. Cha, X. Wang, H. Tan, J. Misiewicza and A. Podhorodeck, *J. Mater. Chem. C,* Vol. 2, p. 9911, 2014.

[212] S. Dühnen, T. Rinkel and M. Haase, *Chem. Mater.,* Vol. 27, p. 4033, 2015.

List of Figures

Appendix

A.1. List of Figures in Appendix

A.2. TEM Histogram

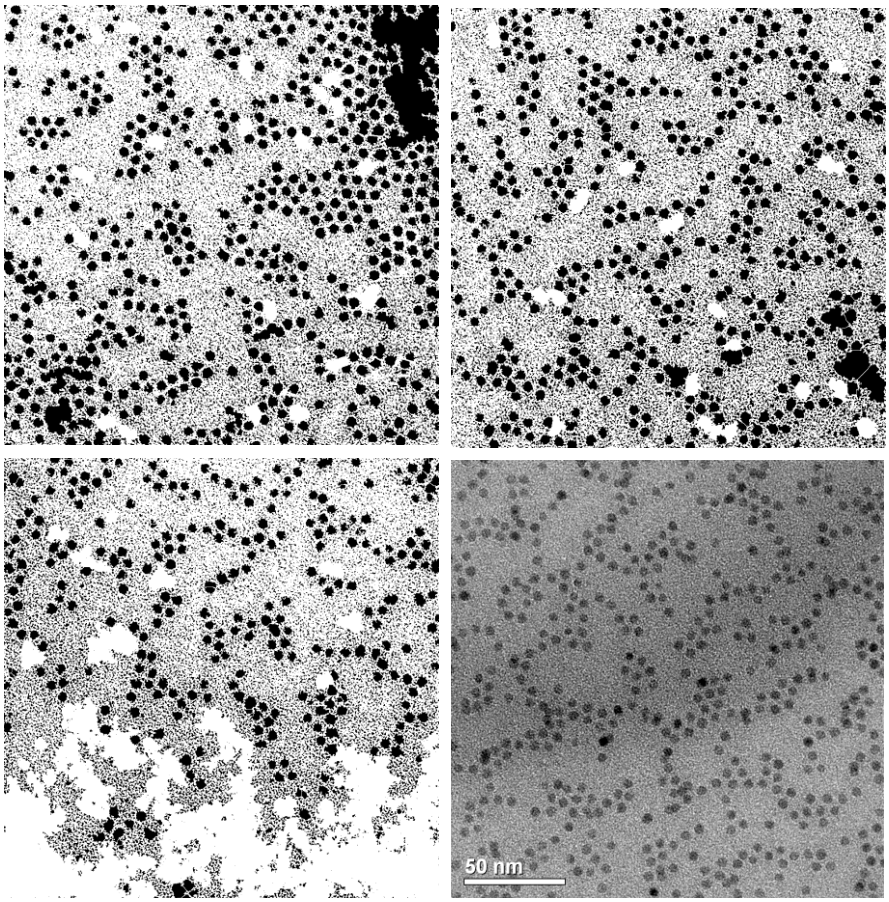

Figure A. 1: Black and white images of the TEM micrograph for the determination of the histogram in the case of NCs of hexagonal β-$NaNdF_4$ obtained the reaction of the rare earth oleates with ammonium fluoride in oleylamine/oleic acid/octadecene for 90 min at 240 °C. The original micrograph is presented at the bottom right to show the scaling.

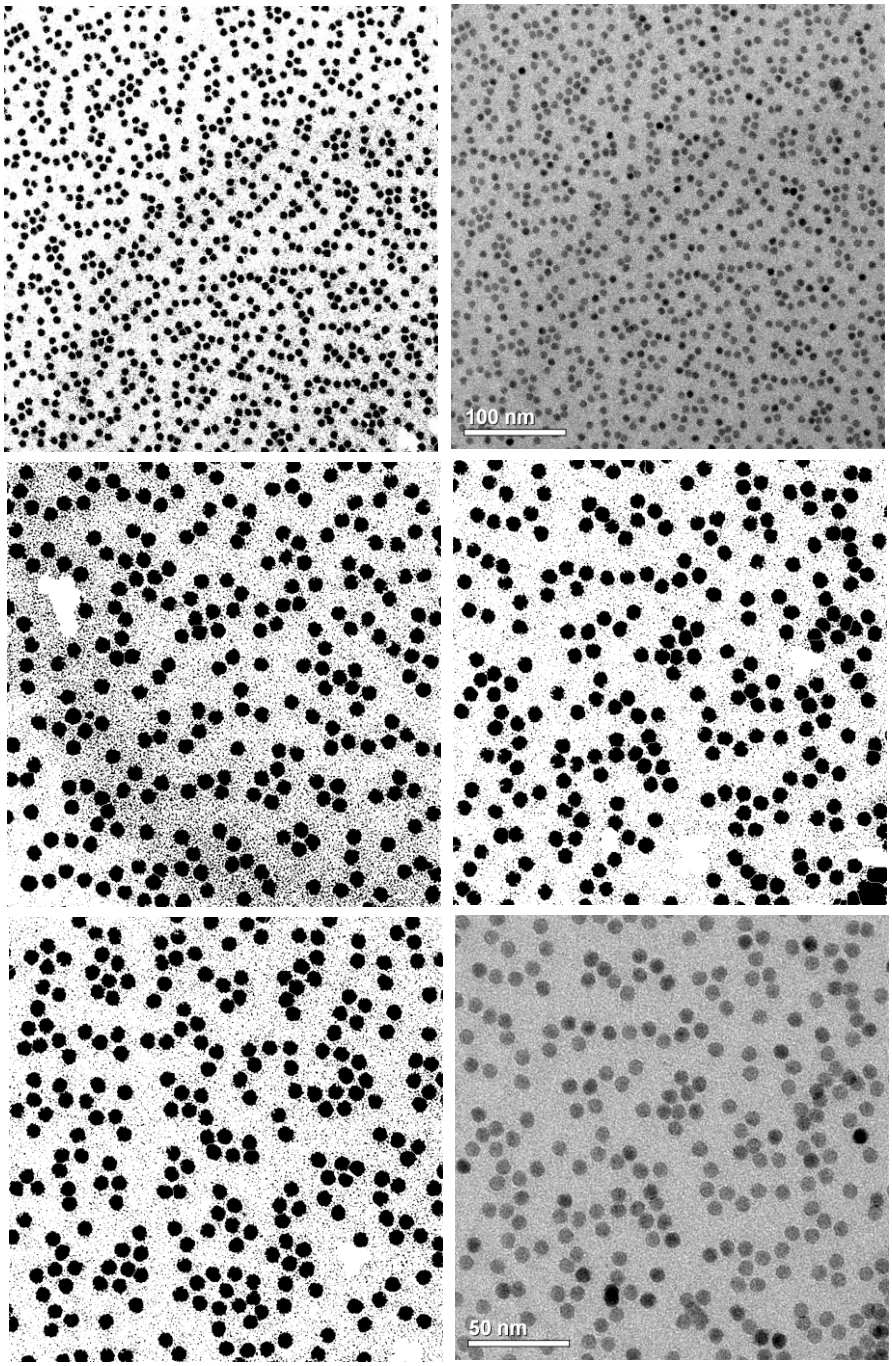

Figure A. 2: Black and white images of the TEM micrographs for the determination of the histogram in the case of NCs of hexagonal β-$NaLaF_4$ obtained the reaction of the rare earth oleates with ammonium fluoride in oleylamine/oleic acid/octadecene for 90 min at 240 °C. The original micrographs are presented at the upper and bottom right to show the scaling.

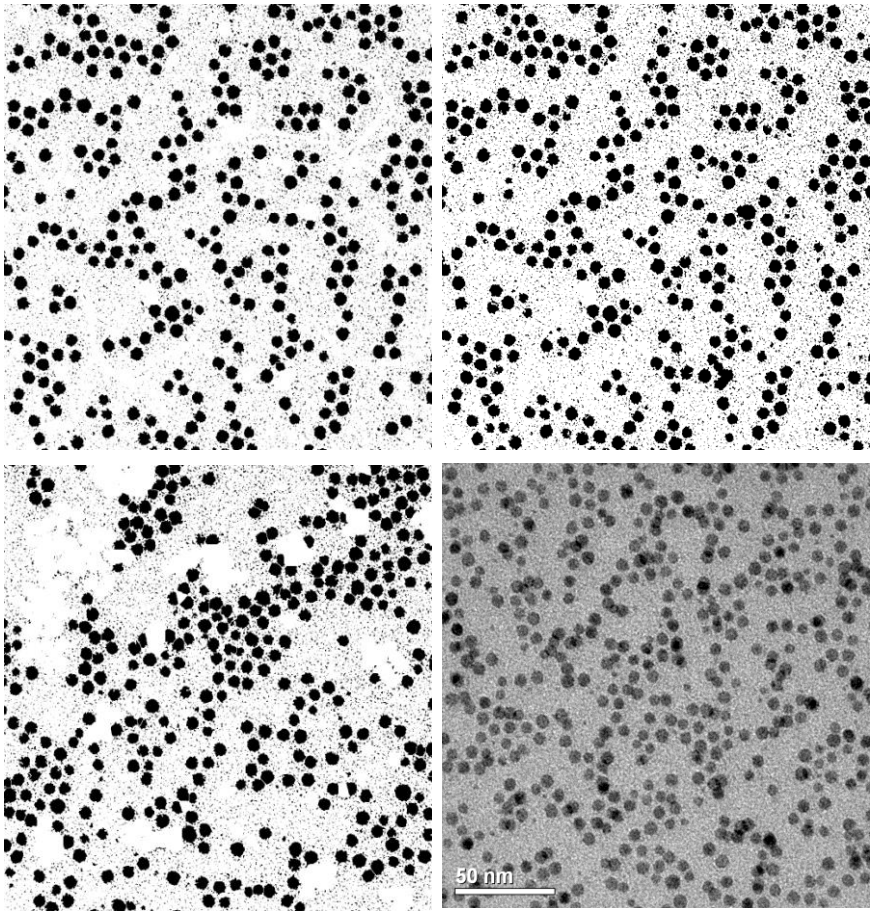

Figure A. 3: Black and white images of the TEM micrograph for the determination of the histogram in the case of NCs of hexagonal β-$NaCeF_4$ obtained the reaction of the rare earth oleates with ammonium fluoride in oleylamine/oleic acid/octadecene for 90 min at 240 °C. The original micrograph is presented at the bottom right to show the scaling.

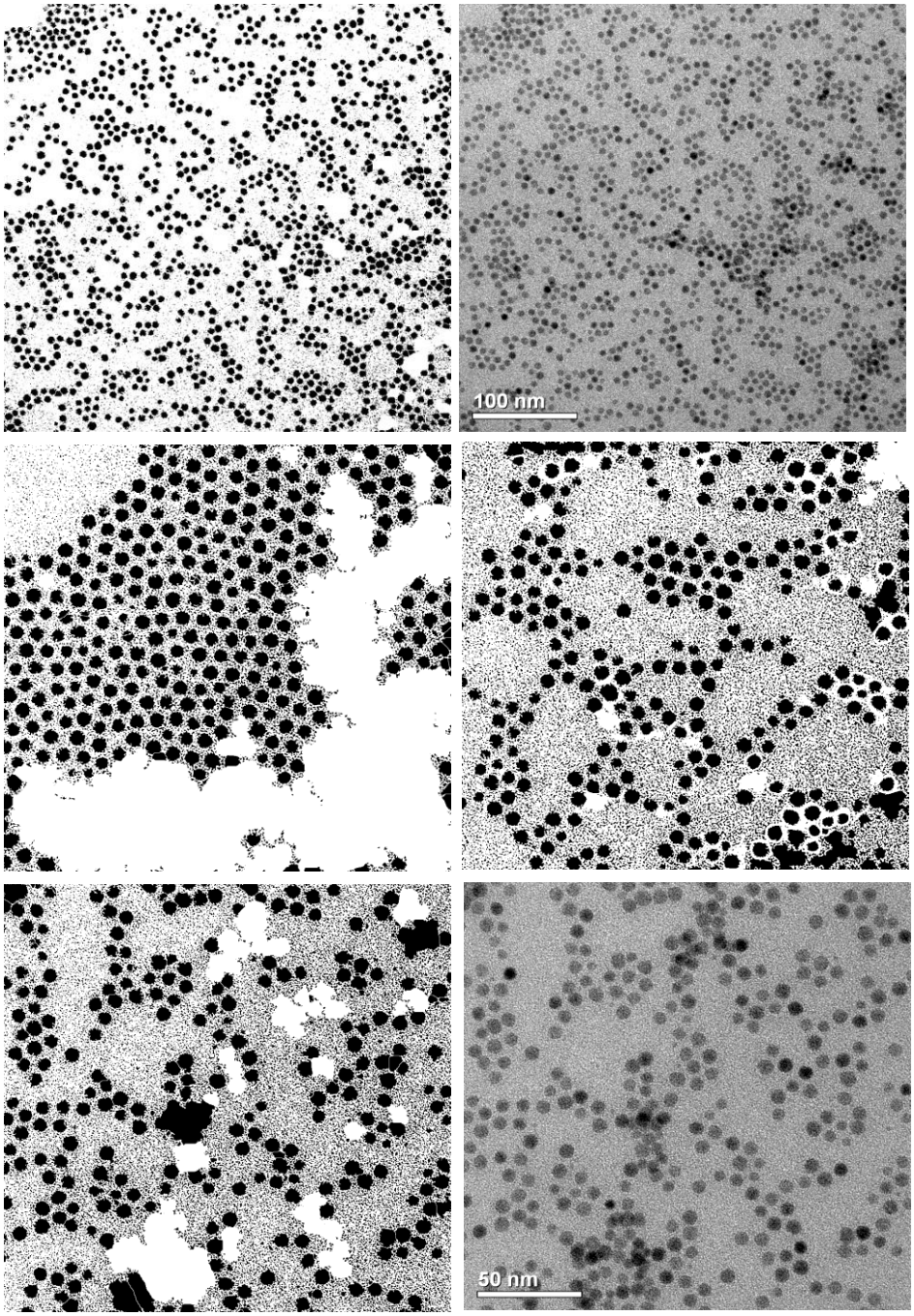

Figure A. 4: Black and white images of the TEM micrographs for the determination of the histogram in the case of NCs of hexagonal β-$NaPrF_4$ obtained the reaction of the rare earth oleates with ammonium fluoride in oleylamine/oleic acid/octadecene for 90 min at 240 °C. The original micrographs are presented at the upper and bottom right to show the scaling.

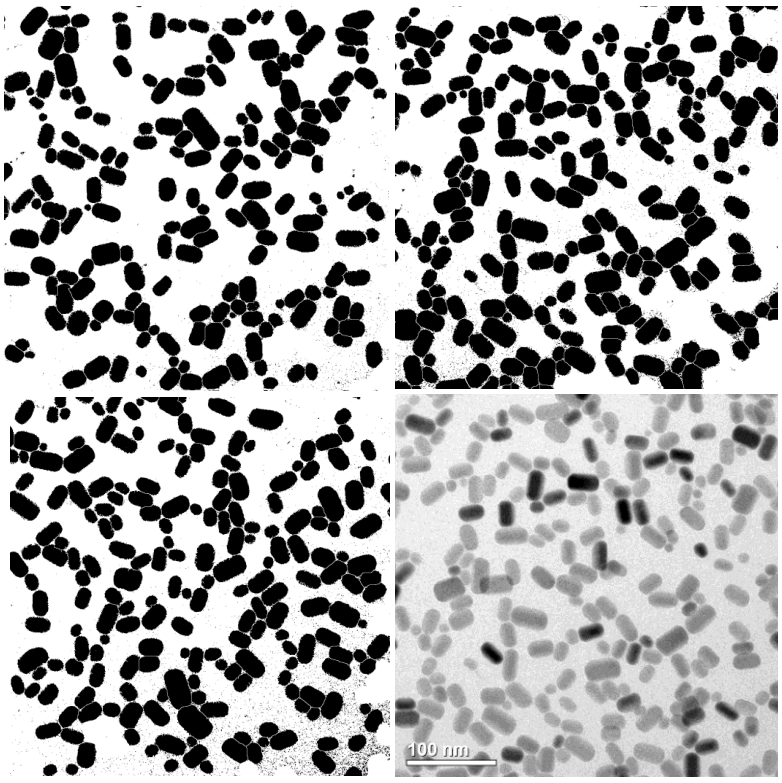

Figure A. 5: Black and white images of the TEM micrograph for the determination of the histogram in the case of NCs of hexagonal β-$NaPrF_4$ obtained by heating small β-$NaPrF_4$ precursor particles in oleic acid/octadecene for one hour at 320 °C. The original micrograph is presented at the bottom right to show the scaling.

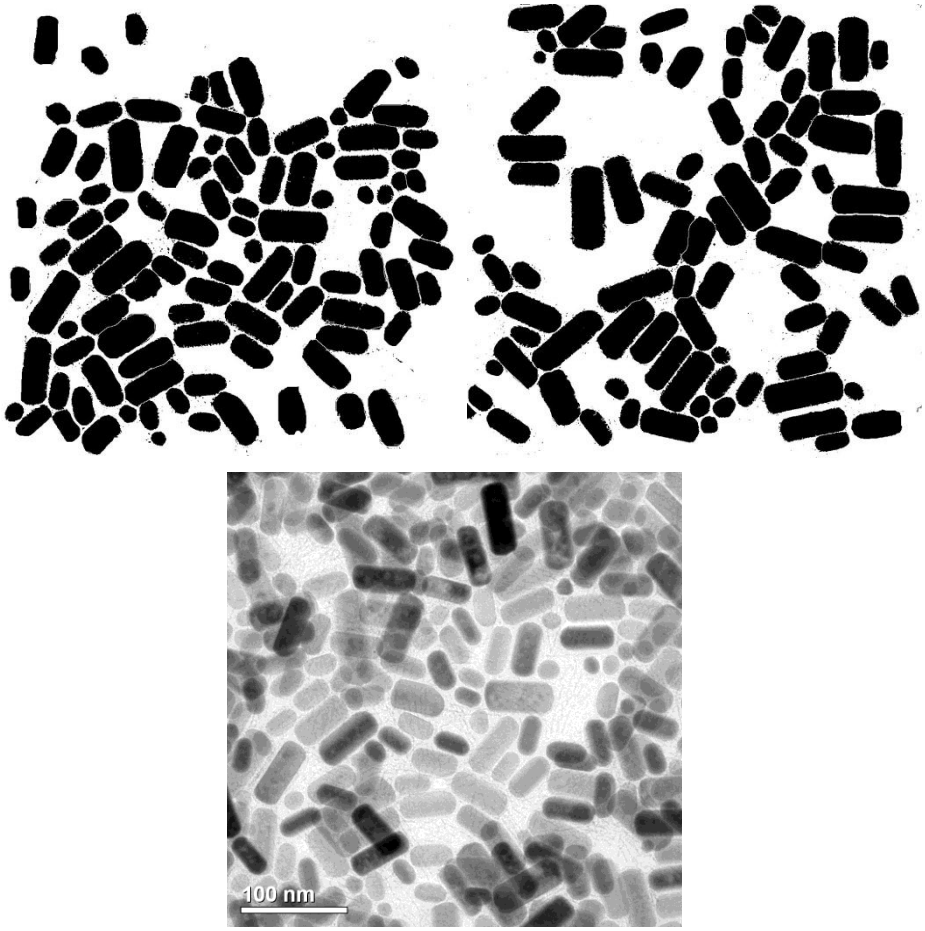

Figure A. 6: Black and white images of the TEM micrograph for the determination of the histogram in the case of NCs of hexagonal β-$NaCeF_4$ obtained by heating small β-$NaCeF_4$ precursor particles in oleic acid/octadecene for one hour at 320 °C. The original micrograph is presented at the bottom to show the scaling.

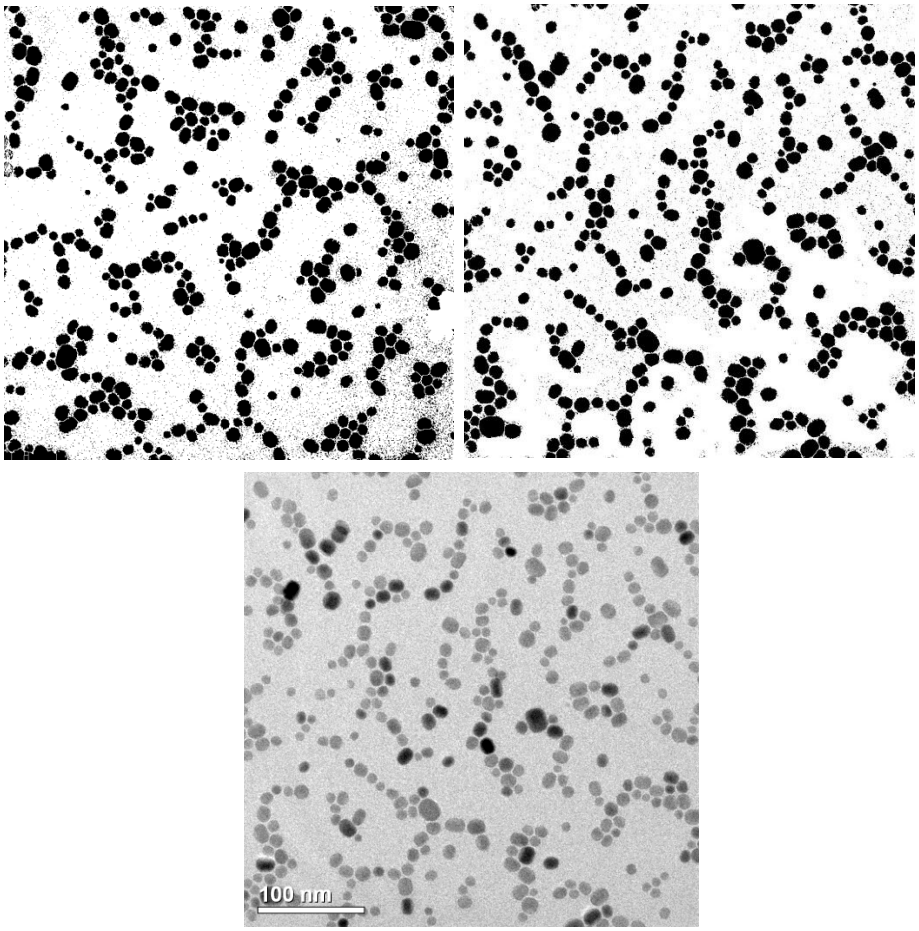

Figure A. 7: Black and white images of the TEM micrograph for the determination of the histogram in the case of NCs of hexagonal β-$NaNdF_4$ obtained by heating of small β-$NaNdF_4$ precursor particles in in oleic acid/octadecene for one hour at 320 °C. The original micrograph is presented at the bottom to show the scaling.

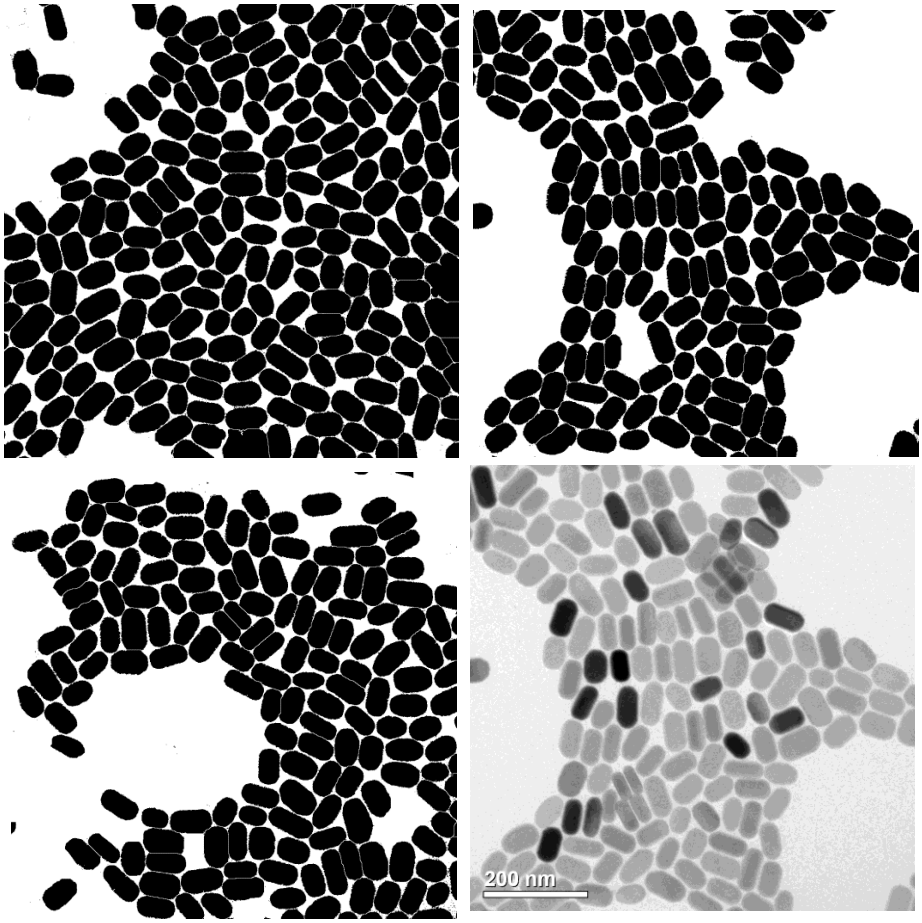

Figure A. 8: Black and white images of the TEM micrograph for the determination of the histogram in the case of NCs of hexagonal β-$NaNdF_4$ obtained by heating sub-10 nm particles of α-$NaNdF_4$ precursor particles in the presence of sodium fluoride at 320 °C in oleic acid/octadecene for one hour. The original micrograph is presented at the bottom right to show the scaling.

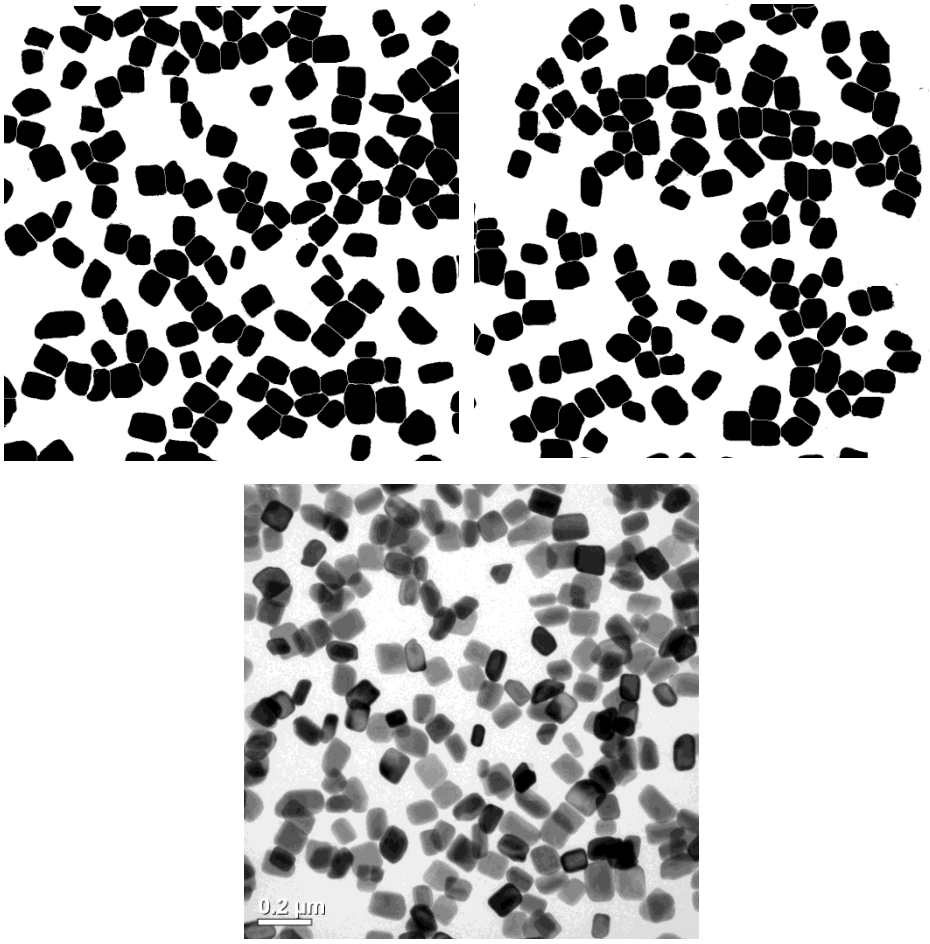

Figure A. 9: Black and white images of the TEM micrograph for the determination of the histogram in the case of NCs of hexagonal β-$NaPrF_4$ obtained by heating sub-10 nm particles of α-$NaPrF_4$ precursor particles in the presence of sodium fluoride at 320 °C in oleic acid/octadecene for one hour. The original micrograph is presented at the bottom to show the scaling.

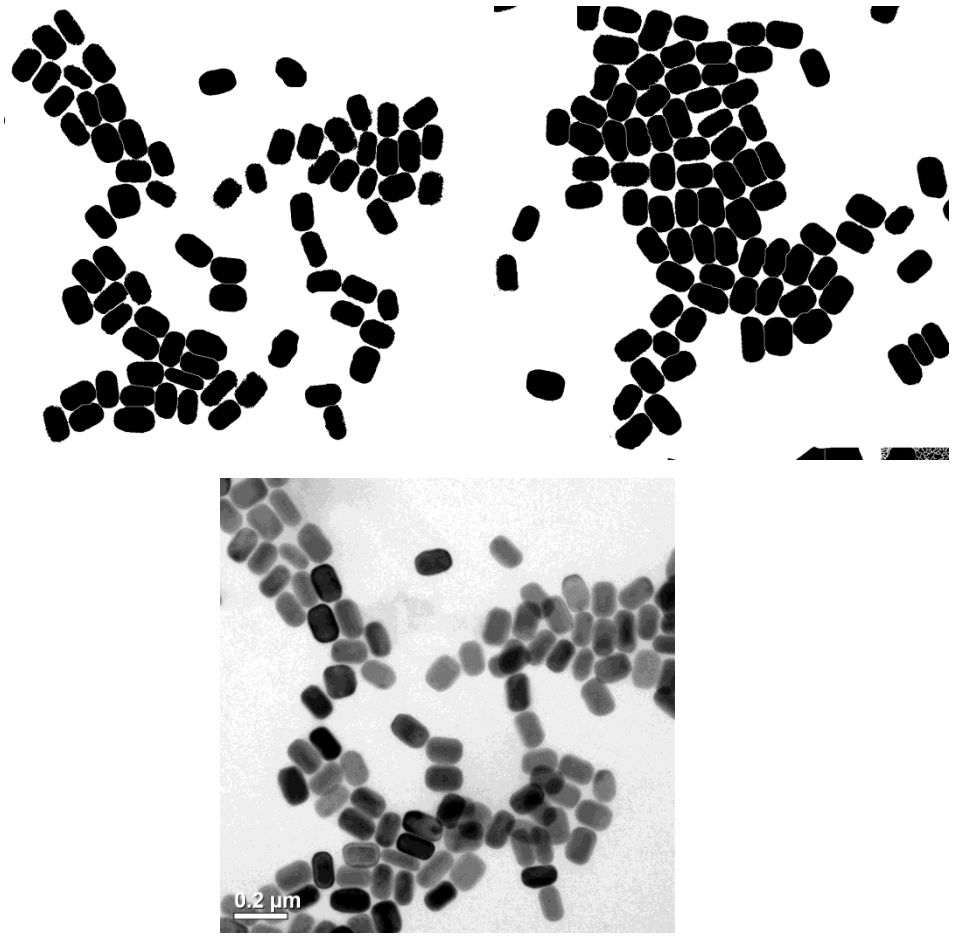

Figure A. 10: Black and white images of the TEM micrograph for the determination of the histogram in the case of NCs of hexagonal β-$NaCeF_4$ obtained by heating sub-10 nm particles of α-$NaCeF_4$ precursor particles in the presence of sodium fluoride at 320 °C in oleic acid/octadecene for one hour. The original micrograph is presented at the bottom to show the scaling.

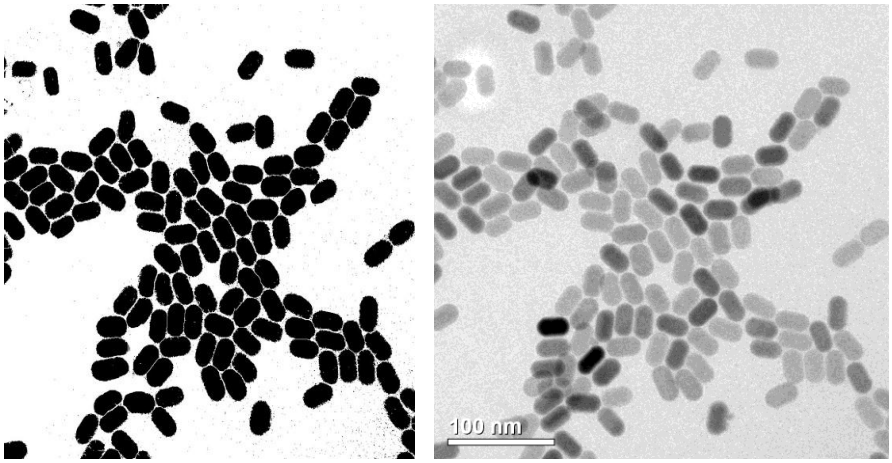

Figure A. 11: Black and white images of the TEM micrograph for the determination of the histogram in the case of NCs of hexagonal β-$NaYF_4$ obtained by heating sub-10 nm particles of α-$NaYF_4$ (Na/Y ratio 0.1) precursor particles in the presence of sodium fluoride at 320 °C in oleic acid/octadecene for one hour. The original micrograph is presented at right to show the scaling.

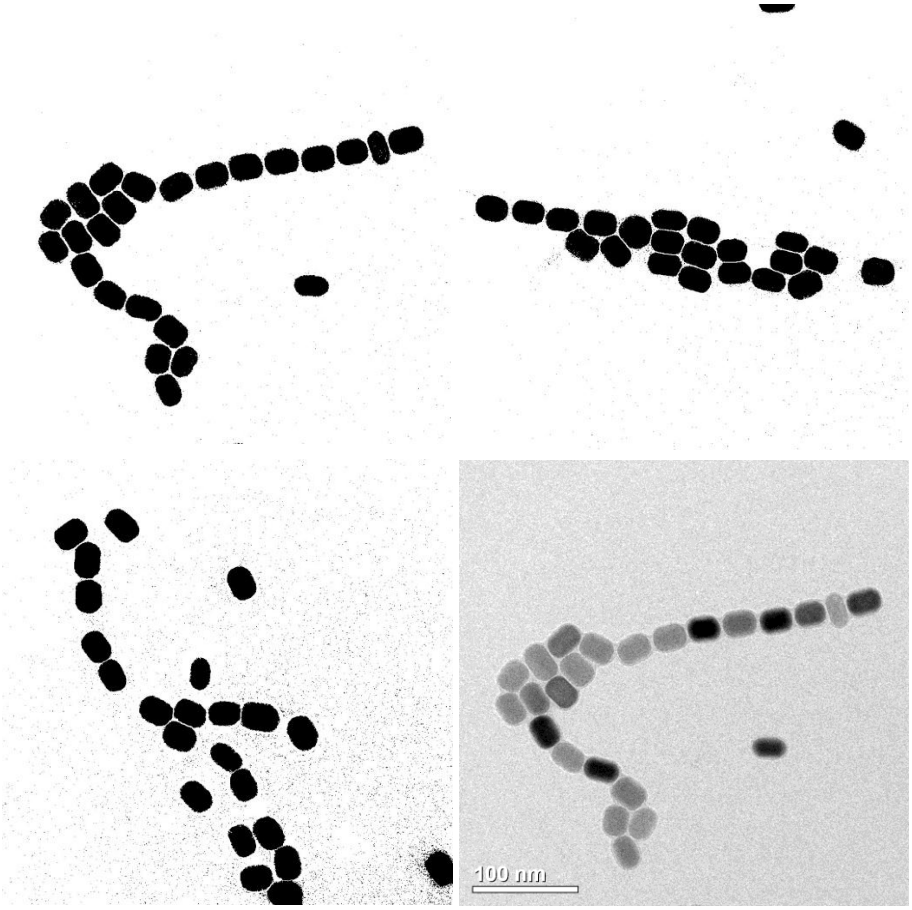

Figure A. 12: Black and white images of the TEM micrograph for the determination of the histogram in the case of NCs of hexagonal β-$NaYF_4$ obtained by heating sub-10 nm particles of α-$NaYF_4$ (Na/Y ratio 0.2) precursor particles in the presence of sodium fluoride at 320 °C in oleic acid/octadecene for one hour. The original micrograph is presented at the bottom right to show the scaling.

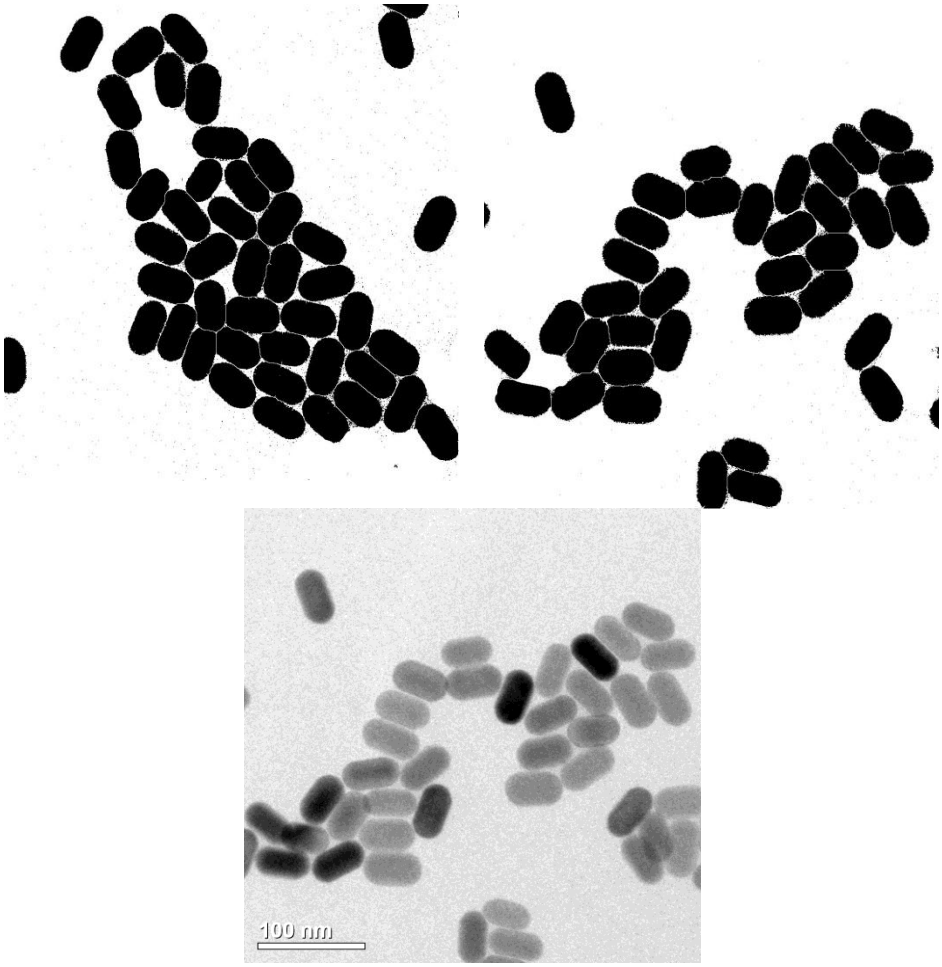

Figure A. 13: Black and white images of the TEM micrograph for the determination of the histogram in the case of NCs of hexagonal β-$NaYF_4$ obtained by heating sub-10 nm particles of α-$NaYF_4$ (Na/Y ratio 0.3) precursor particles in the presence of sodium fluoride at 320 °C in oleic acid/octadecene for one hour. The original micrograph is presented at the bottom to show the scaling.

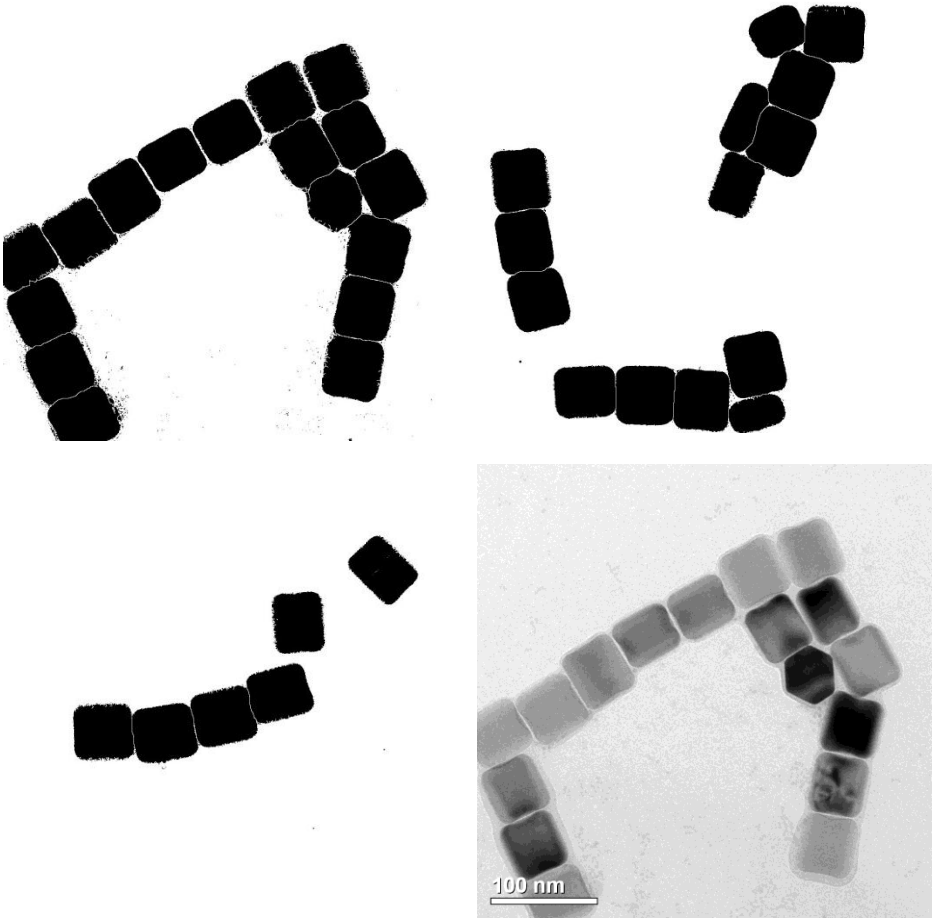

Figure A. 14: Black and white images of the TEM micrograph for the determination of the histogram in the case of NCs of hexagonal β-$NaYF_4$ obtained by heating sub-10 nm particles of α-$NaYF_4$ (Na/Y ratio 0.4) precursor particles in the presence of sodium fluoride at 320 °C in oleic acid/octadecene for one hour. The original micrograph is presented at the bottom right to show the scaling.

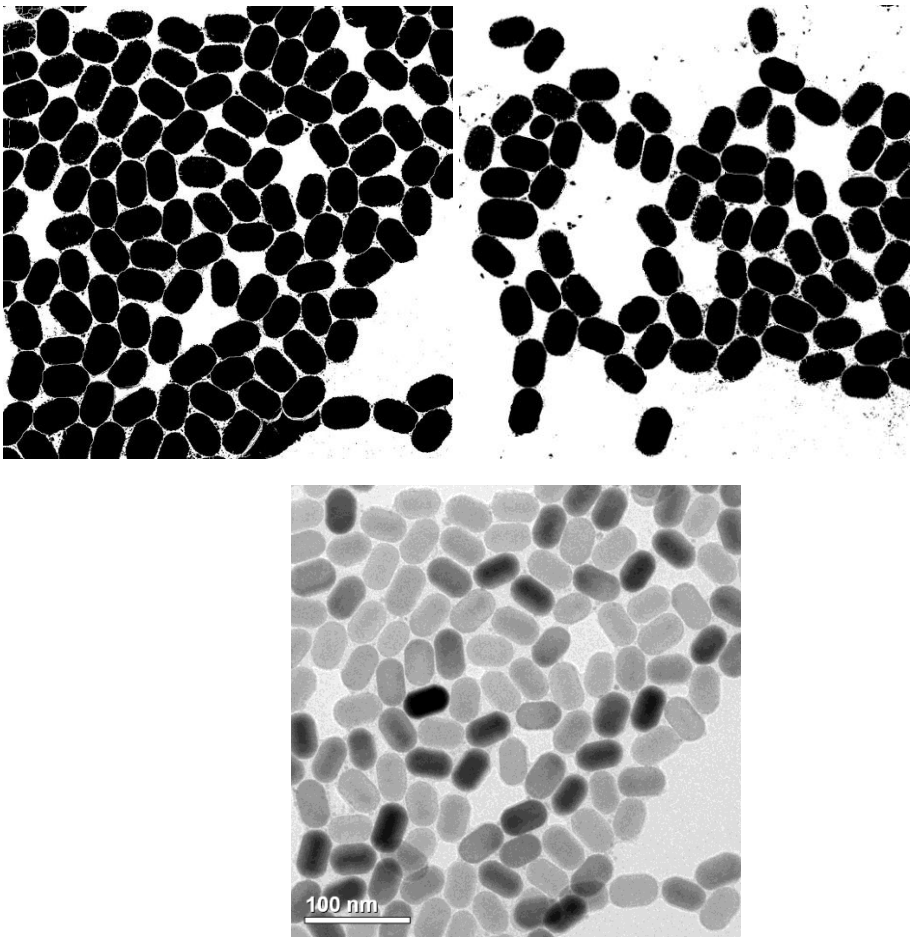

Figure A. 15: Black and white images of the TEM micrograph for the determination of the histogram in the case of NCs of hexagonal β-$NaYF_4$ obtained by heating sub-10 nm particles of α-$NaYF_4$ (Na/Y ratio 0.55) precursor particles in the presence of sodium fluoride at 320 °C in oleic acid/octadecene for one hour. The original micrograph is presented at the bottom to show the scaling.

A.3. Overview of the Synthesis of Nanocrystals

Small hexagonal β-$NaREF_4$ (RE = Ce, Pr, Nd), 290°C/60min

Sample	Sample code	Amount (mmol)	RE-oleate (g)	Na-oleate (g)	OA/OM/ODE (mL)	Restmass. TG (%)
β-$NaLaF_4$	ANR_341	20	19.63	15.2	50/50/100	50
β-$NaCeF_4$	ANR_348	20	19.69	15.2	50/50/100	50
β-$NaPrF_4$	ANR_311	20	19.70	15.2	50/50/100	50
β-$NaNdF_4$	ANR_312	20	19.77	15.2	50/50/100	50

Large hexagonal β-$NaREF_4$ by heating small β-$NaREF_4$ precursor particles

Sample	Sample code	Amount mmol	Small precursor β-$NaREF_4$	Amou nt mmol	Weight (g)	OA/ ODE (mL)	Temp./ Time (°C/Min.)
β-$NaLaF_4$	ANR_343	3	ANR_341	6.25	2.24	12.5/12.5	320/30
β-$NaCeF_4$	ANR_432	3	ANR_431	6.25	2.24	12.5/12.5	320/30
β-$NaPrF_4$	ANR_320a	3	ANR_311	6.25	2.88	12.5/12.5	320/30
β-$NaNdF_4$	ANR_313	3	ANR_312	6.25	2.28	12.5/12.5	320/30

Small cubic α-$NaREF_4$, 200 °C, 60min

Sample Name	Sample code	Amount (mmol)	RE-oleate (g)	NaF (g)	OA/OM/ODE (mL)	Restmass, TG (%)
α-$NaCeF_4$	ANR_335	20	19.69	5.04	50/50/100	30
α-$NaPrF_4$	ANR_328	20	19.7	5.04	50/50/100	57
α-$NaNdF_4$	ANR_329	20	19.77	5.04	50/50/100	52

Product obtained by heating of small cubic α-$NaREF_4$ in OA/ODE

Sample Name	Sample code	Small precursor β-$NaREF_4$	Amount (mmol)	Weight (g)	OA/ ODE (mL)	Temp./ Time (°C/Min.)
$NaPr_3$	ANR_337	ANR_328	6.25	2.354	12.5/12.5	320/30
$NaNdF_4$+NdF_3	ANR_333	ANR_329	6.25	2.31	12.5/12.5	320/30

Large Hexagonal β-$NaREF_4$ from small α-$NaREF_4$ (320°C/30min)

Sample	Sample code	Small precursor β-$NaREF_4$	Amount (mmol)	Weight (g)	NaF (g)	OA/ ODE (mL)
β-$NaCeF_4$	ANR_409	ANR_395	1	1.761	0.315	6/6
β-$NaPrF_4$	ANR_364	ANR_326	0.5	0.262	0.021	5/5
β-$NaNdF_4$	ANR_437	ANR_417	2	1.360	0.840	5/5

Hexagonal Ln^{3+} doped $NaREF_4$ (290°C/60min)

Sample (for 1mmol)	Sample code	RE-oleate (g)	Na-oleate (g)	NH_4F (g)	OA/OM/ ODE (mL)
$NaLaF_4:Pr_{0.05}$	ANR_283	La:Pr=0.934:0.4926	0.76	0.148	5/5/10
$NaCeF_4:Tb_{0.15}$	ANR_244	Ce/Tb oleat-=0.98	0.76	1.482	5/5/10
$NaLaF_4:Ce_{0.05}$	ANR_225	La:Ce=0.934:0.4922	0.76	1.482	5/5/10

Highly sodium deficient small α-$NaYF_4$

stock solution : Y-oleate 59 mmol in 500 mL OA/ODE, 240 °C/90 min

Na/Y ratio	Sample code	Amount (mmol)	RE-oleate (g)	Na-oleate (g)	NH_4F (g)	OA/ODE (mL)	Rest-mass, TG (%)
0.1	ANR_644	13	110	0.5670	1.4926	23/10	55.9
0.2	ANR_643	13	110	0.7915	1.5407	23/10	60.66
0.3	ANR_642	13	110	1.1873	1.5888	23/10	60.79
0.4	ANR_682	13	110	1.5830	1.6370	23/10	60
0.55	ANR_549	13	110	2.1767	1.7093	23/10	60.61

Decomposition of highly sodium deficient α-$NaYF_4$

Na/Y ratio	Sample code	Cubic precursor	Amount (mmol)	Weight (g)	OA/ODE (mL)	Temp./Time (°C/Min.)
0.1	ANR_673	ANR_644	1	0.2685	5/5	300/90
0.2	ANR_675	ANR_643	1	0.2543	5/5	300/90
0.3	ANR_677	ANR_642	1	0.2607	5/5	300/90
0.4	ANR_692	ANR_682	1	0.2707	5/5	300/90
0.55	ANR_574	ANR_549	1	0.2788	5/5	300/90

Heating of highly sodium deficient small α-$NaYF_4$

Na-oleate and NH_4F (1:1); 300 °C/80 min

Na/Y ratio	Sample code	precursor (mmol)	Weight (g)	Na-oleate (g)	NH_4F (g)	OA/ODE (mL)
0.1	ANR_678	1	0.2685	0.3044	0.0370	5/5
0.2	ANR_679	1	0.2543	0.3044	0.0370	5/5
0.3	ANR_680	1	0.2607	0.3044	0.0370	5/5
0.4	ANR_693	1	0.2707	0.3044	0.0370	5/5
0.55	ANR_681	1	0.2788	0.3044	0.0370	5/5

$LiYF_4$ NCs using sodium deficient α-$NaYF_4$ precursor particles

Stock solution: 10 mmol $LiOH.H_2O$ in 10 mL OA

Na/Y ratio	Precursor (1mmol)	Sample code	Weight (g)	Li-oleate (mL)	NH_4F (g)	OA/ODE (mL)
0.1	ANR_644	ANR_650	0.2685	1	0.037	5/5
0.2	ANR_643	ANR_649	0.2543	1	0.037	5/5
0.3	ANR_642	ANR_647	0.2607	1	0.037	5/5
0.4	ANR_682	ANR_683	0.2707	1	0.037	5/5

$LiYF_4$ nanocrystals using YF_3

Stock solution: 10 mmol $LiOH.H_2O$ in 10 mL OA

Sample code	Amount (mmol)	Li-oleate (mL)	YF_3 (g)	NH_4F (g)	OA/ODE (mL)	Temp./Time (°C/Min.)
ANR_595	2	2	0.2918 restmass46.73%	0.07407	10/10	300/60

$LiYF_4$ nanocrystals using molecular precursors with sodium

Stock solution:10 mmol $LiOH.H_2O$ in 10 mL OA; 3 mmol Y-oleate in 18 mL OA, 300 °C/90min

Na/Y ratio	Sample code	Amount (mmol)	Y-oleate (mL)	Na-oleate (g)	NH_4F (g)	OA/ODE (mL)
0.1	ANR_581	3	18	0.0913	0.4777	0/15
0.2	ANR_610	3	18	0.1827	0.5111	0/15
0.3	ANR_640	3	18	0.2739	0.5444	0/15
0.4	ANR_645	3	18	0.3653	0.5777	0/15

$LiYF_4$ nanocrystals using molecular precursor

Stock solution: 10 mmol $LiOH.H_2O$ in 10 mL OA

Sample code	Amount (mmol)	Li-oleate (mL)	Y-oleate (mL)	NH_4F (g)	OA/ODE (mL)	Temp./Time (°C/Min.)
ANR_621	3	3	18	0.4444	0/15	300/60

$LiLuF_4$ nanocrystals using LF_3

Stock solution: 10 mmol $LiOH.H_2O$ in 10 mL OA

Sample code	Amount (mmol)	Li-oleate (mL)	LuF_3 (g)	NH_4F (g)	OA/ODE (mL)	Temp./Time (°C/Min.)
ANR_600	2	2	0.49392 Restmass61.35%	0.07407	10/10	300/60

$LiLuF_4$ nanocrystals using molecular precursor

Stock solution: 10 mmol $LiOH.H_2O$ in 10mL OA; 3 mmol Lu-oleate in 18 mL OA

Sample code	Amount (mmol)	Li-oleate (mL)	Lu-oleate (mL)	NH_4F (g)	OA/ODE (mL)	Temp./Time (°C/Min.)
ANR_537	3	3	18	0.4444	0/15	300/90

$LiLuF_4$ NCs using sodium deficient α-$NaLuF_4$ precursor particles

Stock solution: 10 mmol $LiOH.H_2O$ in 10 mL OA, 300 °C/90 min

Na/Y ratio	Sample (1mmol)	precursor	Weight (g)	Li-oleate (mL)	NH_4F (g)	OA/ODE (mL)
0.3	ANR_695	ANR_686	0.3465 Restmass 70.58 %	1	0.037	5/5

Highly sodium deficient small α-$NaLuF_4$

Lu-oleate stock solution: 30 mmol in 120 mL OA/ODE), 240 °C/90 min, (TG 60.79 %)

Na/Y ratio	Sample code	Amount (mmol)	RE-oleate (g)	Na-oleate (g)	NH_4F (g)	OA/ODE (mL)
0.3	ANR_686	10	40	1.1873	1.2222	10/50

Core/shell $LiYF_4$:Yb,Er/$LiYF_4$

Li-oleate stock solution 10 mmol in 10 mL OA

Sample	Precursors	Li-oleate (mL)	NH_4F (g)	OA/ODE (mL)	Temp./Time (°C/Min.)
Core ANR_572 (3 mmol)	$NaYF_4$:Yb,Er(Na/Y=0.2) 60 % Rest mass 0.8634 g	3	0.111	15/15	300/60
Core/ shell ANR_573	Core LYF_4:Yb,Er (0.5mmol)	3	0.111	5/5	300/40

A.4. List of Chemicals

Properties	Oleic aicd	1-octadecene	n-Hexane	Ethanol
CAS Nr.	112-80-1	112-88-9	110-54-3	64-17-5
Formula	C18H34O2	C18H36	C6H14	C2H6O
Molarmass	282.47 g/mol	252.49 g/mol	86.178 g/mol	46,07 g/mol
Form	Liquid	Liquid	Liquid	Liquid
Melting point	13-14 °C	14-16 °C	-95.35 °C	-114.5 °C
Boiling point	360°C	315 °C	28.5 °C	78.325 °C
Density	0.887 g/mL	0.789 g/mL	0.6606 g/mL	0.78939g/mL
Flash point	189°C	148 °C	-22 °C	12 °C
Hazard Statement	H315-H319	H304	H225 H361f H304 H373 H315 H336 H411	H225
Precautionary Statement	P280-P264-P305+P351+P338-P362-P321-P332+P313-P337+P313-P302+P352	P301 + P310-P331	P201 P202 P210 P240 P241 P242 P243 P260 P261 P264 P271 P273 P280 P281 P301+310 P302+352 P303+361+353 P304+340 P308+313 P312 P314 P321 P331 P332+313 P362 P370+378 P391 P403+233 P403+235 P405 P501	P210 P233 P240 P241 P242 P243 P280 P303+361+353 P370+378 P403+235 P501

Properties	Sodium oleate	Sodium fluoride	Ammonium fluoride	Silver nitrate
CAS Nr.	143-19-1	7681-49-4	12125-01-8	7761-88-8
Formula	C18H33NaO2	NaF	NH_4F	AgNO3
Molarmass	304.45 g/mol	41.99 g/mol	37.04 g/mol	169.87 g/mol
Form	White to yellowish solid	White solid	White solid	White solid
Melting point	232-235 °C	993 °C	100 °C	209.7 °C
Boiling point	530 °C	1704 °C		440 °C
Density		2.79 g/cm^3	1.009 g/cm^3	4.35 g/cm^3
Hazard Statement	H319	H301 H319 H315	H331 H311 H301	H272, H314, H410
Precautionary Statement	P305+P351+P338	P261 P264 P270 P271 P280 P301+310 P302+352 P304+340 P305+351+ 338 P311 P312 P321 P322 P330 P332+313 P337+313 P361 P362 P363 P403+233 P405 P501	P261 P280 P301+P310 P311	P220, P273, P280, P305+351+338, P310, P501

Properties	Lanthanum chloride -7-hydrate	Cerium chloride chloride-7-hydrate	Praseodymium chloride-7-hydrate	Neodymium chloride-6-hydrate
CAS Nr.	20211-76-1	18618-55-8	10361-79-2	13477-89-9
Formula	$LaCl_3.\ 7H_2O$	$CeCl_3.\ 7H_2O$	$PrCl_3.\ 7H_2O$	$NdCl_3 \cdot 6H_2O$
Molarmass	371.37 g/mol	372.58 g/mol	373.77 g/mol	250.598 g/mol
Form	White solid	White solid	Light green solid	Mauve solid
Melting point	371.37 g/mol	817 °C	786 °C	758 °C
Boiling point	1000 °C	1727 °C	1710 °C	1600 °C
Density	3.84 g/cm^3	3.97 g/cm^3	2.25 g/cm^3	4.13 g/cm^3
Hazard Statement	H315-H319-H335	H315-H319-H335-H303	H319	H315-H319-H335
Precautionary Statement	P261-P280-P305+P351+P338-P304+P340-P362-P312-P321-P405-P403+P233-P501a	P261-P280-P305+P351+P338-P304+P340-P362-P312-P321-P405-P403+P233-P501a	P280-P264-P305+P351+P338-P337+P313	P261-P305 + P351 + P338

Properties	Yttrium chloride-6- hydrate	Gadolinium chloride -6-hydrate	Lutetium chloride-6-hydrate	Erbium chloride-6-hydrate	Ytterbium chloride-6-hydrate
CAS Nr.	10361-92-9	13450-84-5	15230-79-2	10025-75-9	10035-01-5
Formula	$YCl_3.6H_2O$	$GdCl_3.\ 6H_2O$	$LuCl_3.6H_2O$	$ErCl_3.6H_2O$	$YbCl_3.6H_2O$
Molarmass	303.26g/mol	371.61g/mol	389.33g/mol	381.62g/mol	387.34g/mol
Form	White solid	White solid	White solid	Violet solid	White solid
Melting point	721 °C	609 °C	905 °C	776 °C	854 °C
Boiling point	1507 °C	1580 °C	sublimes above 750°C	1500 °C	1453 °C
Density	2.67 g/cm^3	2.42 g/cm^3	3.98 g/cm^3	4.1 g/cm^3	2.58 g/cm^3
Hazard Statement	H315-H319-H335			H315-H319-H335	
Precautio-nary Statement	P261-P280-P305+P351+P338-P304+P340-P362-P312-P321-P405-P403+P233-P501a			P261-P280-P305+P351+P338-P304+P340-P362-P312-P321-P405-P403+P233-P501a	

Properties	**Lithium hydroxide-1-hydrare**	**Tetra methyl ammonium fluoride-4-hydrate**
CAS Nr.	1310-66-3	17787-40-5
Formula	$LiOH.H_2O$	$C_4H_{12}FN{\cdot}4H_2O$
Molarmass	41.962 g/mol	165.20 g/mol
Form	White solid	White solid
Melting point	450-471°C	39-42 °
Hazard Statement	H314,318,331,H361,H370,H372	H302, H315, H319
Precautionary Statement	P280-P305 + P351 + P338-P310	P261-P305 + P351 + P338

Acknowledgment

My PhD work would not have been possible without the help and support from many people whom I owe a great debt of gratitude.

Foremost, I express my deep sense of gratitude and respect to my research supervisor Prof. Dr. Markus Haase for giving me such an opportunity. His guidance, support, patience and encouragement have been endless and indispensable. I am extremely privileged to have him as my 'Doktorvater'.

I owe my gratitude to Prof. Dr. Lorenz Walder for having time and interest to examine my thesis as a second expert in the doctoral committee. His valuable advice and comments helped to improve the thesis.

Sincere thanks to Prof. Dr. Jacob Piehler, for fruitful association and scientific discussions, and I want acknowledge him and his team, especially Mr. Christoph Drees, for the collaborative work and manuscript.

I am indebted to my present and previous colleagues at Inorganic Chemistry-I department for providing an inspiring and fun filled environment. I wish to thank Dr. Jörg Nordmann, Dr. Benjamin Voss and Dr. Karsten Kömpe for sharing their research expertise and advice in the synthesis and analysis of research data. I wish to thank Dr. Thorben Rinkel and Dr. Simon Dühnen for the creative discussions and inputs for the successful completion of my work.

I am thankful to Ms. Kerstin Rücker not only for the thermogravimetric analysis but also for all other help and comfort provided in and off-campus. I would like to thank Ms. Marianne Gather for the XRF measurements as well as, with Dr. Ulli Walbrik, for creating a friendly and relaxed atmosphere in the office. Furthermore, I am thankful to Mr. Henning Eickmeier for analysing TEM samples. Also, I thank Mr. Christian Homann and Ms. Frederike Heiker for their nice companionship and I wish them all the very best for their doctoral work.

I want to thank Ms. Anna Hodge for reading the final version of the thesis for reviewing the language and for the compilation of the official documents.

I would also like to express my gratitude to Ms. Susanne Hassenfuss and Mr. Dirk Jaquemotte for their warm heartedness to share the apartment and for making Osnabrueck as my second home.

Finally, I would like to express my deepest gratitude to beloved family and friends for their unconditional support in all these years. Most of all, I express my sincere thanks to my husband, Dr. Rajesh Komban, for the understanding, motivation and never-ending support throughout the period and life.

Curriculum Vitae

Personal Details

Name	Athira Naduviledathu Raj
Date of Birth	02. 01. 1985
Place of Birth	Thodupuzha, Kerala
Nationality	Indian
Address	Hasetorwall 8, 49076, Osnabrueck
E-mail	anaduviledat@uos.de

Academic Qualification

Ph. D. April 2011 - to date	Institute of Chemistry of new Materials, University of Osnabrueck, Germany. (Supervisor: Prof. Dr. Markus Haase)
Master of Science August 2005 - July 2007	School of Chemical Science, Mahatma Gandhi University, Kerala, India.
Bachelor of Science June 2002 - April 2005	Mahatma Gandhi University, Kerala, India.

School Education

June 1991 - March 2000	Primary & High School, Kerala Secondary Education Examination Board, Kerala, India.
June 2000 - March 2002	Higher Secondary School, Board of Higher Secondary Education, Kerala, India.

Research Experience

April 2011 - to date	Ph. D. student, Institute of Chemistry of new Materials, Osnabrueck (Group: Prof. Dr. Markus Haase).
March 2008 - May 2010	Research Project Fellow, Materials and Minerals Division, National Institute for Interdisciplinary Science and Technology (NIIST-CSIR), Trivandrum, Kerala, India.
January 2007 - June 2007	Master Degree Project, Materials and Minerals Division, National Institute for Interdisciplinary Science and Technology (NIIST-CSIR), Trivandrum, Kerala, India. Project Dissertation: "Sol-Gel Nanocrystalline Photo Luminescent Europium Doped Lanthanum Phosphate Particulates and Coatings."

Publications

A. Naduviledathu Raj, T. Rinkel and M. Haase, Ostwald ripening, particle size focusing, and decomposition of sub-10 nm $NaREF_4$ (RE = La, Ce, Pr, Nd) nanocrystals, Chem. Mater., **2014**, 26, 5689.

C. Drees, **A. Naduviledathu Raj**, R. Kurre, K. B. Busch, M. Haase and J. Piehler, Engineered upconversion nanoparticles for resolving protein interactions inside living cells, Angew. Chem. Int. Ed., **2016**, 55, 11668.

T. Rinkel, **A. Naduviledathu Raj**, S. Dühnen and M. Haase, Synthesis of 10 nm β-$NaYF_4$:Yb,Er/$NaYF_4$ core/shell upconversion nanocrystals with 5 nm particle cores, Angew. Chem. Int. Ed., **2016**, 55, 1164.

T. Rinkel, J. Nordmann, **A. Naduviledathu Raj** and M. Haase, Ostwald-ripening and particle size focusing of sub-10 nm $NaYF_4$ upconversion nanocrystals, Nanoscale, **2014**, 6, 14523.

J. Nordmann, B. Voß, R. Komban, K. Kömpe, **A. Naduviledathu Raj**, T. Rinkel, S. Dühnen and M. Haase, Synthesis of β-phase $NaYF_4$:Yb,Er upconversion nanocrystals and nanorods by hot-injection of small particles of the α-phase, Z. Phys. Chem., **2015**, 229, 247.

S. Sankar. **A. Naduviledathu Raj**, C. K. Jyothi, K. G. K. Warrier and P. V. A. Padmanabhan, Room temperature synthesis of high temperature stable lanthanum phosphate-yttria nano composite, Materials. Res. Bulletin, 47, **2012**, 1835.

Conference paper/poster

A. Naduviledathu Raj, T. Rinkel and M. Haase, Investigation of $LiYF_4$ nanocrystals as host material for Yb/Er based upconversion luminescence, 14-16 May 2015, Bochum, Germany (poster).

J. Nordmann, B. Voß, **A. Naduviledathu Raj**, K. Mummenhoff and M. Haase, Hot-injection and seeded growth with "sacrificial particles" as precursors: synthesis of hexagonal phase $NaYF_4$:Yb,Er nanoparticles from "sacrificial" cubic phase $NaYF_4$:Yb,Er 4 nm particles, 29-31 May 2014, Hamburg, Germany (presentation).

A. Naduviledathu Raj and M. Haase Ostwald ripening, focusing and destruction of $NaREF_4$ nanocrystals of RE = Ce, Pr and Nd, Bunsentagung, 29-31 May 2014, Hamburg, Germany (poster).

A. Naduviledathu Raj, S. Dühnen and M. Haase, Monodispersed Sub-10 nm sized $NaLnF_4$ nanocrystals of the lighter lanthanides La, Ce, Pr and Nd, Bunsentagung, 9-11 May 2013, Karlsruhe, Germany (poster).

A. Naduviledathu Raj, V. Jendrock, T. Rinkel and M. Haase, Synthesis of rare-earth trifluoride nanoparticles based on small sacrificial particles, Bunsentagung, 9-11 May 2013, Karlsruhe, Germany (poster).

Declaration

I hereby declare that I have written this thesis without any inadmissible help of third parties and without use of any other than the allowed auxiliaries. Data and concepts taken directly or indirectly from other sources are marked with indication of the source.

Further persons were not involved with the content-related writing of the work concerned. Notably, I have not made use of intermediary or advisory services (doctoral consultants or other persons).

Nobody has received monetary benefits for work related to the content of the submitted dissertation.

The dissertation has so far neither been presented either in Germany or abroad, and has not been presented in equivalent or similar form to any other examination office.

Osnabrueck, 29.11.2016

_____

Athira Naduviledathu Raj